AD

USAAVLABS TECHNICAL REPORT 67-65

FABRICATION AND FULL-SCALE STRUCTURAL EVALUATION OF SANDWICH SHELLS OF REVOLUTION COMPOSED OF FIBER GLASS REINFORCED PLASTIC FACINGS AND HONEYCOMB CORES

By

Gene M. Nordby

W. C. Crisman

Charles W. Bert

November 1967

U. S. ARMY AVIATION MATERIEL LABORATORIES
FORT EUSTIS, VIRGINIA

CONTRACT DA 44-177-AMC-164(T)

UNIVERSITY OF OKLAHOMA RESEARCH INSTITUTE
NORMAN, OKLAHOMA

DEPARTMENT OF THE ARMY
U. S. ARMY AVIATION MATERIEL LABORATORIES
FORT EUSTIS, VIRGINIA 23604

This program was carried out under Contract DA 44-177-AMC-164(T) with the University of Oklahoma Research Institute.

The data contained in this report are the result of research conducted on sandwich shells of revolution composed of fiber glass reinforced plastic facings and honeycomb cores to determine the mode of shell failure in bending, torsion, and a combination of the two.

The report has been reviewed by the U. S. Army Aviation Materiel Laboratories and is considered to be technically sound. It is published for the exchange of information and the stimulation of future research.

TASK 1F121401A14176
CONTRACT DA 44-177-AMC-164(T)
USAAVLABS Technical Report 67-65
November 1967

FABRICATION AND FULL-SCALE STRUCTURAL EVALUATION OF SANDWICH SHELLS OF REVOLUTION COMPOSED OF FIBER GLASS REINFORCED PLASTIC FACINGS AND HONEYCOMB CORES

Final Report

By

Gene M. Nordby
W.C. Crisman
Charles W. Bert

Prepared by

University of Oklahoma Research Institute
Norman, Oklahoma

for

U. S. ARMY AVIATION MATERIEL LABORATORIES
FORT EUSTIS, VIRGINIA

SUMMARY

Large sandwich cylinders, truncated cones, and curved panels composed of fiber glass-epoxy facings and honeycomb cores were fabricated and tested as a part of a larger research program designed to bring acceptability of reinforced plastics for primary load-bearing members of Army aircraft structures. The many aspects of tooling for and fabrication of these large shells (up to 58-inch diameter and 72 inches long) by autoclave cure were examined in detail. To generate preliminary data on this mode of shell failure, the shells were designed to fail in buckling. The tests were carried out on a testing machine capable of applying 3,000,000 inch-pounds of bending moment, of torque, or of each in combination. Curved-panel compressive test values agreed reasonably well with the approximate theoretical analyses available, but agreement of test and analysis was not good for the shear loading. Preliminary interaction relations were confirmed tentatively for the combined torsion and bending of the cylinders and truncated cones.

FOREWORD

This report was prepared by the University of Oklahoma Research Institute (OURI) under phases IV and V of U. S. Army Aviation Materiel Laboratories (USAAVLABS) Contract DA 44-177-AMC-164(T) for research conducted during the period from May 10, 1965 to March 31, 1967. Work under this contract has encompassed material properties as well as structural evaluations. Phases I and III were reported separately as Technical Report 65-66, titled The Effect of Resin Content and Voids on the Strength of Fiberglass-Reinforced Plastics for Airframe Use, and Phase II was reported as Technical Report 65-60, Dynamic Elastic, Damping, and Fatigue Characteristics of Fiberglass-Reinforced Sandwich Structure. The research effort is a continuation of the work accomplished under two other contracts which resulted in the following reports: Technical Report 65-15, Strength Properties and Relationships Associated with Various Types of Fiberglass-Reinforced-Facing Sandwich Structure, and Technical Report 64-37, Research in the Field of Fiberglass-Reinforced Sandwich Structure for Airframe Use.

The present report was written by Dr. Gene M. Nordby, project director and Dean of the College of Engineering at the University of Oklahoma; Mr. W. C. Crisman, project director; and Dr. Charles W. Bert, research engineer and Professor of Aerospace and Mechanical Engineering.

CONTENTS

ILLUSTRATIONS

TABLES

SYMBOLS

a	length of buckle or panel, inches; subscript used with σ_{cr} to denote axial compression
b	width of buckle or panel, inches; subscript used with σ or σ_{cr} to indicate bending
c	thickness of core, inches; subscript used with M_{cr} to indicate cylinder; subscript used with G to denote effective core value.
cr	subscript used with τ, σ, T, and M to indicate the critical buckling values
d_1, d_2, d_3	parameters defined by Equations (49), (50), (51)
f	subscript used with σ, T, and M to indicate values at material failure or used with E and ν to indicate effective facing value
h	thickness of sandwich measured between facing centerlines (c+t), inches
i	subscript used with μ and ϕ to denote isotropic
n	number of buckles in the circumferential direction $(2\pi R_c/b)$
t	one facing thickness, inches
A_1, A_2, A_3, A_4	parameters defined by Equations (25), (27), (28), (29)
B	parameter defined by Equation (43)
B_1, B_2	parameters defined by Equations (23), (24)
C_o	orthotropic-facing correction factor
C_1, ..., C_8	parameters defined by Equations (38), ..., (45)
D	flexural rigidity of shell, pound-inches
E_x, E_y, E_{45}	Young's moduli of the facings in the axial, circumferential, and 45-degree directions, psi
F	$(1/3)\ (t/h)^2$
G_{xz}, G_{yz}	transverse shear moduli of the core, psi

H	total thickness of sandwich ($h + t$), inches
I	area moment of inertia of the facings about specimen neutral axis, $inch^4$
I_f	area moment of inertia of the facings per unit width and about centroidal axis of cross section, $inch^3$
J	parameter $L^2/R_c h$
K	buckling coefficient used in large-deflection axial compression analysis
K'	buckling coefficient used in small-deflection axial compression analyses; see Equation (70)
K_f	buckling coefficient used in torsional analysis
K_{xa}	buckling coefficient used in Reference 40 axial compression analysis; see Equation (65)
L	axial length of shell, inches
M	pure bending moment, pound-inches
N_{cr}	critical buckling load (uncorrected for orthotropic facings), pounds per inch of width
P	compressive load applied to curved panels, pounds
Q	parameter defined by Equation (47)
R_1, R_2	smallest and largest radii of the shell middle surface, respectively, inches
R_c	radius of middle surface of cylinder, inches
$\overline{RC}$	resin content by weight, percent
S_x, S_y	parameters defined by Equations (30), (31)
T	pure torsional moment, pound-inches
T_1, T_2	parameters $(\gamma + \rho)$, $(\gamma - \rho)$
V	parameter defined by Equation (69)
W_x, W_y	parameters defined by Equations (54), (55)
α	semivertex angle of cone, degrees
β_1, β_2, β_3, β_4	parameters defined by Equations (33), (36), (37), (46)

γ	inclination of torsional buckles from cylinder axis, degrees; shear strain, inches/inch
Δ	denotes increment in the quantity denoted by the symbol following Δ
δ	side deflection of curved panels, inches
ε_{45}	measured normal strain at 45 degrees to the shell axis, inches/inch
ζ	aspect ratio of buckles (b/a)
η	parameter $n^2 h/R_c$
Θ	parameter defined by Equation (9)
θ_σ	principal stress direction, measured from axis of major material symmetry, degrees
θ_ε	principal strain direction, measured from axis of major material symmetry, degrees
λ	factor $(1 - \nu_{xy}\ \nu_{yx})$
μ_{xy}	shear modulus of the facings, psi
ν_{xy}, ν_{yx}	Poisson's ratios of facing material
ρ	parameter $\pi R_c/nL$
σ	compressive stress in facings, psi
σ_b	maximum bending stress, psi
τ	shear stress in the facings, psi
ϕ, ϕ_1, ϕ_2	shear-stiffness factors defined by Equation (57)
ψ_1, ψ_2	parameters defined by Equations (18), (21)
ω	parameter defined by Equation (8)

BLANK PAGE

DISCUSSION

1. Introduction

For the past four years, the University of Oklahoma Research Institute (OURI) has been conducting research in the area of fiber glass reinforced plastics (FRP) of the type suitable for primary aircraft structure of U. S. Army aircraft. The initial phase of the program was to determine the optimum employment of raw materials and fabrication processes to develop maximum stress levels in the sandwich material. This work has consisted of (1) the evaluation of several sandwich fabrication techniques (Reference 25) and the relation between strength and fabrication variables for the facing laminates alone (References 25, 27, and 31), (2) the evaluation of several sandwich configurations sized to fail in face rupture and in the various buckling modes (References 15, 25, and 26), and (3) the evaluation of the dynamic properties of a sandwich material (References 30, 28, and 5). In items (2) and (3), the test results were compared with the results of calculations.

The second phase has as its final objective the development of optimum-design methods for aircraft-type structures. The first step toward this objective was the static testing of full-size structures of simple geometry (cylindrically curved panels, complete cylinders, and truncated cones), in order to evaluate the methods of analysis. The present report covers this step.

The next step in the second phase would involve the optimization of the orientation of the layers of the laminate, optimum design of structural joints, and dynamic testing of full-size structures of simple geometry (such as a truncated cone). The final step would be the optimum design, fabrication, and testing of a typical complex aerodynamic structure such as a wing. In this final step, it would be necessary to use the results generated in all of the preceding parts of the program.

The objectives of the present work were (1) to evaluate the three basic FRP sandwich structures and the corresponding methods of analysis, and (2) to develop tooling and fabrication procedures necessary to produce the various shells. Since instability is the most critical and often the most difficult to predict of the static failure mechanisms, the shells were designed for buckling (see Section 3.) This decision necessitated rather large specimens, especially since the construction is sandwich, which has a high effective stiffness (References 36 and 16).

The loads and the boundary conditions were made as uncomplicated as possible in an effort to obtain more basic information and to minimize unnecessary obscuration of the findings. In particular, the loads consisted of compression and shear on the curved panels and pure torsion, pure beam flexure, and a combination of the two on the complete shells.

As was anticipated from the beginning, the tooling required more project time and funds than any other facet of the research. Yet, the

tooling was rather inexpensive, relatively speaking, because plastics were used throughout. A task almost as consuming as the tooling was the design and assembly of the special equipment to fabricate and test the large shell specimens within the funding and time schedule of the program. Hence, only a small sampling from each specimen configuration could be made for comparison with existing theory. The data generated must, therefore, not be considered more than preliminary and should be supplemented by future tests.

The sandwich facing-laminate constituent materials used in this research were those best suited for aircraft application four years ago when the program began. Though advances have been made in resins, glasses, and finishes, the materials are still very much in use, and thus, the principles derived here are believed to be basic to the design and fabrication of FRP structures.

The facing materials used are Epon 828 epoxy resin activated by curing agent Z and Volan A finished, E-glass, used in the form of 181-style fiber glass fabric. The other materials used in the sandwich construction are (1) AF-110B film-supported adhesive and (2) the 1-mil nonperforated foil 5052 aluminum honeycomb core with 1/4-inch hexagonal cells.

2. Special Research Equipment

a. Fabrication Equipment

The major items of fabrication equipment that were especially constructed for this program consisted of plaster-mold forming and handling tools, a resin prepregging machine, and a plastics-curing autoclave system. Each item will be discussed in detail in the following subsections.

(1) Plaster Equipment

The device used to shape the plaster molds is shown in Figure 1. This plaster sweep consists of a three-column steel frame which supported each of the mold frameworks (A in Figure 1) in the vertical position, and a screed system (B and C in figure 1) mounted on bearings which permitted rotation of the screed around the molds to establish the surface of the plasters. The screed bar is accurately positioned relative to the mold axes by means of a set of micrometer slides (C in Figure 1). Adjustment of the slides establishes the desired end radii of the cylindrical or conical molds. The bare frameworks and the completed plaster molds are installed or removed from the sweeping device by an overhead hoist.

A special dolly system was designed and constructed to handle the plaster molds as well as the plastic tools. The use of the dollies in maneuvering the plasters is shown in Figure 2, where a newly constructed cylindrical mold is being lowered

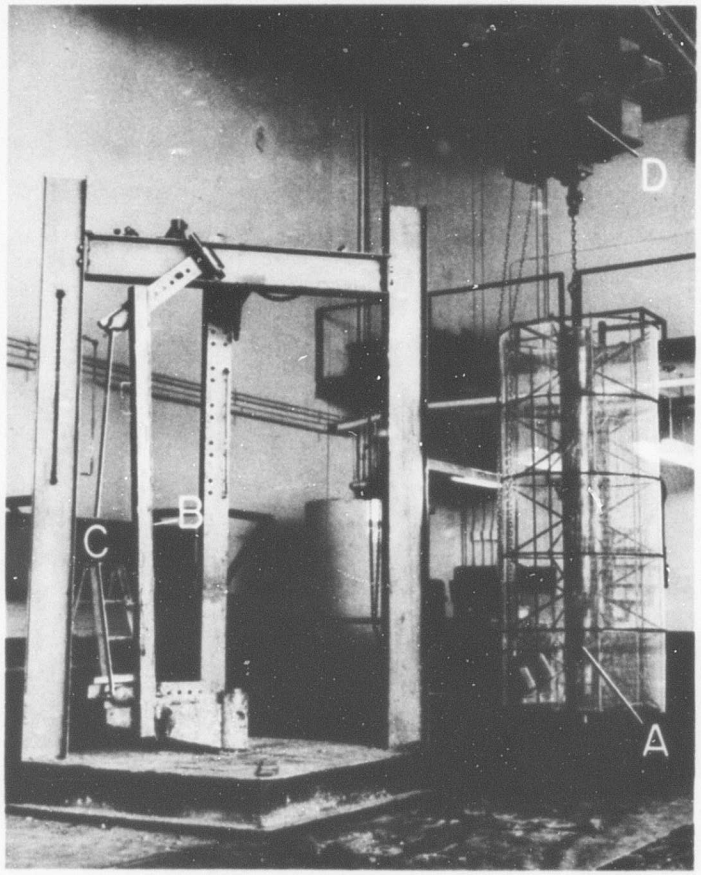

BEFORE ASSEMBLY

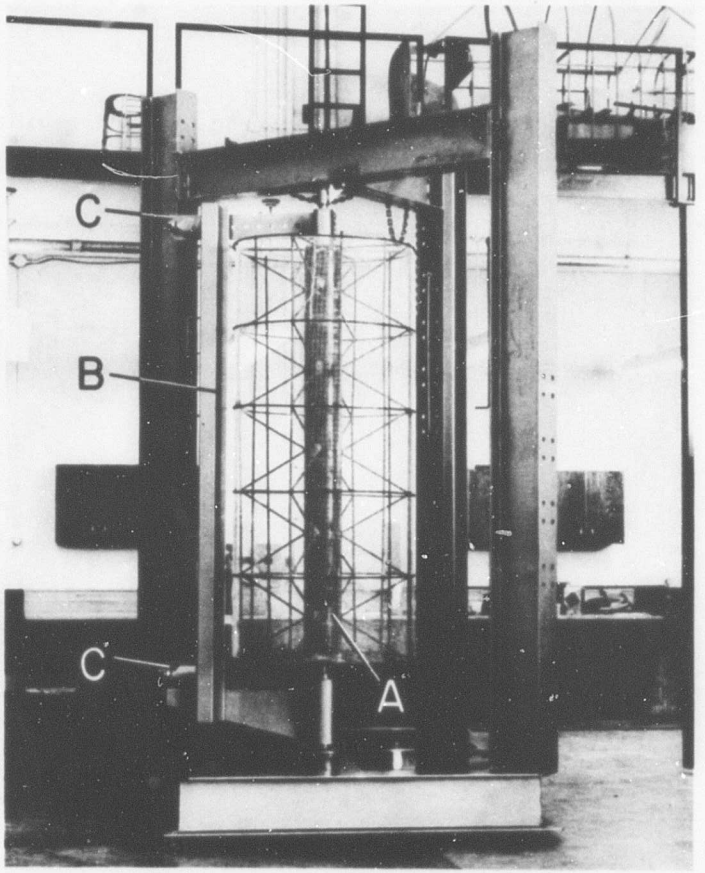

COMPLETED ASSEMBLY

Figure 1. Plaster-Sweeping Device Showing Typical Mold Framework Installation: A, Steel Framework to Support Plaster (Cylinder Shown); B, Sweep for Screeding Plaster Mold; C, Slides for Micrometer Adjustment of Sweep Radius; D, Scale for Weighing Molds.

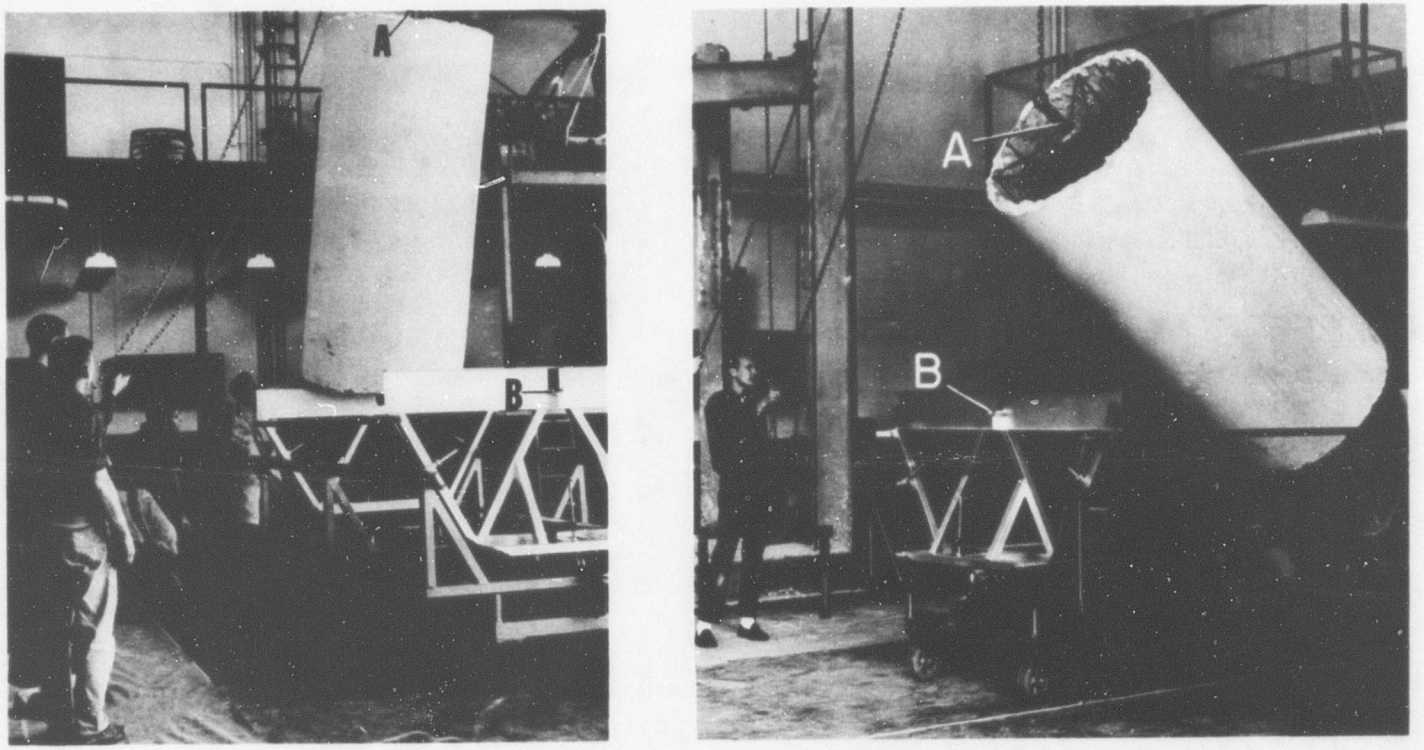

Figure 2. Typical Installation of Plaster Mold Into Autoclave Dolly System: A, Plaster Mold Support Shaft and Lifting Eye; B, Front Saddle Support for Plaster Mold Shaft.

from the vertical to the horizontal position for completion of the tooling cycle.

The system is actually composed of two components: an upper skeleton-like dolly for supporting components in the autoclave and a lower dolly for transporting the components, plaster or plastic. The dual function of the dolly system and a description of its special parts are shown in Figure 3. Here a cylindrical plaster mold suspended in the upper dolly is being rolled off the transportation dolly into the autoclave for drying. The component weight is carried by V-grooved wheels rolling on the autoclave track, and balance is provided by outriggers (two on each end) that rest lightly against the autoclave air duct. Thus, by virtue of the system design, the upper dolly itself is unusually lightweight and occupies very little space in the vessel.

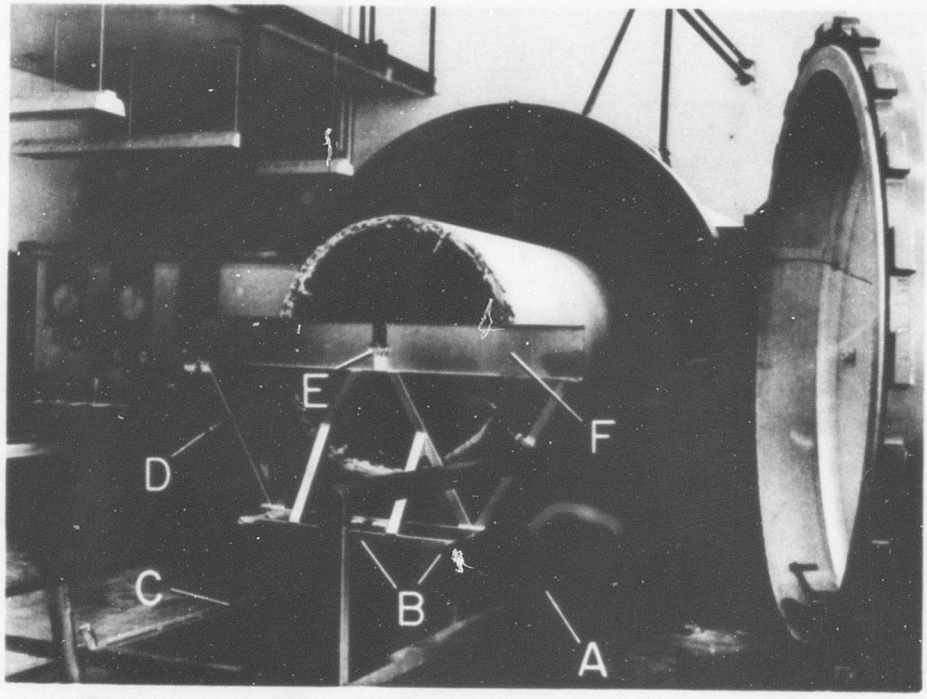

Figure 3. Loading of Component Into Autoclave Showing Function of Dolly System: A, Transportation Dolly; B, Autoclave Dolly; C, Track for Dolly Wheels; D, Autoclave Dolly Outrigger; E, Saddle Support; F, End plate.

(2) Multilayer Prepreg Machine

The resin prepreg machine is essentially the same machine presented in References 9 and 31 with minor exceptions. The main modification made for the present program was the widening of

the system to impregnate up to 54-inch-wide fiber glass fabric. The other change was the addition of larger rolls of films, polyethylene and nylon, eliminating the need for periodically rerolling a supply of film onto the machine. The rerolling seemed to cause excessive stretching of the film, which fostered detrimental wrinkles and even air seepage into the impregnate during the initial B-staging period.

Figure 1 of Reference 9 adequately describes the operation of the apparatus which produces the much desired uniform-resin-content (±1 percent) multilayered preimpregnate of very low void content; but, for clarity, a sketch of the two-ply system is shown in Figure 4. As indicated, the turning of the take-up cylinder (B) pulls the fabric off the supply rolls (C), into the heated resin vat (J) for impregnation, through the first set of pressure rollers (L) for prepreg assembly, and finally through the main pressure rollers (D) for establishment of the final resin content and introduction of the cover films (E).

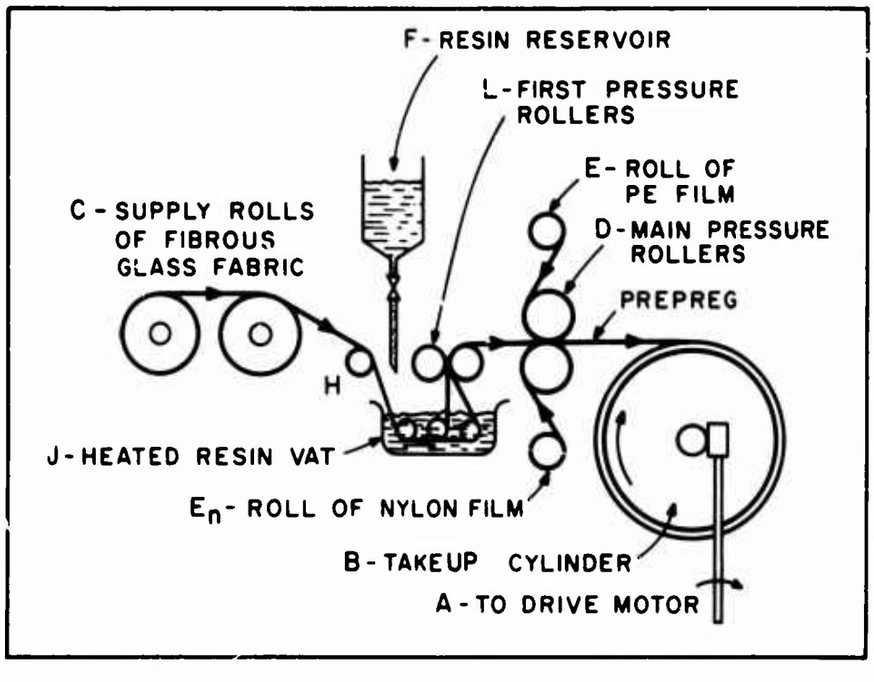

Figure 4. Schematic of Multilayer Prepreg Machine.

(3) Autoclave System

As mentioned previously, the autoclaving system was designed and constructed by the University of Oklahoma Research Institute for the purpose of fabricating large sandwich shells composed of fiber glass-reinforced plastic facings and honeycomb

cores (Reference 29). The system consists primarily of an ASME-code pressure vessel which is insulated and outfitted with an electric heating system, a control console consisting of a battery of recorder-controllers, and a high-volume air supply in the form of a 300-cfm compressor. The main components are shown in Figures 5 through 9.

The autoclave is equipped with a ring-lock quick-opening door and contains a 6-foot-diameter by 12-foot-long working space with the capability of operating at 150 psi and 350 degrees Fahrenheit outside wall temperature. The 7-foot-diameter steel vessel is insulated with a lining of 3-inch-thick fiber glass wool sandwiched between two sheets of asbestos paper. The insulation is covered on the ends of the vessel by 3/16-inch-thick steel heads and covered in the cylindrical portion by a 16-gage galvanized steel shell which also forms an annular air duct (C in Figure 8). The cutaway of Figure 5 shows the construction in detail.

The vessel air space is heated by 48 finstrip electrical heaters totaling 60,000 watts. The 25-inch-long heaters are mounted in the rear head of the vessel in eight hexagonal-shaped rings encircling the 22-inch-diameter blower. Heating is accomplished by the blower (see Figure 9) inducing air from the working space of the vessel (see H in Figure 8) and forcing it radially through the heaters into the annular air duct. The duct in turn channels the air forward to the door area, where it is redirected back into the working space. The temperature in the vessel is controlled by the Honeywell pulse-type controller (E in Figure 6) which proportions the time that the 220-volt heaters are on by opening and closing a 3-phase contactor. The control thermocouple (all thermocouples are the iron-constantan type) measures vessel air temperature rather than specimen temperature. This is to prevent large temperature overshoots after the temperature acceleration period, since temperature reduction is accomplished by heat loss through the vessel walls.

The air pressure in the vessel is controlled by the modulation of the inlet and outlet control valves (E and H in Figure 7) that is produced by a pneumatic signal from the Honeywell controller mounted on the console (D in Figure 6). The Honeywell controller, which is equipped with a proportional band, reset and rate functions, and the control valves was furnished to the project by OURI. The high-volume compressor (D in Figure 9) was obtained by modifying the original equipment, designed for 150-cfm delivery at 3000 psi, by paralleling two low-pressure stages, essentially doubling the capacity.

The vacuum and therocouple lines are introduced into the vessel through a 12-inch-diameter blind flange (see E in Figure 8). The blower drive shaft is supported in the center of the

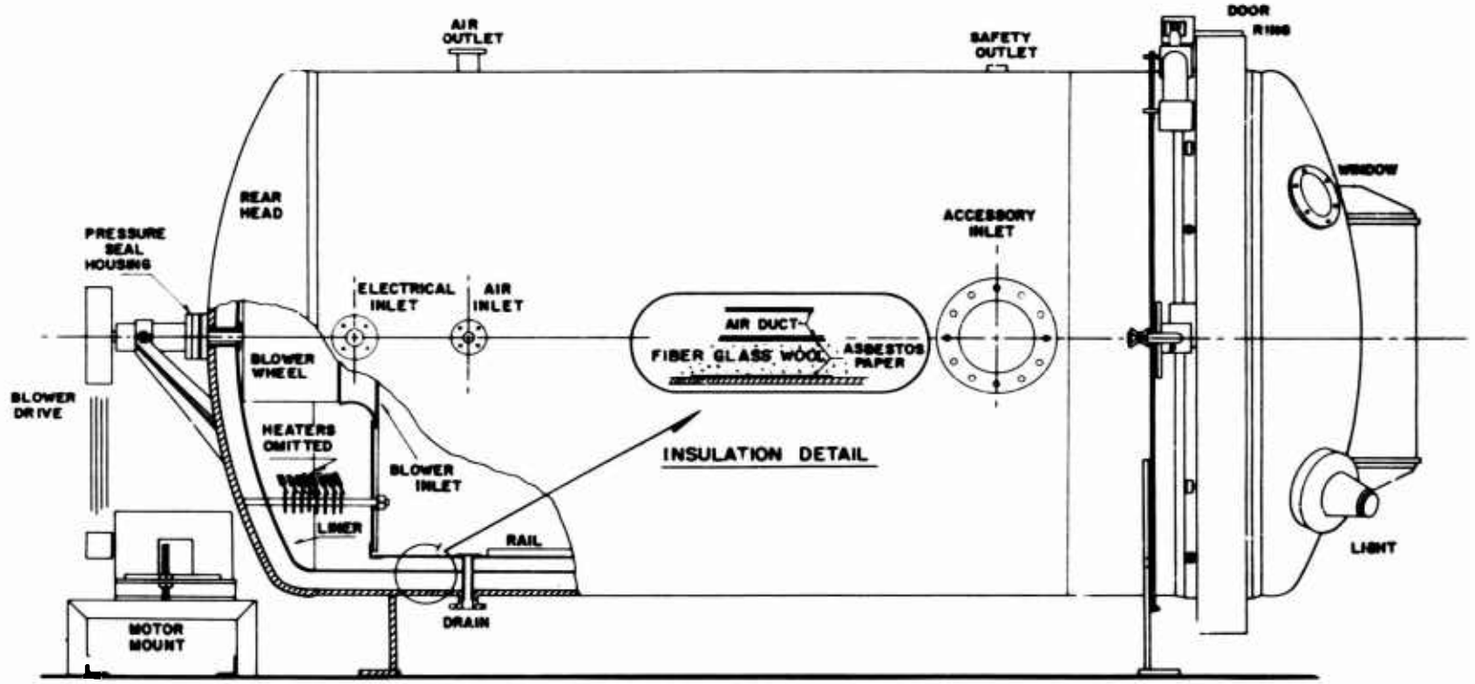

Figure 5. Cutaway of 150 psi, 350° F Autoclave Showing Construction Details.

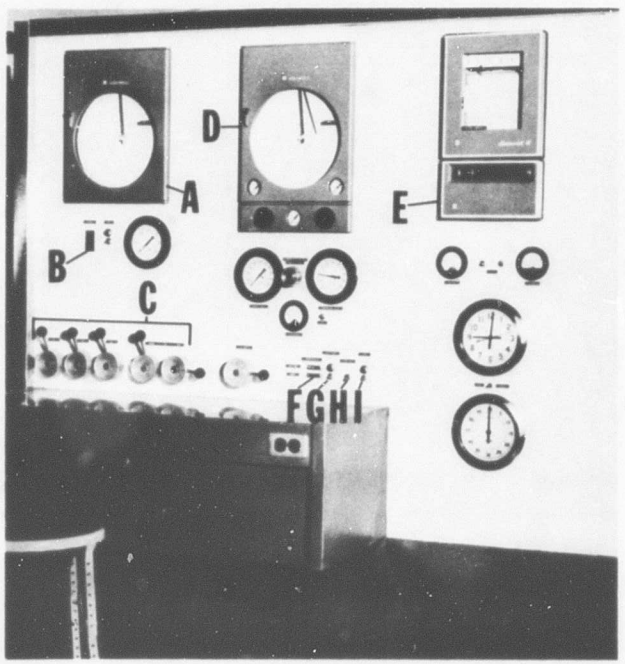

Figure 6. Autoclave Control Console: A, Vacuum Recorder; B, Vacuum Control; C, Vacuum Line Selectors; D, Pressure Recorder-Controller; E, Temperature Recorder-Controller; F, Thermocouple Connectors; G, Heater Power Switch; H, Door Switch; I, Light Switch.

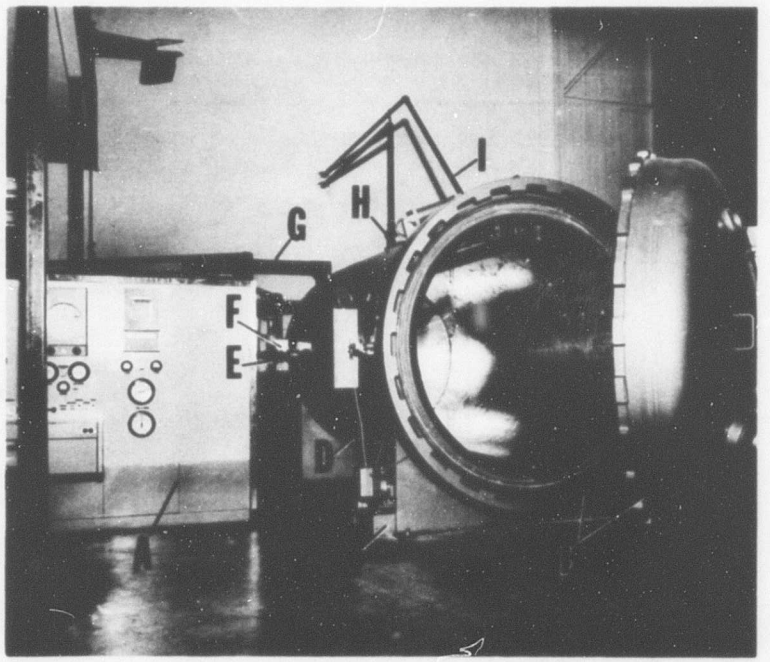

Figure 7. Front View of Autoclave System: A, Control Console; B, Door and Lock Ring; C, Hydraulic Pump for Door Lock Ring; D, Pressure Vessel; E, Air Inlet Control Valve; F, Junction Box for Heater Power Lines; G, Wireway Containing Thermocouple and Vacuum Lines; H, Air Exhaust Control Valve; I, Air Exhaust Pipe From Vessel Safety Valve.

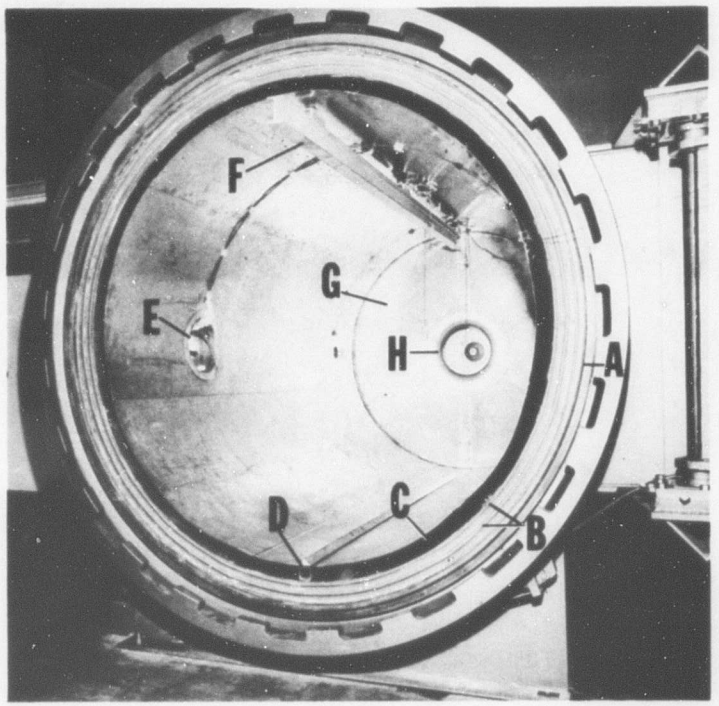

Figure 8. Interior View of Autoclave: A, Door Pressure Seal; B, Door Heat Seals; C, Annular Air Duct; D, Track for Specimen Dolly; E, 12-Inch-Diameter Port for Thermocouple and Vacuum Line Entrance; F, Overhead Rail Suspension; G, Heater Cover Panel; H, Blower Inlet.

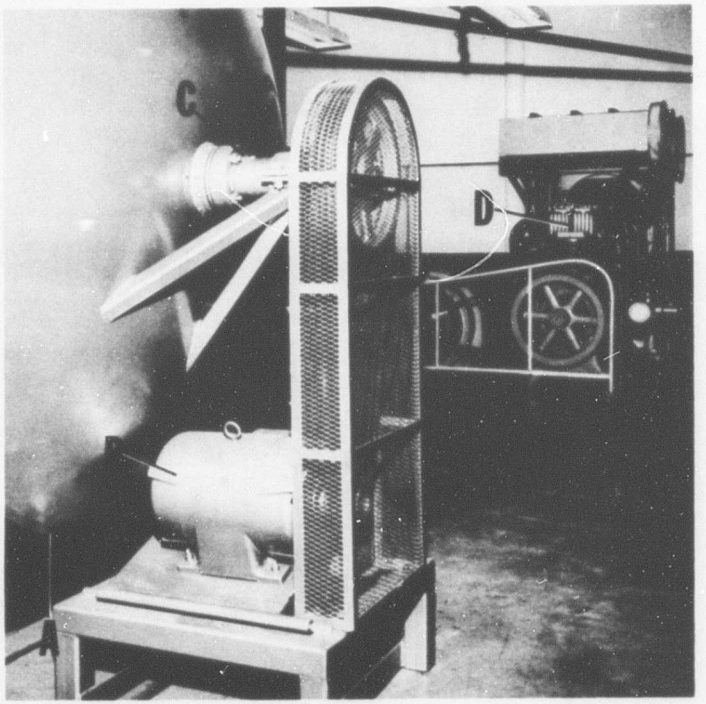

Figure 9. Rear View of Autoclave Showing Blower Drive System: A, Rear Head of Pressure Vessel; B, Blower Motor; C, Housing for Blower Drive-Shaft Pressure Seal (Tungsten Carbide Ring Rotating Against Carbon); D, Autoclave Compressor (300-cfm Capacity).

rear head of the vessel by a 3-inch-diameter studding outlet and is made airtight by a dry seal consisting of a tungsten carbide ring rotating against a carbon insert. The plastic specimens may be introduced and supported in the vessel by way of the removable overhead rail (F in Figure 8) or by way of the angle iron track (D in Figure 8). The latter was used for the very large sandwich shells in conjunction with a skeleton-like dolly (Section 2.a.(1) and Figure 3) which occupies a minimum of space inside the vessel.

(4) Table Saw Cradle

The roller cradle shown in Figure 10 was designed to accurately position and guide the sandwich shells while they were sawed to length. This fixture, which rotates the specimens (whether curved panel, cylinder, or cone) about their longitudinal axes, is essentially a steel table on which are mounted one fixed center row and four adjustable outer rows of rollers that can be moved in the plane of the table. The roller table is bolted to the frame of the table saw with its axis perpendicular to the abrasive blade of the saw. The specimens were rotated by hand as they were sawed.

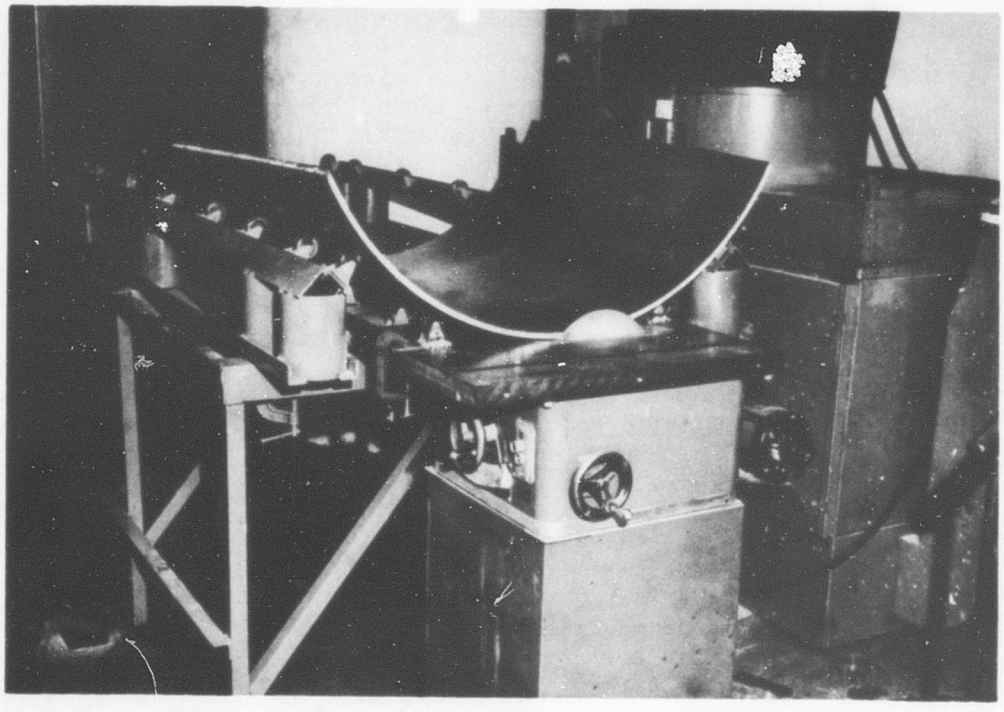

Figure 10. Roller Cradle Attachment to Table Saw.

b. Torsion-Bending Testing Machine

The testing machine, which was designed for the application of pure torsion, pure bending, and combined loadings is shown schematically in Figure 11 and by the photograph of Figure 12. In this machine, shells up to 6 feet in diameter and 12 feet in length may be mounted and subjected to combined moments of over, 3,000,000 inch-pounds. This machine is based on the same loading concepts used in the California Institute of Technology machine, which had a considerably smaller capacity (Reference 8). These moments are developed by jack loads applied to the ends of the 10-foot-long arms or frames, as shown in the illustrations. To apply a pure bending moment, the two moment arms are connected to a centrally located hydraulic jack by means of 5/8-inch-diameter steel cables (D in Figure 12). The entire loading system is reacted by the large I-beams of the main frame to minimize the floor loading.

Axial freedom is provided, to eliminate the possibility of any direct tensile or compressive forces, by resting one loading head of the machine on a set of six hardened-steel rollers. Rotational freedoms are achieved by connecting each specimen loading plate (composed of I-beams welded flange-to-flange) to a universal joint (A in Figure 11). Note that the specimens are connected to the loading plates by bonding their ends between concentric steel rings, which were in turn bolted directly to the loading plates.

Hydraulic pressure to operate the loading jacks was developed by an air-driven hydraulic pump located in the Sprague Engineering and Sales test panel labeled A in Figure 12. The specific jack loads at specimen failure were obtained from calibration curves relating gage pressure and jack load.

3. Specimen Design

The previous research performed by OURI, as outlined in the introduction, involved small, flat sandwich panels which were tested under nearly ideal conditions. However, this work showed that excellent structural sandwich of fiber glass-reinforced plastics can be fabricated and the strength predicted under given boundary conditions. Now these initial determinations are extended to assess the material's application to full-size structures. In order to keep the conclusions as clear as possible, these first extensions into complete structures were held to simple geometries and boundary conditions before evaluating the more complex aircraft-type component and filling in the details on optimum laminate selection; details of design of joints, attachments, etc.; and details of such effects as access openings in the structure.

Probably the most perplexing problem in designing an efficient shell structure is the prediction of buckling. Thus, the sandwich shells in the present study were sized for buckling in order to observe the structure's response to this static failure mode. Again it must be mentioned that the shells had to be large in size to offset the high

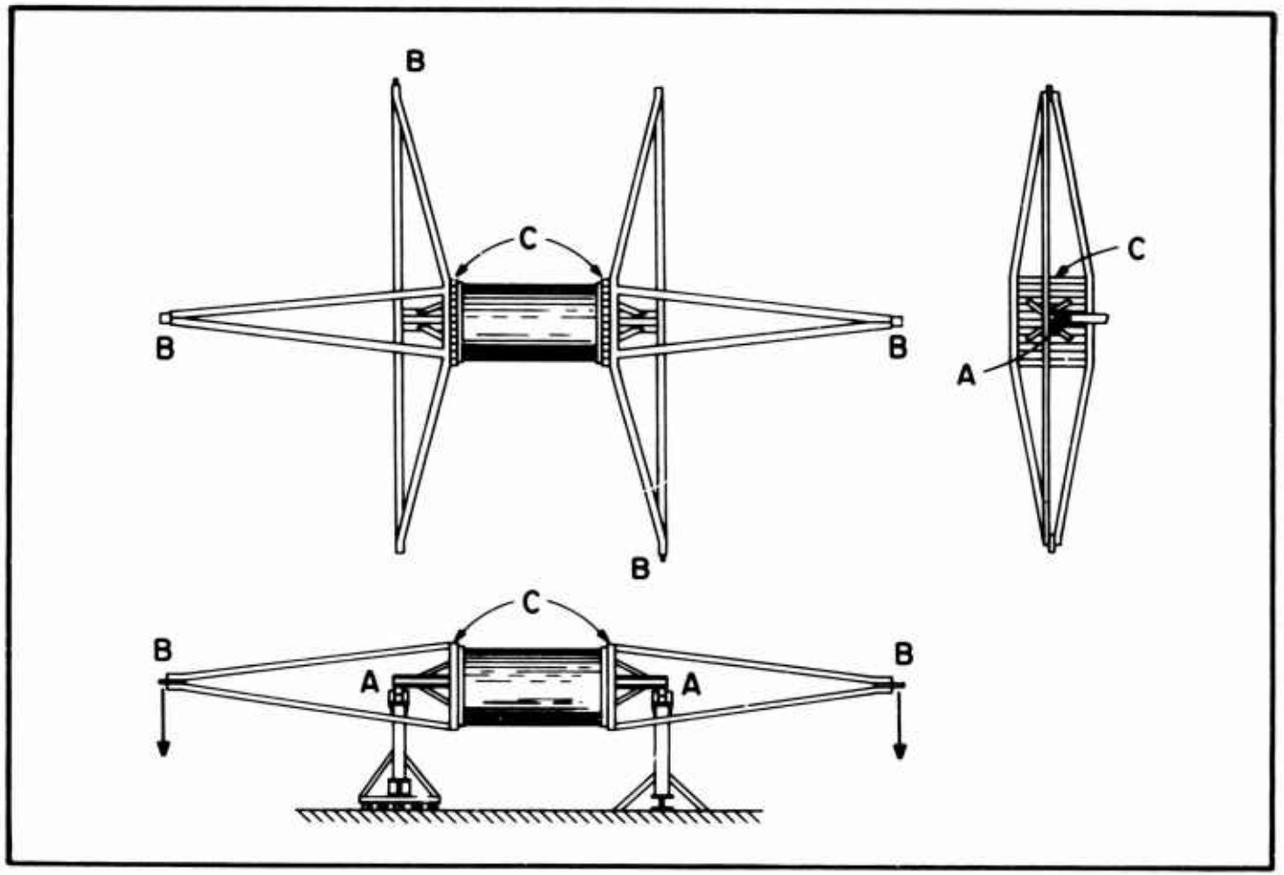

Figure 11. Schematic of 3,000,000 Inch-Pound Torsion-Bending Testing Machine: A, Universal Joints; B, Loading-Arm Cable Connections; C, Specimen Mounting Plates.

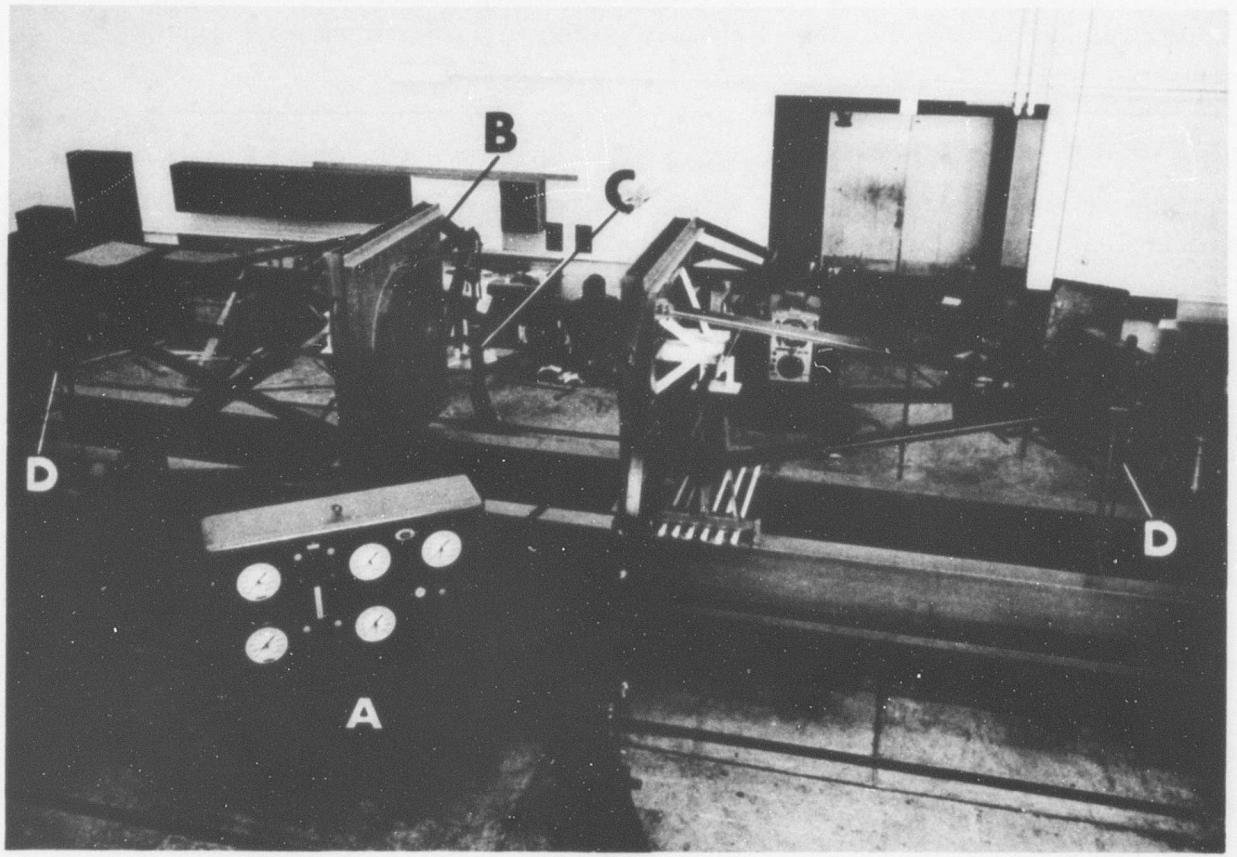

Figure 12. Overall View of Torsion-Bending Testing Machine: A, Hydraulic Control Panel; B, Specimen Mounting Rings; C, Torsion-Arm Loading Jack; D, Bending-Arm Loading Cable Connecting With Jack (Not Visible) Located in Center of Main Frame.

effective stiffness of the sandwich construction. It is interesting to note that the design of sandwich shells for buckling tests is almost the converse of the design of successful sandwich shell structures. The reason for this is that to design a successful sandwich shell structure, one wants to prevent structural buckling from occurring before the facing and core materials fail locally; while to assure a "successful" buckling test, one wants to be certain that structural buckling does occur before local failure of the component materials.

Since the data scatter in thin, monolithic shell buckling tests (Reference 39) is on the order of ±33 percent, the difference between the two experimental data bands, that for buckling and that for material failure, takes on unusual significance and must be made as great as possible to insure a successful buckling test. Thus, in sandwich structural design, though the buckling data scatter is expected to be much lower than in the monolithic case, the lower bound of buckling scatter band is most important; conversely, in setting up a buckling test program, the upper bound is of most importance (to ensure that buckling occurs before material failure).

a. Design Criteria

The basic criteria used in the design of the cylindrical and conical frustum shells are listed in the following paragraphs. For the sake of economy, the same sandwich construction was used for the curved panels, and the panels were sized to permit testing in the available university equipment.

(1) As discussed above, the overriding requirement is that there must be a reasonable assurance that the specimens buckle before the component materials fail locally. To quantify this requirement, it was decided that the ratio of the estimated upper bound of the buckling stress be no greater than or approach no closer than 75 percent of the stress required for local material failure.

(2) It goes without saying that the specimens must fit inside the autoclave to be used in their manufacture. The vessel which was especially designed for this program was made as large as possible under the existing funding and has available an inside diameter of 73 inches. Thus, to allow room for air circulation and cooling reinforcement, the maximum active diameter of the FRP shells was set at 58 inches. Although some 140-inch-long axial space is available in the autoclave, the shells need not be longer than about 1.5 times their average diameter; therefore, to also allow space for gripping the molds and tools, the active length of the shells was established at 72 inches.

(3) The thickness of the facing and of the core and as many of the other geometrical parameters as possible are desired to be as typical of possible Army aircraft applications as is

consistent with the other requirements.

(4) All specimens of a given geometrical class (cylinder or conical frustum) are to be identical for two reasons: (1) to reduce manufacturing cost and (2) to permit comparison of data for the different combinations of loading: pure bending moment, pure torque, and combined torque and bending moment.

(5) The conical frustum specimens should be as different geometrically from a cylinder as possible in order to provide the widest possible range of geometrical parameters.

b. Shell Assembly

Before continuing with the selection of the shell sizes, the method of shell assembly and the splicing of component materials must be considered. Accuracy in shell fabrication is very important in any program to verify a theoretical analysis by structural tests; thus in the case of the sandwich shell, the most desirable method of fabrication would be that which produced smooth, uniform-thickness facings well bonded to the core. As discovered during the early flat panel research at OURI (Reference 26, page 14), the waviness in the facings that precipitates early buckling can best be minimized by prelaminating the facings to the required curvature and then bonding them to the core in a separate operation. This method of sandwich assembly was applied to the structures at hand and is illustrated in Figure 13.

Although wide fiber glass fabric (50-inch width was finally chosen) could be used for the curved-panel facings in conjunction with only one core splice at most, the assembly of a closed structure such as the cylinder and the cone must be facilitated by some type of facing joint, as Figure 13 indicates. Since joint optimization was not a part of the present program, ease of fabrication was the primary consideration in choosing the single-shear butt joint shown in Figure 13, with sufficient lap provided to insure structural soundness. All the joints in the facings, except the final closing joint, were to be laminated in place with the facings, and it was originally reasoned that the core and outer facing could be made to conform to the increased facing thickness at these joints with no problem. This was later verified as shown in Figure 26 of Section 4.c.

For the core joint, the simple butt splice was considered adequate. The number of longitudinal joints in the core and in each of the facings was held to two and three, respectively, for the cylinder, and to three and four, respectively, for the cone. As stated in the beginning, those various decisions were made somewhat arbitrarily because of the lack of basic information; thus, a systematic study of the joining problem is badly needed to obtain optimums, where due consideration is given to such factors as specific strength, fabrication, and aerodynamic smoothness.

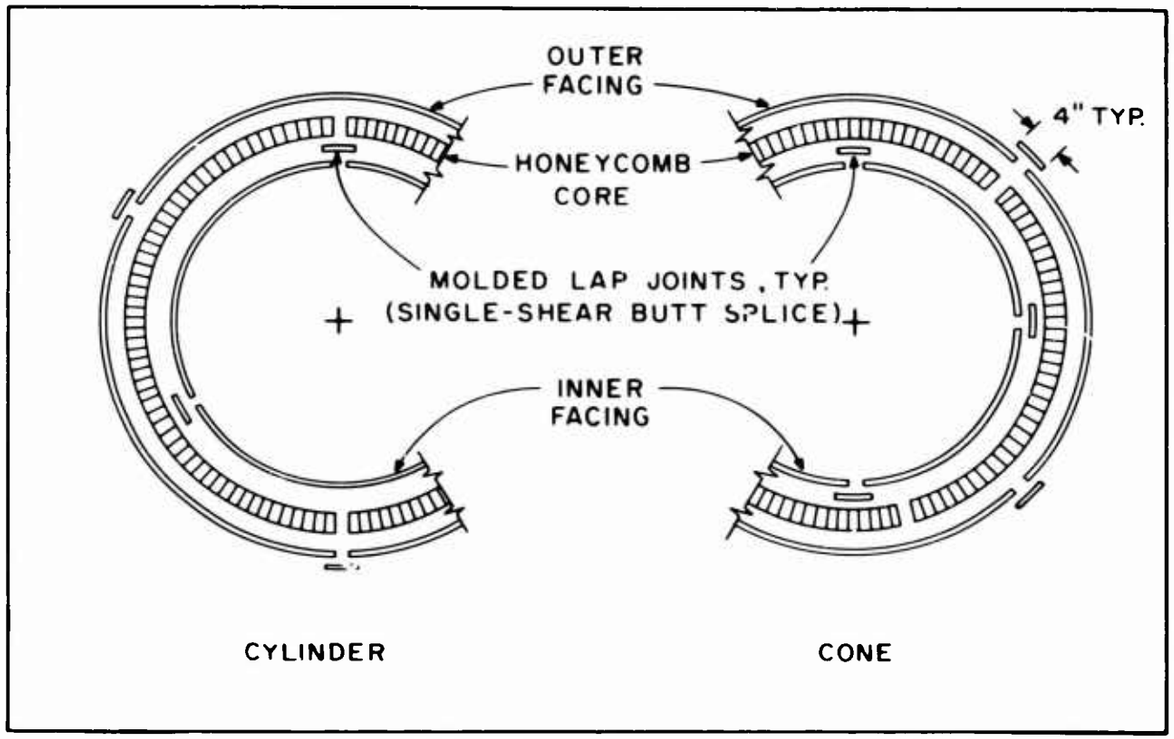

Figure 13. Exploded End Views Showing Shell Assembly.

Next, to continue with the design of the shells regarding size, it is first advisable to review suitable methods of analysis. The stable stress analysis will be discussed and then followed by discussions of the various buckling analyses leading to final design statements in Subsections f, g, and h.

c. Stable Stress Analysis

The maximum torsional shear stress τ induced by a pure torque T in a uniform-thickness sandwich shell of revolution is

$$\tau = T/4\pi R_1^2 t \qquad (1)$$

where
t is a single facing thickness, and
R_1 is the smallest radius of the neutral surface.*

The maximum normal bending stress σ_b induced by a pure bending moment M in a uniform-thickness sandwich shell of revolution is

$$\sigma_b = M/2\pi R_1^2 t. \qquad (2)$$

The values of T and M, respectively, required to produce local failure are readily obtained by setting τ in Equation (1) equal to the facing shear strength τ_f, and by setting σ_b in Equation (2) equal to the facing compressive strength σ_f. The values available at the beginning or design phase of the program were τ_f = 17,700 psi (Reference 34) and σ_b = 30,450 psi (average two-ply value, Table 14, Reference 26; see Section 4.b. for a more accurate value).

Recent research by Tsai (Reference 42) indicates that anisotropic generalizations of the distortion-energy theory of failure used for isotropic ductile materials are applicable to the failure of glass-fiber, epoxy-resin composite materials under biaxial loading. The ordinary (isotropic) distortion-energy theory predicts a ratio of shear strength to compressive strength τ_f/σ_f = 0.577. However, for the particular two-ply laminate used for the facing here, τ_f/σ_f = 17,700/30,450 = 0.582. Since these values differ by less than 1 percent, it is concluded that the ordinary distortion-energy theory describes adequately the failure behavior of our laminate.

For an element loaded in torsion combined with axial bending, application of Equations (1) and (2) and the Mohr-circle concept gives

*In shell theory, the neutral surface corresponds to the neutral axis in beam theory. In a symmetrical sandwich construction (equal facing thicknesses) such as used here, the neutral surface is located at the center of the core thickness.

the following equation for the principal stresses σ_1 and σ_2:

$$\sigma_{1,2} = (4\pi R_1^2 t)^{-1} (M \pm \sqrt{M^2 + T^2}). \quad (3)$$

For such a biaxial-stress system, the ordinary distortion-energy theory can be written as follows:

$$\sigma_1^2 - \sigma_1\sigma_2 + \sigma_2^2 = \sigma_f^2 \quad (4)$$

Equations (3) and (4) can be combined to give the following interaction equation:

$$(M/M_f)^2 + (T/T_f)^2 = 1 \quad (5)$$

where M_f and T_f are the bending moment and torque required to produce failure when acting singly. Equation (5) is plotted in Figures 14 and 15 for comparison with the buckling interaction equations that are discussed in the following paragraphs.

d. Buckling Analysis of Sandwich Cylinders

The simple circular cylinder is the only kind of sandwich shell of revolution for which buckling analyses are available for torque, bending moment, or combined torque and bending moment loadings. Of these, the most general and the most accurate torsional buckling anlaysis is that of March and Kuenzi (Reference 23), which is presented for reference in Appendix I along with the flow chart of the computer program written by the present authors.

Apparently, the only analyses available for buckling under pure bending moment are those of Wang and Sullivan (Reference 44) and Gellatly and Gallagher (Reference 12), in which it was predicted that buckling occurs in bending at a stress σ_b, given by Equation (2), equal to the critical buckling stress for axial compression. This prediction is the same as that of the classical (small-deflection) buckling of homogeneous circular cylindrical shells (References 6 and 38). However, in both the homogeneous case (Reference 41) and the sandwich case (Reference 13), the only test results available at the time that the present cylinders were designed indicated a critical buckling stress in bending equal to approximately 1.3 times the critical buckling stress for axial compression. Thus, at that time it appeared that the best estimate for buckling of sandwich cylinders in bending would be to use a critical buckling stress equal to 1.3 times the critical buckling stress under axial compression, estimated by means of the analysis of March and Kuenzi (Reference 22). This analysis is given in Appendix II along with the computer program developed.

The only buckling analysis known to us for sandwich cylindrical

shells subjected to a combination of torque and bending moment is the approximate analysis of Wang, Vaccaro, and DeSanto (Reference 45), who derived the following interaction equation:

$$(T/T_{cr})^2 + M/M_{cr} = 1 \qquad (6)$$

where T_{cr} is the buckling torque for pure torque loading and M_{cr} is the buckling torque for loading by a pure bending moment. Figure 14 shows the use made of Equation (6) in designing the cylinder specimens. A comparison of material failure and buckling failure cases under combined torsion and bending stresses can be made readily from this figure.

e. Extension to Buckling Analysis of Sandwich Cones

At the beginning of the research, no specific analysis of buckling of sandwich cones was available to us. However, Seide et al (Reference 39) had made extensive analyses and experiments on buckling of homogeneous conical frustum shells under various loadings and had arrived at some fairly simple approximate equations for design purposes. The approach used here is to adapt these to sandwich conical frustum shells. To show the preliminary design condition, the resulting interaction equation is plotted in Figure 15 in a form identical to the case of the cylinder (Reference 45).

For pure torque loading, Seide (References 37 and 39) used:

$$T_{cr}/\pi D = 1.70\pi^2 (\omega/L)^2 [(1-\nu^2) (L^2/\omega t)]^{3/4} \qquad (7)$$

where
- D is the flexural rigidity of shell,
- L is the axial length of shell,
- ν is Poisson's ratio, and
- ω is given by:

$$\omega = (R_1 \cos \alpha) (1 + \theta - \theta^{-1}) \qquad (8)$$

where
- α is the cone semivertex angle, and

$$\theta = [1/2 (1 + R_2/R_1)]^{1/2} \qquad (9)$$

where
- R_1, R_2 are the smallest and largest radii of the cone, respectively.

It is noted that Equation (7) is identical in form to that for a cylindrical shell of moderate length, since $\alpha = 0$ and $R_1 = R_2 = R_c$, where R_c is the cylinder radius. This fact will be used subsequently

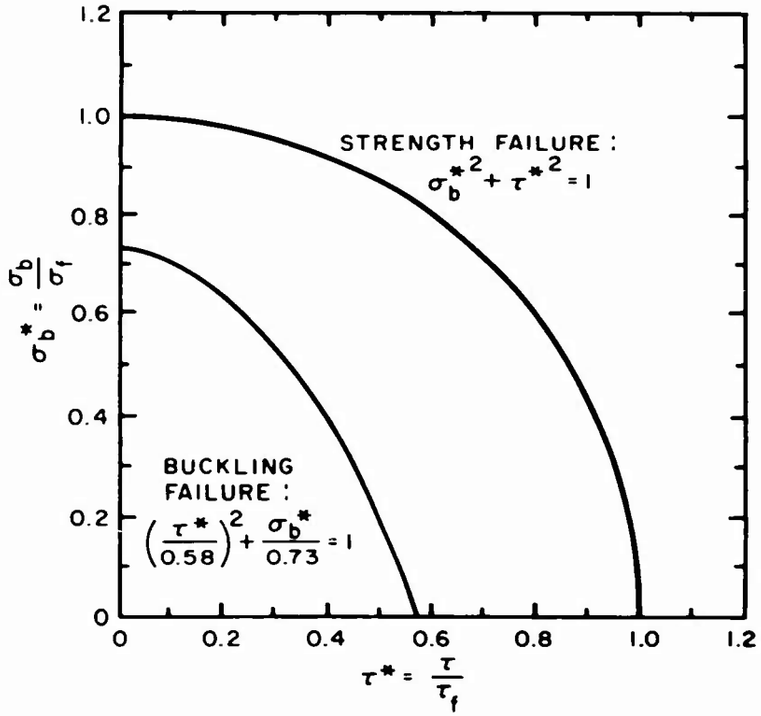

Figure 14. Preliminary Design Interaction Curves for Sandwich Cylinders.

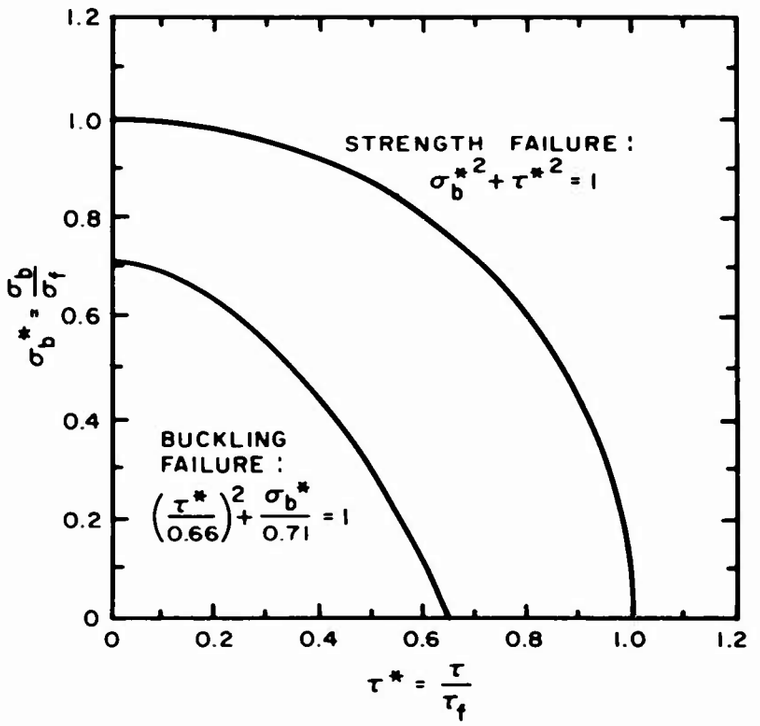

Figure 15. Preliminary Design Interaction Curves for Sandwich Cones.

to adapt Equation (7) to the sandwich case. Equation (7) has been verified experimentally (Reference 39) in a limited number of tests on homogeneous cones. In 18 tests where α took on values of 60 degrees, 30 degrees, and zero degrees (cylinders), ratios of experimental to theoretical values ranged from 0.68 to 1.22.

For cones loaded by pure bending moment, Seide et al (Reference 39) used:

$$M_{cr} = (M_{cr})_c \cos^2\alpha \tag{10}$$

where $(M_{cr})_c$ is the critical bending moment for buckling of a cylinder having a radius R_c equal to the smallest cone radius R_1.

To apply the preceding equations, which are for homogeneous isotropic shells, to fiber glass-facing, honeycomb-core sandwich shells (which have orthotropic facings and shear-flexible orthotropic cores), the principles of dimensional analysis will be used. The elastic properties of the sandwich are defined as follows: E_x, E_y = facing elastic moduli in the meridional and circumferential directions, respectively; G_{xz}, G_{yz} = transverse shear moduli of the core; ν_{xy}, ν_{yx} = facing Poisson's ratios. It is obvious that these factors can affect the results in the following dimensionless ways only:*

$$f(E_y/E_x),\ g(G_{yz}/G_{xz}),\ \text{and}\ h(G_{xz}/E_x), \tag{11}$$

where f,g, and h are the unknown functions of the dimensionless quantities appearing inside the parentheses.

Since we are holding all of the core and facing mechanical and dimensional parameters the same for all shell geometrical configurations, here we do not need to know the nature of the functions f, g, and h at all. This is because we are interested only in ratios, the ratio of the critical stress of the cone to that of the cylinder, and not absolute quantities; hence, the functions cancel out.

f. Specimen Design: Cylinder

In view of the many conflicting requirements listed previously, many design compromises had to be made. Preliminary calculations, using the analyses of Appendixes I and II (the numerical values are tabulated in the appendixes), indicated that in order to meet requirement 1, Section 3.a., it is necessary to use two-ply facings, each

*The difference between the isotropic quantity ν^2 and the orthotropic quantity $\nu_{xy}\,\nu_{yx}$ is assumed to be negligible. This is a very reasonable assumption for the facing laminate used in this program.

approximately 0.02 inch thick (two-ply rather than three-ply which is more typical of good design), and a core with a thickness of 0.30 inch and a hexagonal cell size of 1/4 inch in conjunction with a 1-mil-thick foil.

Using the buckling analysis of Reference 22 (see Appendix II) for a sandwich cylinder in axial compression, and a factor of 1.3 to convert critical buckling stress from axial compression to bending stress, it was found that for a core thickness of 0.3 inch, the smallest even integer cylinder radius meeting requirement 1, Section 3.a., under pure bending-moment loading is 22 inches. This corresponds to a diameter of 44 inches which is less than the permissible value of 58 inches of requirement 2 and thus is satisfactory. Checking requirement 1, we have $M_{cr}/M_f = 1.3(17,200/30,450) = 0.73$, which is less than 0.75 and thus is ample.

Using the buckling analysis of Reference 23 for a sandwich cylinder in torsion (see Appendix I) and the already determined dimensions of L = 72 inches and R_c = 22 inches, the ratio $T_{cr}/T_f = 10,300/17,700 = 0.58$ is also less than 0.75 and thus is ample.

g. Specimen Design: Cone

In view of requirement 5, tempered by requirement 3, a cone semivertex angle of 5 degrees was selected as a compromise. Then in view of requirement 1, the largest diameter ($2R_2$) of the conical frustum was selected to be as large as possible, namely, 58 inches. Combining these dimensions with the frustum length of 72 inches gives a small-end radius of 22.7 inches. Using Equations (7) and (9) to convert from cylinders to cones gives $\omega/R_1 = 1.126$; thus, the following values check out as satisfactory under requirement 1:
$T_{cr}/T_f = (1.126)^2 (1.126 \times 22.7/22) - 3/4 (0.58) = 0.66$;
$M_{cr}/M_f = 1.3 (16,650) (\cos 5°)^2/30,450 = 0.71$.

Table I, on the next page, summarizes the complete-shell designs. It should be mentioned again that the various preliminary buckling stresses calculated in order to arrive at the final designs are included in the appendixes with their respective analyses.

h. Selection of Combined Torsion-Bending Loading Condition

Again, Figures 14 and 15 show the general buckling and local-failure interaction curves for the cylindrical and conical-frustum shells, respectively. As can be seen, the nature of the general-buckling interaction curves is such that a small amount of torque has little effect on bending moment required for buckling; yet a small amount of bending moment has a somewhat larger effect on the torque required for buckling. These facts favor the use of a relatively small amount of bending moment in the combined loading test to get a large exaggeration from the individual-loading test results.

Consideration of the fact that the experimental determination of combined-loading buckling data is merely to fill in a third test point between the two individual-loading test points, favors a combined-loading M/T ratio of one.

Consideration of combined loadings on the aft portion of an aircraft fuselage indicates that M/T ratios of 15 to 30 are typical.

In view of all the considerations discussed above, an M/T ratio of one was selected. This means that throughout the combined-loading tests, the bending moment and torque were both increased together and maintained equal to each other. Since the area moments of inertia for torsion and bending are in the ratio of 2 to 1, the resulting stresses will be in the ratio of 1 to 2.

TABLE I
SUMMARY DESIGN OF SANDWICH SHELLS

A. Sandwich Constituents

Constituent	Description	Thickness	Orientation*
Facing	828-Z Epoxy, 181-E Volan A Fiber glass	Two-ply	=W
Core	5052 Aluminum, 1-mil Nonperforated Foil, 1/4-inch Hexagonal Cell	0.3 inch**	=R
Adhesive	AF-110B Film-Supported Epoxy	0.015 inch	-

B. Shell Geometry

Shell	Radius, R_1 or R_c (in.)	Radius, R_2 (in.)	Length, L(in.)**	Angle, α(°)
Cylinder	22	-	72	0
Cone	21.7	58	72	5

*The symbols =W and =R indicate that the warp and ribbon directions of the facings and cores, respectively, are aligned with the shell axis.
**See Table V for curved panel deviations.

4. Experimental Procedure

a. Tool Construction and Evaluation

The tooling for these shells of revolution consisted of (1) main plaster molds, (2) concave plaster molds, and (3) FRP working tools or bonding fixtures, as indicated in the schematic of Figure 16 on the next page. The first step in constructing the main plaster molds for each shell configuration was the assembly of a welded steel framework to support the thin shells of plaster, as illustrated in Figures 1 and 2 on pages 3 and 4. To contain the plaster on the frames, a 1/4-inch-mesh hardware cloth was wired to the rings which were welded to the main trusses of the shaft. Next, the completed framework was placed in the plaster-sweeping device which was designed for vertical operation to eliminate the shaft deflection in bending that would occur in horizontal operation. The molds were then constructed by splash casting about 2 inches of gypsum cement on the framework (Figure 1).

The thickness of the plaster was brought to within about 1/4 inch of the desired surface and scraped with a saw-toothed screed attached to the sweep (Figure 1), in order to insure a good mechanical bond to the finish coat. A 30-minute-set cement (Ultracal 30) was found to be suitable for this foundation layer. After the castings had set sufficiently to obtain wet strength, the final layer was splashed on, and the precise contour of the mold was established by screeding with an accurately ground straightedge attached to the sweep. A 60-minute-set-gypsum cement (Ultracal 60) was found to be the most suitable for this finish layer, as water loss to the dryer foundation layer seemed to reduce the period of plasticity that is so important to the screeding of such a large surface. It should be mentioned that one of the most important factors in producing a glassy surface on the plaster and preventing the formation of grooves was the cleaning of the screed at regular intervals.

After the castings had dried for approximately 24 hours in the screeding device, they were lowered to the horizontal position and into the special dolly system designed to support the molds during the subsequent operations. The lowering procedure is shown in Figure 2. After the plaster surface was inspected and minor repairs were made, the mold was dried in hot air and then sealed to prevent water absorption from the atmosphere. It was found that drying could best be accomplished at 120 degrees Fahrenheit for at least 24 hours. Figure 3 shows a mold being introduced into the autoclave for drying. The molds were sealed by spraying on a compound compatible with the resin to be applied to the surface (in this case, vinyl Epofilm 990A). It should be noted that, as experience was gained with these plasters, autoclave drying was eliminated in favor of air drying since these molds were used only once (for making the concave castings).

After the final screeding, the main plasters possessed the contours

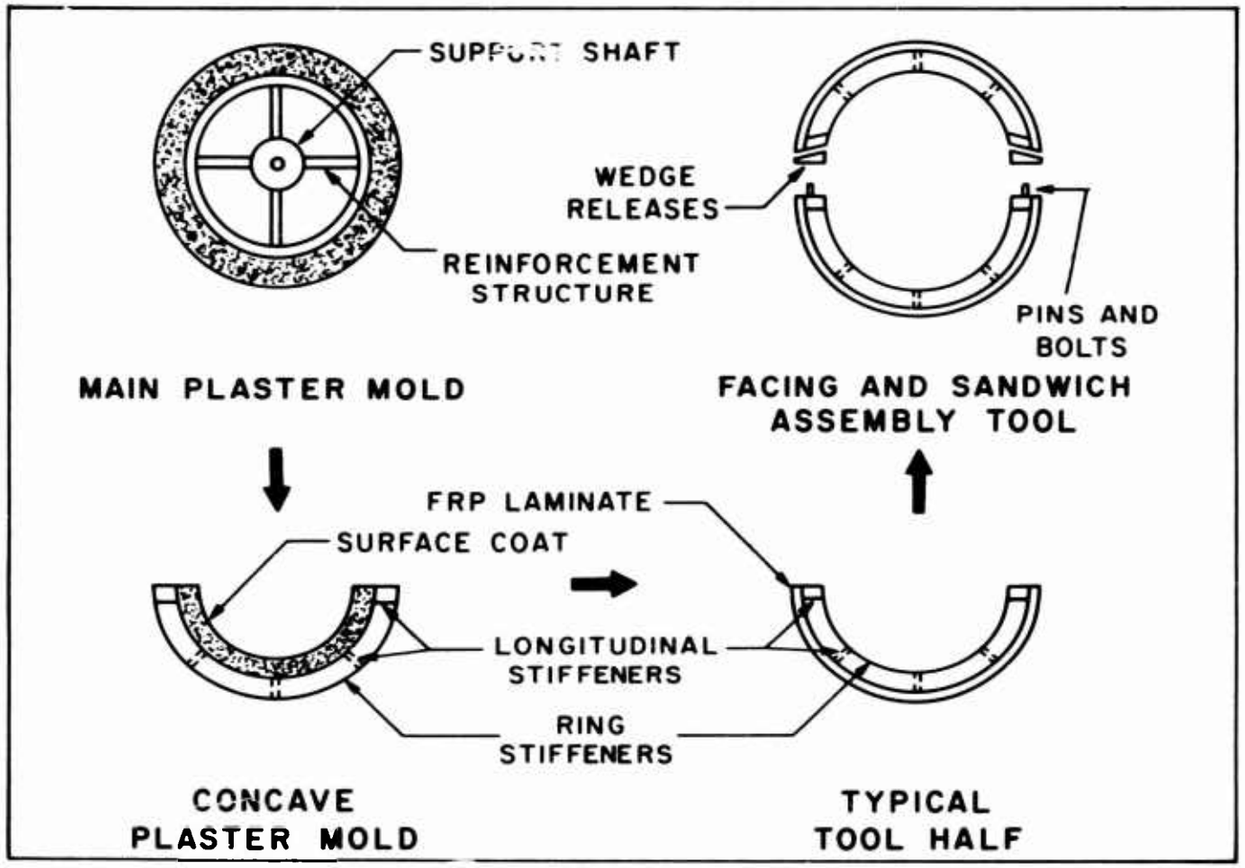

Figure 16. Schematic of Tooling Components for Sandwich Shells. The cylinder assembly tool is shown rather than the cone in order to indicate its special collapse feature.

to which the specimen facings were molded. As the plasters are damaged by high temperatures and repeated use, it is normally standard practice to build working tools from the plaster molds. In most cases it would be desirable to construct matched tools for the inside and outside facings of the sandwich specimens; however, in the present application, the thin facings are usually flexible, which permits the use of one common tool, as will be discussed in the section on fabrication. A male or convex tool was believed to be the most practical on which to lay up and cure the specimens; hence, a concave plaster mold on which to fabricate the tools had to be made next.

The concave plaster molds were cast off the main plasters by spraying a parting agent (Teflon Release H) onto the sealed surface of the master mold, and applying a surface coat by hand to about 1/8-inch thickness. When the surface coat had become tacky, a plywood framework composed of rings and longerons and containing a grid of steel reinforcing rod was set in place to contain the plaster. The plaster was then splashed directly onto the tacky surface coat. For the cylindrical plaster, wads of hemp saturated with plaster were pushed into the surface coat to obtain a good bond to the plaster. However, it was found that the hemp caused formation of air voids and poor plaster saturation. Thus, the use of hemp was eliminated for the conical plaster. These intermediate plasters were built up to about 3 inches in thickness and sealed after air drying as before (Figure 17).

For economy of time and money, the working tools were made from room-temperature-curing reinforced plastics by laying up 3/8-inch-thick laminates directly in the concave plasters and subsequently reinforcing them with rings and longerons similar to the so-called egg-crate backup structure often used in industry. The laminates for the tools were fabricated using a high-temperature surface coat (31C and 9216 hardener), one layer each of 120- and 181-style fiber glass fabric, and approximately 30 layers of 10-ounce fiber glass tooling fabric saturated with high-temperature epoxy tooling resin (31A and 9234 7-hour hardener). The surface coat was used primarily to prevent surface air entrainment, and thus surface flaws, during the hand layup of this laminate. The buildup was usually accomplished in three separate layups which were squeegeed and cured under vacuum. After curing for 24 hours at room conditions, each new layer was rough sanded to insure bonding to the next layup.

A number of the tooling materials were new to the project fabricators, and thus difficulties were encountered from time to time. For example, the first of the tool laminates was lost because of parting-agent failure, necessitating extensive repair of the cylindrical concave plaster mold. In this case, a repeat occurrence was prevented by spraying an intermediate film on the plasters and by

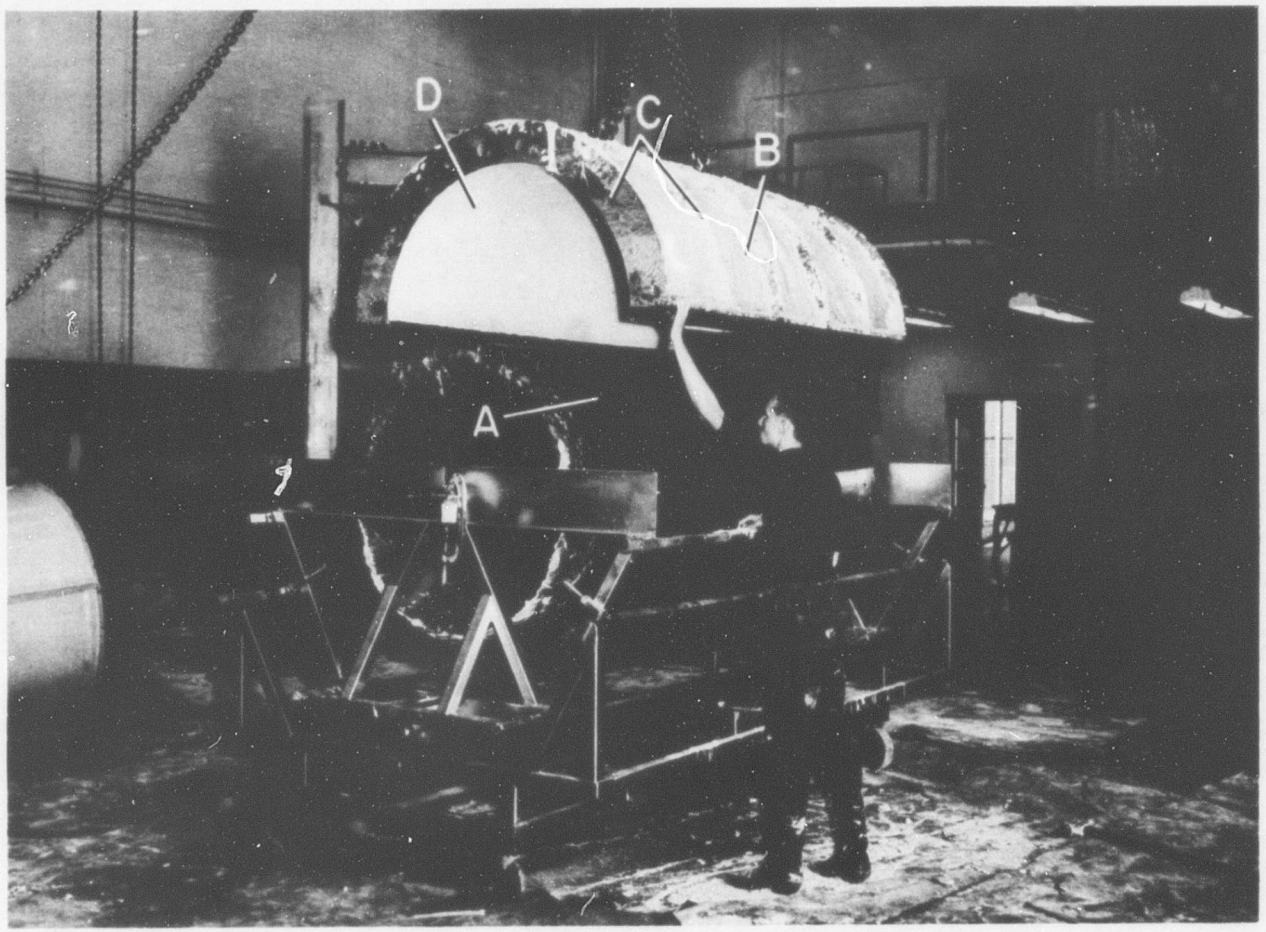

Figure 17. Parting of Concave and Main Plaster Molds: A, Master Plaster Mold Sealed With Vinyl Spray-On Film; B, Concave Plaster Mold; C, Reinforcing Rings; D, Surface Coat Compatible With Wet Plaster.

spraying the Teflon parting agent in an extremely wet condition.

The reinforcing rings and longerons were fabricated by wrapping 3/4-inch-thick plywood forms with resin-saturated tooling fabric to about the 3/8-inch thickness. After the laminate had been sanded, the backup members were bonded in place using a glass-powder tooling-resin putty and subsequently reinforced with resin-fabric fillets.

The two halves of each tool were then carefully faired together by sanding where necessary and fastened by (1) bolts through the edge longerons and by (2) alignment pins through the wedges and longerons in the case of the cylinder tool and by bonding at these longeron faces in the case of the cone. High-temperature zinc chromate tape (sealant number 200) compressed in a groove oriented lengthwise on each side of the wedges was used to obtain the vacuum seal between the halves of the cylinder tool. Since it was not necessary to dismantle the cone tool for specimen removal and since its diameter was rather large, making it more vulnerable to heat distortion, an orthogonal system of cross bracing was added at each ring stiffener (see B of Figure 21).

As the final step in the construction of the tools, they were heat treated to the maximum anticipated specimen bonding temperature (350 degrees Fahrenheit) before being placed into use. Some surface cracking occurred on the cylinder tool as a result of heating, since it was the first tool made and probably contained air voids. However, these flaws were easily repaired. Warping of the longerons at the wedge locations was also noted, and these places had to be sanded down for good fitting of the tool halves.

To provide a vacuum under the film blankets that covered each layup (and thus a resultant pressure under autoclave conditions), lines were connected directly into the tooling laminate in the beginning of the program. Considerable difficulty in preventing vacuum leaks was experienced with this approach due to differential expansion of materials. This was the case even when the connection was made with a room-temperature-vulcanizing (RTV) silicone rubber adhesive. Thus, these holes were plugged and the vacuum lines were then introduced through the zinc chromate blanket seal on each individual specimen layup. Inside the sealed area, the vacuum lines (1/4-inch copper tubing) were bent so as to encircle each end of the tools. They were drilled with closely spaced holes to provide uniform venting and were covered with felt to prevent blanket puncture.

b. Materials Fabrication and Evaluation

Since the shell specimens were fabricated from fiber glass-reinforced plastic (FRP) laminate facings separately bonded to an aluminum honeycomb core, it is important to discuss the properties and the processing of the constituent materials. A preliminary discussion was presented in Reference 4. Two advances in materials processing of influence here are (1) development of a multilayer impregnating

machine to minimize air voids and increase facing uniformity and (2) determination of effects of process variables on properties.

The prepreg machine (Figure 4) is a modification of a previous machine, reported in References 9 and 31, to handle wider fabric (up to 54 inches). The machine produced two-ply prepreg of 828-Z epoxy and 181-style fiber glass fabric in lengths over 700 inches while maintaining previously achieved uniformity ($\pm$1 percent resin content).

Table II lists properties of the shell-facing laminate. The sampling from the autoclave cured laminates, although not large, was sufficient to establish the properties for the various shell analyses. Test coupons were taken from flat laminates fabricated identically to the curved-facing laminates discussed in Section 4.c.(1). Cure was accomplished at 160 degrees Fahrenheit laminate temperature for 100 minutes at a total pressure of 70 psi (10 psi vacuum plus 60 psi autoclave) with a zero-pressure precure of 23 minutes. Postcure usually took place during the bonding cycle, but a small oven was used for these special laminates. This cure closely approximates one in which optimum surface finish and laminate uniformity were obtained previously in an electrically heated press (Reference 31).

Test specimens and procedures were similar to previous ones (References 25, 26, and 31). Figure 18 shows a typical compressive stress-strain curve for parallel-to-warp loading. Stress-strain curves for perpendicular-to-warp loading were similar, but the 45-degree-to-warp ones were nonlinear.

Other investigators (Reference 43) have noted that a coupon test at any direction but the material-symmetry axes (fiber directions) is merely a resin shear test only, since fiber edges are cut and not loaded as they would be in a continuous structure. This was revealed at completion of the present program by plotting strain data from the 45-degree arm of a strain rosette on a shell tested in torsion (Figure 47, Appendix III). At higher strains, tangent values of E_{45} calculated from the measured shear modulus (see Appendix III) were much higher than coupon-obtained values but were somewhat below the values used by Norris (Reference 32) for 181-style fiber glass cloth/epoxy.

Of all the major process variables investigated, resin content is the most usuable parameter for relating laminate fabrication to final strength properties. Numerous test data showing the effect of resin content on strength properties were determined previously for the three-ply press-made laminate (References 27 and 31). Figure 19 shows the modulus data along with the limited test data for the newest two-ply laminate; compressive strength data are shown in Figure 20. In comparing the two- and three-ply laminate data, the usual thickness effect of strength degradation is evident. The modulus data suggest the same trends in relation to resin content and thus all the new two-ply curves were drawn parallel to their

TABLE II
AUTOCLAVE CURED
FLAT LAMINATE STRENGTH PROPERTIES

Property	Laminate A*			Laminate B_1*			Laminate B_2*		
	=	⊥	45°	=	⊥	45°	=	⊥	45°
Tensile Modulus (psi x 10^{-6})	2.25	2.11	0.31	2.20	1.86	0.31	2.23	1.98	0.26
Tensile Strength (psi x 10^{-3})	39.0	40.1	23.2	40.5	35.8	23.4	43.9	39.7	21.8
Specimen Resin Content (% By Weight)	32.7**	30.8**	39.2**	31.1**	32.5**	36.9	31.4	32.7	38.4
Number of Specimens	9	6	7	9	7	8	10	10	10
Average Specimen Resin Content (%)		-			-			34.2	
Compressive Modulus (psi x 10^{-6})	3.16	3.52	-	3.29	3.61	0.475	3.67	3.01	0.431
Compressive Strength (psi x 10^{-3})	-	-	-	32.0	27.3	-	23.8	32.4	-
Specimen Resin Content (%)	36.1	29.5	-	34.5	31.2	36.6	30.1	36.1	38.1
Number of Specimens	5	7	9	7	6	8	8	9	9
Average Specimen Resin Content (%)		35.1			34.9			34.3	
Prepreg Resin Content (%)		50.8			49.0			49.5	
Average Laminate Resin Content (%)		35.1				34.6***			
Average Laminate Thickness (in.)		0.022				0.021***			

*181 epoxy (828-Z), 2-ply laminates cured at 160° F and 70 psi for 100 minutes and postcured 2 hours at 300° F. Loads oriented parallel (=), perpendicular (⊥) and at 45° to fabric warp direction. Modulus recorded for terminal straight-line portion of stress-strain curves for = and ⊥ cases and for terminal slope (approximately a straight line) for 45° case. Tensile specimen notches 10 and 7 mils for (=, ⊥) and 45°, respectively.

**Values estimated by using resin content from compressive specimens in conjunction with same within-laminate variation of resin content as found in laminate B_2.

***Laminates B_1 and B_2 included in averages as they are identical, within fabrication tolerances.

respective three-ply counterparts; however, the thickness effect is not as pronounced as for strength (see Figure 20).

Being able to make these comparisons vividly points out the great value of continuing with one set of basic materials throughout a program which encompasses material property studies and full-scale structural evaluations. As the last step in obtaining the material properties, these newly generated two-ply data plots together with the average resin contents for the specimen facings were used to obtain the specific properties for shell analysis, and these properties are recorded in Table III along with core shear data.

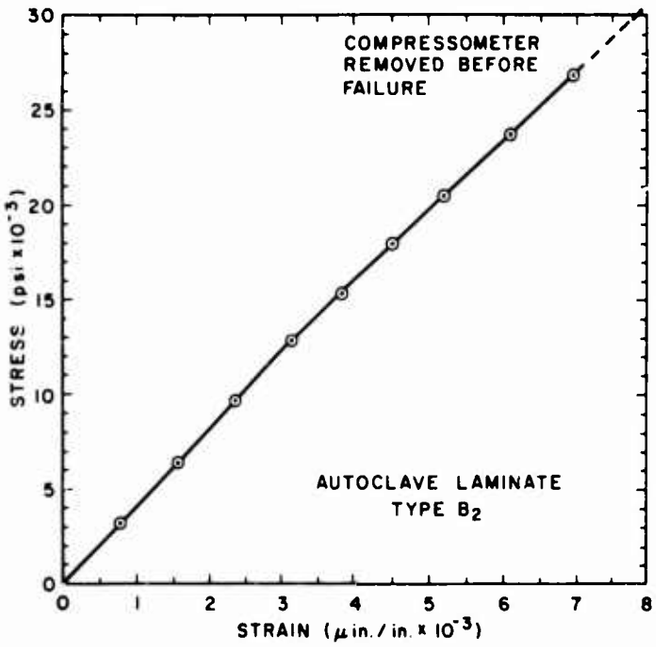

Figure 18. Typical Compressive Stress-Strain Curve for Parallel-to-Warp Loading.

TABLE III
SHELL CONSTITUENT PROPERTIES

Description	Type	Facing** Resin Content* (%)	Facing** Thickness* (in.)	Modulii (psi x 10^{-6})*** ∥ Initial	∥ Secondary	⊥ Initial	⊥ Secondary	G	45° 8,560 psi	45° Secondary
Two-ply, 181-Style 828-Z Epoxy Facing	A	35.1	0.022	4.14	3.23	3.96		-	2.03	0.478
	B	34.6	0.021	4.19	3.28	4.0	3.14		2.08	0.482
5052 Nonperforated Aluminum Honeycomb Core, 1/4-in. Cell, 1-mil Foil	C	-	-	0.0320		0.0183			-	-
	D	-	-	0.0306		0.0179			-	-

*Average values obtained from each of the laminate types tested. Poisson's ratio ν (=0.13) obtained from Reference 32.

**Initial and secondary tangent compressive moduli of the facing laminates were obtained by plotting parallel resin content-property curves using values from the original stress-strain curves, such as shown in Figure 19 for the secondary modulii.

***Symbols ∥, ⊥, and 45° indicate orientation of facing fabric warp or core ribbon to shell axis as follows: parallel, perpendicular, and 45 degrees, respectively. All laminates were parallel plied. Core C = 0.3 in. thick, and core D = 0.4 in. thick.

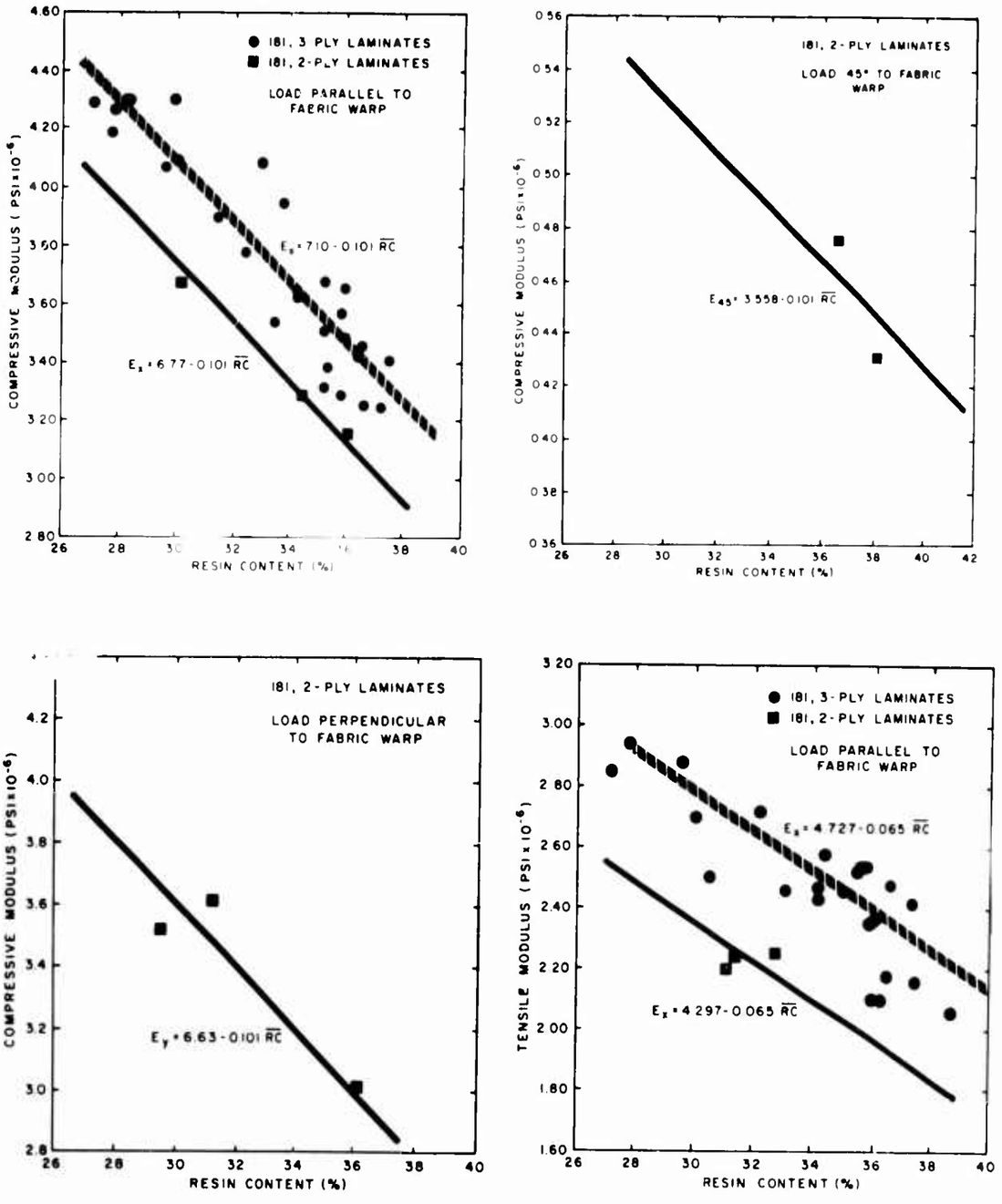

Figure 19. Effect of Resin Content on Laminate Secondary Modulus. The individual graphs are labeled as to type and orientation of load. See page 30 for a discussion on the inaccuracy of the 45-degree loading results.

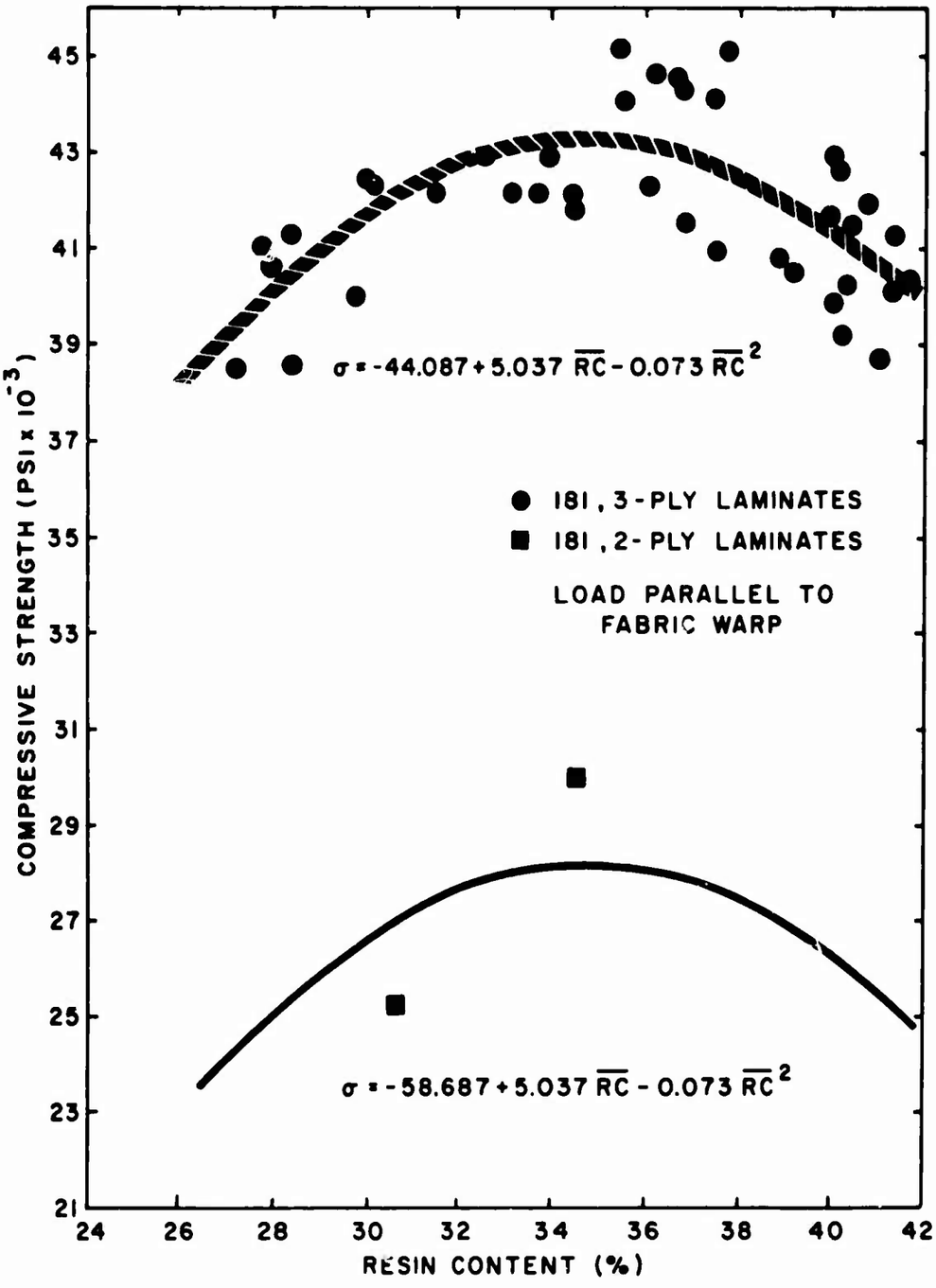

Figure 20. Effect of Resin Content on Laminate Compressive Strength Parallel to Fabric Warp.

c. Specimen Fabrication and Evaluation

The fabrication of the shells on the working tools was accomplished in three phases which consisted of facing lamination, core rolling, and sandwich bonding. There are many unique features to the layup procedure developed for these shells; hence, the facing lamination phase, especially, will be discussed in detail. (A preliminary discussion is given in Reference 4.) First, it should be mentioned again that both the inside and the outside facings were cured on the same tool. This technique was possible because the facings were thin and very flexible so that an inside facing could be warped into an outside facing position with no adverse effects.

(1) Facing Lamination

A dry layer of 181-style fiber glass fabric was used for a bleeder to improve resin content uniformity and to insure that uniform venting occurred over the entire facing surface during vacuum and autoclave pressure application. One-half-mil-thick Teflon FEP film perforated with 1/16-inch-diameter holes spaced about 1/2 inch apart was used as the parting agent between the bleeder and the prepreg. The bleeder fabric was stretched against the tool or over the prepreg to obtain an outside or inside facing, respectively. This unique procedure resulted in a smooth outside surface for the outside facing and a smooth inside surface for the inside facing.

Another innovation was prepreg curing with one cover film (see Figure 4) left on. The film was the same 3-mil-thick heat-stabilized nylon (Kapran 80) used for the vacuum-pressure blankets. This procedure was used because the film provided support for handling the prepreg and thus prevented misalignment of the fibers and deviation (from the desired contour) which produces wrinkles on the cured facings.

The procedure for layup of the facings for the complete shells and curved panels (partial cylinders) consisted of removing precut pieces of prepreg from cold storage and laying them out on a flat table. For the cylinders, three such pieces (four for the cones) were butted together and connected by 4-inch-wide single-shear lap splices of prepreg, as shown in A of Figure 21. The perforated Teflon film was next placed on the sticky prepreg, which had usually B-staged about 7 hours at this point. For an inside facing, the prepreg was then wrapped onto the tool with the nylon cover film toward the tool, using the 181-style fabric bleeder wrapped under tension to press the prepreg tightly against the tool. In the case of an outside facing, the bleeder had already been spiral wrapped on the tool; hence, the prepreg was wound over the bleeder with the perforated Teflon side against the tool, using a very closely woven fabric (to avoid an imprint) to apply the hold-down force and provide venting.

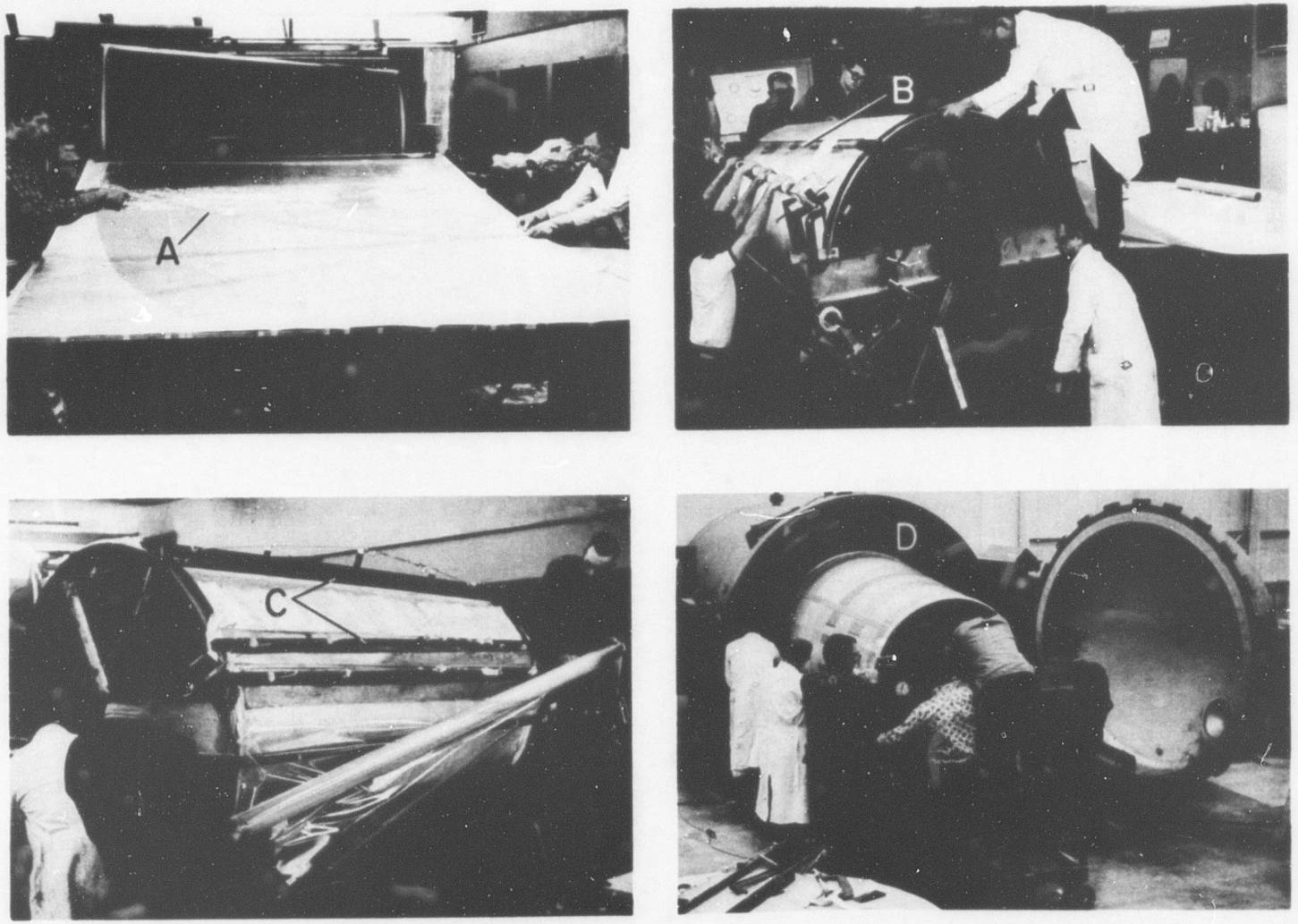

Figure 21. Photos Showing Layup of Facings: A, Splicing of Prepreg on the Flat; B, Pressure Wrapping Prepreg Onto Tool; C, Clamping for Last Joint; D, Loading of Layup Into Autoclave.

The layup of the facings for the cones was slightly more complicated than for the cylinders, in that the wrapping in each case was accomplished by rotating the tools on their axes with a hand-cranked chain drive, as shown in B of Figure 21. As can be seen, the bleeder fabrics for the cones could not be tensioned directly in a simple manner because of the taper of the cone; therefore, the layups were pressed against the tool by tension wrapping narrow strips of film over the layup as it was made. These 9-inch-wide strips would stretch sufficiently to stay uniformly tight, even though the tool radius varied across their widths.

A longitudinal bar clamp with a sponge-rubber-padded face held the elements (bleeder, prepreg, tension wrap material, and vacuum blanket) at one of their ends during the wrapping process. Another such clamp was then used to hold the tension while the closing prepreg joint was made (same as A in Figure 21) and the vacuum blanket sealed. It was often found beneficial to install the blanket in a separate step; hence, a third clamp was used inside each of the former ones to prevent loss of tension during the operation (C in Figure 21). The outside facing layup was closed simply by overlapping the prepreg and preventing the laminate from bonding during cure. The overlap provided the extra length needed for the circumference of the outside facing. A 10-psi vacuum was applied, the clamps were removed, and the layups were permitted to stay under the vacuum at room temperature for completion of a 10-hour B-stage time. It should be mentioned that the procedure for layup of the curved panels was similar but much simpler than that just described for the complete shells.

Each layup was rolled into the preheated autoclave (Reference 29), suspended in the same dolly as used for the layup (D in Figure 21). The cure was conducted as described in Section 4. b. A typical temperature cycle for these large components is shown in Figure 22 for reference. After cooling and removal from the autoclave, the facing laminates were stripped of bleeder and films, and the bonding surface was lightly sanded. The outside-type facing was removed from the tool and stored on end, with care being taken to maintain its shape. The inside-type facing was left on the tool for the buildup of the sandwich.

Evaluations of the facing layup showed, more than anything, that the facing prepreg assemblies were rather difficult to handle and to apply to the tools because of (1) their large surface area (over 12,000 square inches), (2) their thinness (only two-ply), and (3) their susceptibility to local stretching or bulging which invariably resulted in wrinkles in the cured facings. The main trouble spots encountered in working with the prepregs were (1) the coiling and uncoiling of the precut slabs, which were required for cold storage, (2) maintaining

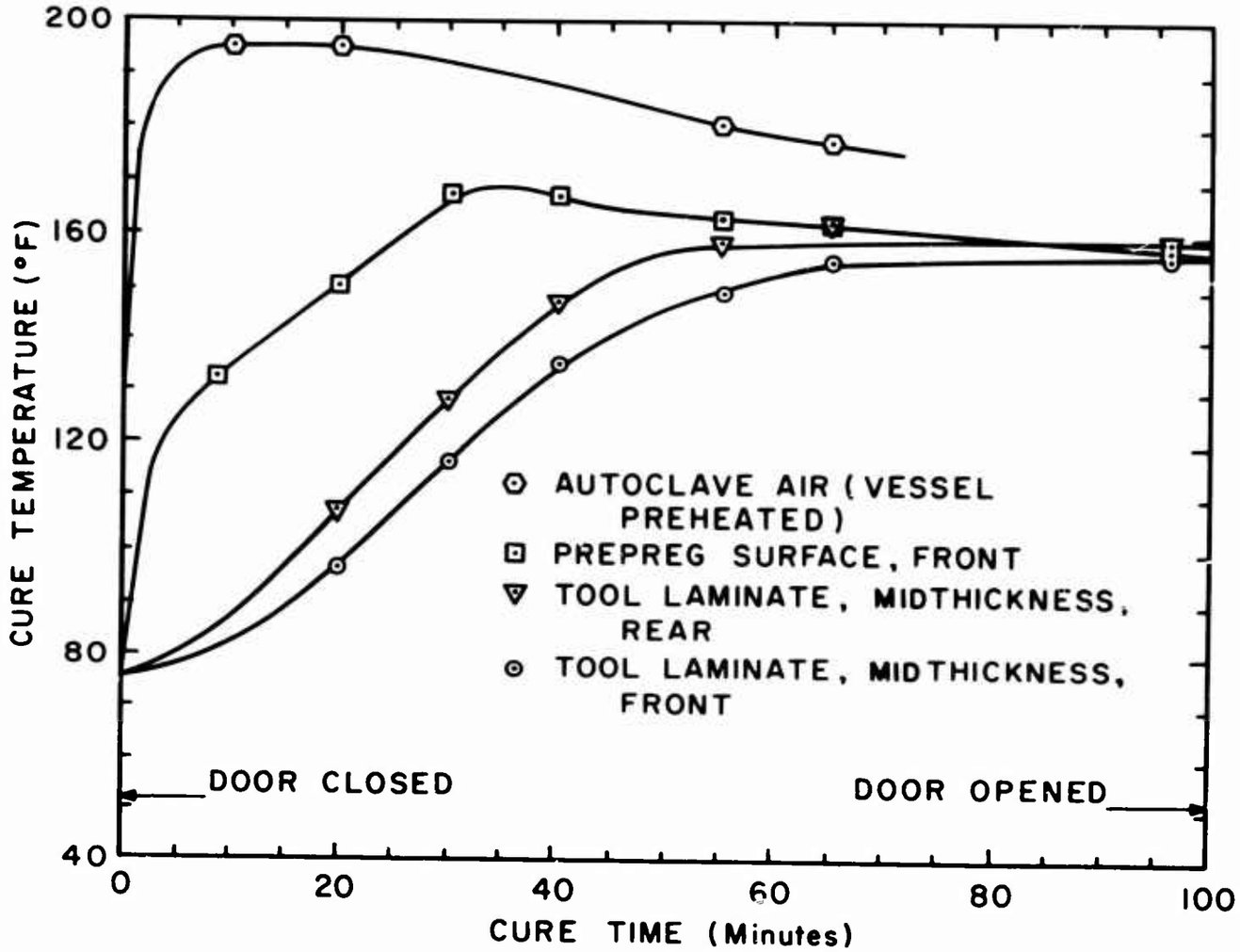

Figure 22. Typical Temperature History of Autoclave Cures.

enough flatness and trueness during splicing, and (3) the installing of the large assembly on the tools. Also, great care had to be exercised in the production of the thin, 50-inch-wide prepreg to prevent wrinkles from developing at the coating machine.

Although this was the initial development of the fabrication procedure and thus time was limited, the facing wrinkles were held to a minimum and finally eliminated on the curved panels. However, this was accomplished to a lesser degree on the cylinders and cones, in that order. One method found effective in reducing the wrinkles was the use of the inside-type layup for the outside facing. The disadvantage of this procedure was a reduction in surface smoothness caused by bleeder imprint.

One of the most difficult problems encountered in the present fabrication effort was the occurrence of leaks in the layups during autoclave cure. Numerous facings were lost because of air entrainment and poor compaction as a result of system leaks. The layups had to be checked very carefully to locate the smallest leaks (normally arising from such causes as blanket punctures, blanket folds at zinc chromate joints, poorly stuck zinc chromate sealant, etc.), as these would increase in size and effect with heat and pressure during the cure. The use of film blankets and edge sealant constituted the best approach for this exploratory effort; however, more durable blankets and self-tightening edge seals should be used in a production situation.

The next logical step in the fabrication program would be the layup of a doubly curved specimen such as a tangent ogive. It is very likely that solutions to the layup problems encountered on the present ruled surfaces would suggest themselves in such an extension of the program.

(2) Core Rolling

Four slabs of honeycomb were used in the construction of each cylinder, two slabs for the curved panels, and at least six for the cones (three circumferentially). The core slabs were formed into the cylindrical or conical shape without anticlastic curvature by rolling in the sheet metal roll-forming machine shown in Figure 23. The fully expanded core was sandwiched between sheets of heavy Kraft paper and sheets of 1/32-inch-thick soft aluminum while lying on the flat. Then the assembly was introduced into the three-roller system. The center roller was lowered into the core in small increments each time it was cranked through, until the desired curvature was obtained. Next, the assembly was draped over a work stand, the aluminum sheets were removed, and the core was cut to size using a modeler's knife and a metal straightedge.

Figure 23. Rolling of Honeycomb Core: A, Center Roller; B, Edge of Core and Protective Sheets.

(3) Sandwich Bonding

After sanding, a 3-foot-wide, film-supported adhesive (AF-110B) was wrapped onto the inner facing while it was still on the tool (A in Figure 24). The core slabs were then pressed into this adhesive layer by hand (B in Figure 24) and connected using bonded compressive butt splices (C in Figure 24). The outer layer of adhesive was next wrapped over the core, and the outside facing was installed and stuck down by hand (D in Figure 24) so that the joints of each facing were symmetrically staggered. The final shell joint was made with a 4-inch-wide precured strip and the same adhesive. A layer of fiber glass fabric was wrapped over the sandwich layup to insure uniform application of vacuum, and, as the final step, the vacuum blanket of 3-mil-thick heat-stabilized nylon was wrapped on and sealed with zinc chromate tape. The sandwich layup was rolled into the preheated autoclave and cured at approximately 300 degrees Fahrenheit temperature under 10-psi vacuum for a total of 150 minutes, including 70 minutes for warmup (Figure 25).

After a slow cooldown, the specimens were removed while the tools were suspended vertically. Prior to removal of the cylinder specimen, the tool was collapsed by removal of the two wedges. Of course, the curved panels could be removed by simply lifting them directly off the tool while in the horizontal position.

A peculiar problem was encountered with the sandwich assemblies and, in particular, the cones. During the installation of outside facing, because of the large surface area, it was often difficult to keep the facing pressed in its final position until the vacuum pressure was applied. When this condition occurred, the facing was required to slide on the core to its final position as the adhesive was warmed during cure. Should the proper sliding not occur, the facing would be bent sharply into a wrinkle at places where the facing circumference was too great. Where these small wrinkles did form, they were repaired by filling with a syringe (see Section 4.d.(2) for adhesive) to insure a good core-to-facing bond. Then the overall integrity of each shell was determined by tapping lightly with a coin.

The facing splices were excellent in these shells, in that the splices were so much an integral part of the parent facing that the core, along with the opposite facing, conformed well to the increased thickness at the joints. This is demonstrated in the photograph of Figure 26. No unbonded areas were apparent, and none of the failures in the structural tests of the shells initiated at facing splices.

To give an indication of the time and effort required to fabricate large sandwich shells, special records were made for each fabrication step on the third cylinder and are summarized in Table IV. The extra cost of bookkeeping prohibited generating

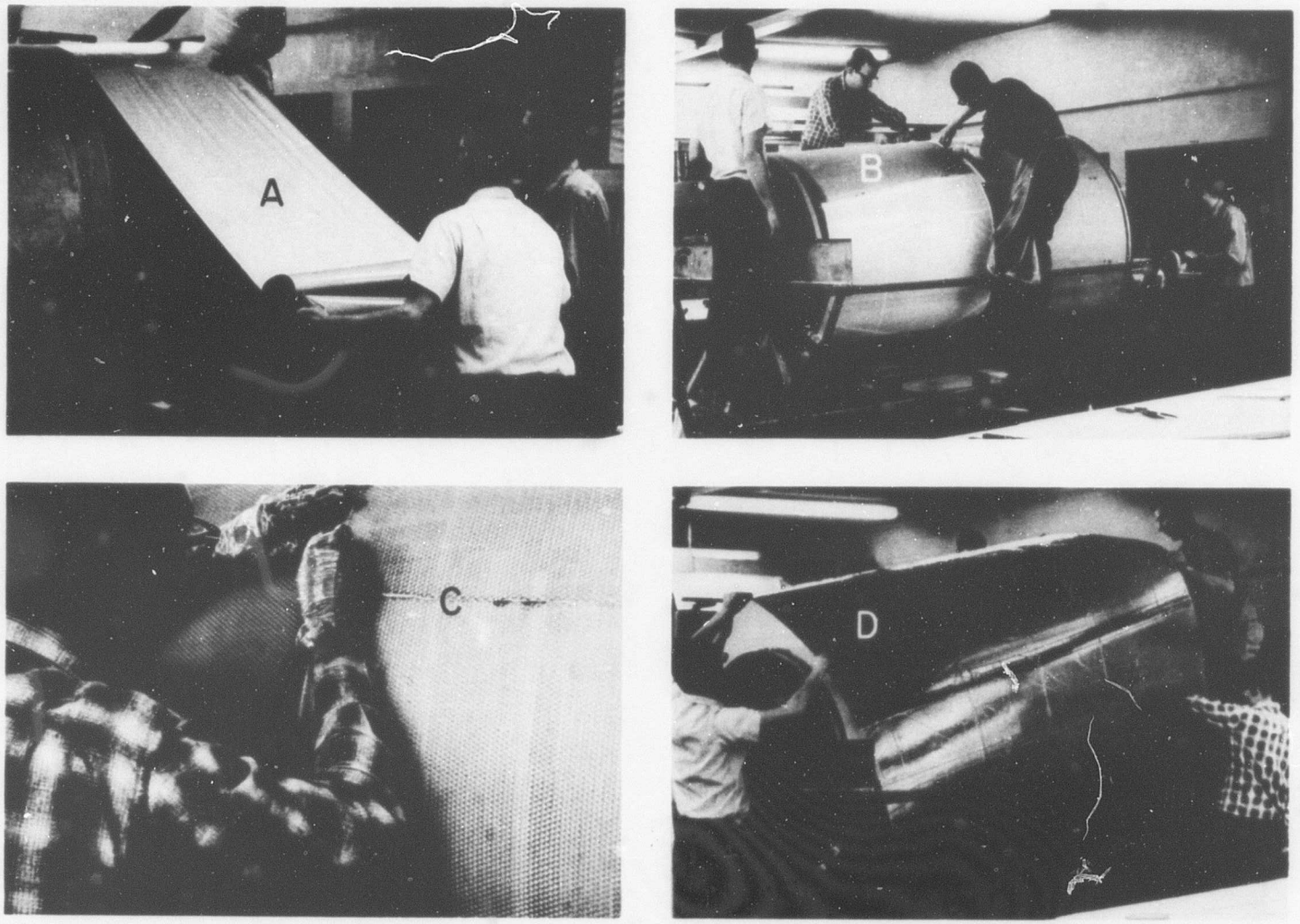

Figure 24. Photos Showing Method of Sandwich Shell Assembly: A, Inside Facing Adhesive Wrap; B, Core Positioning; C, Core Butt Splicing; D, Outside Facing Installation.

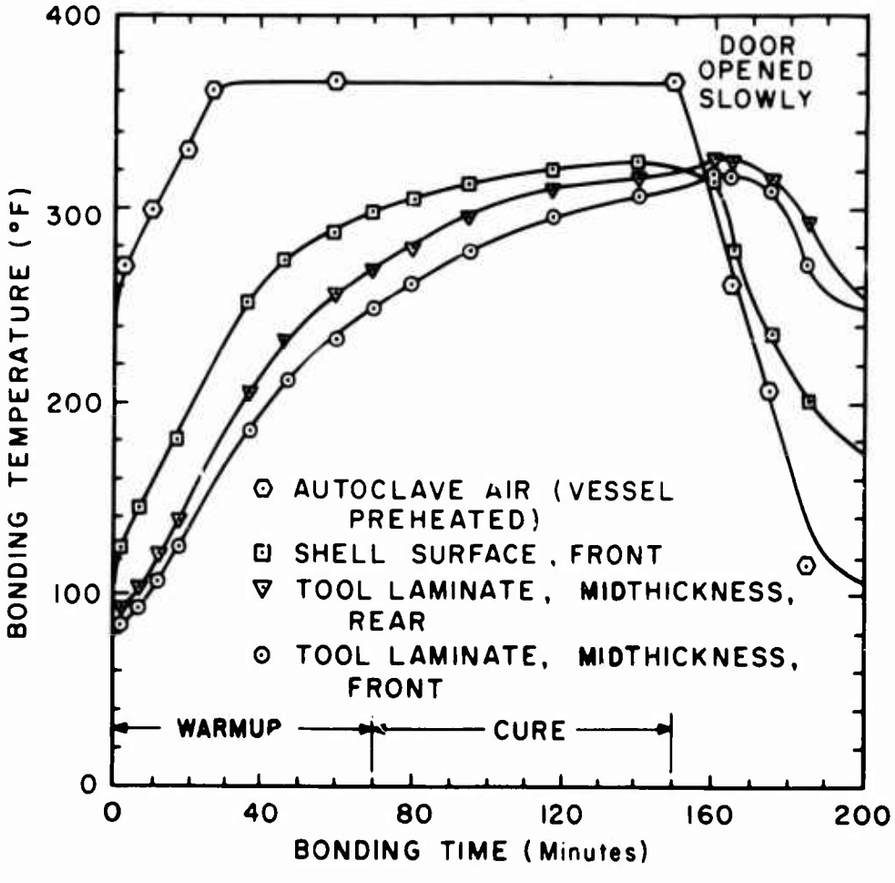

Figure 25. Typical Temperature History of Autoclave Bonding Cycle.

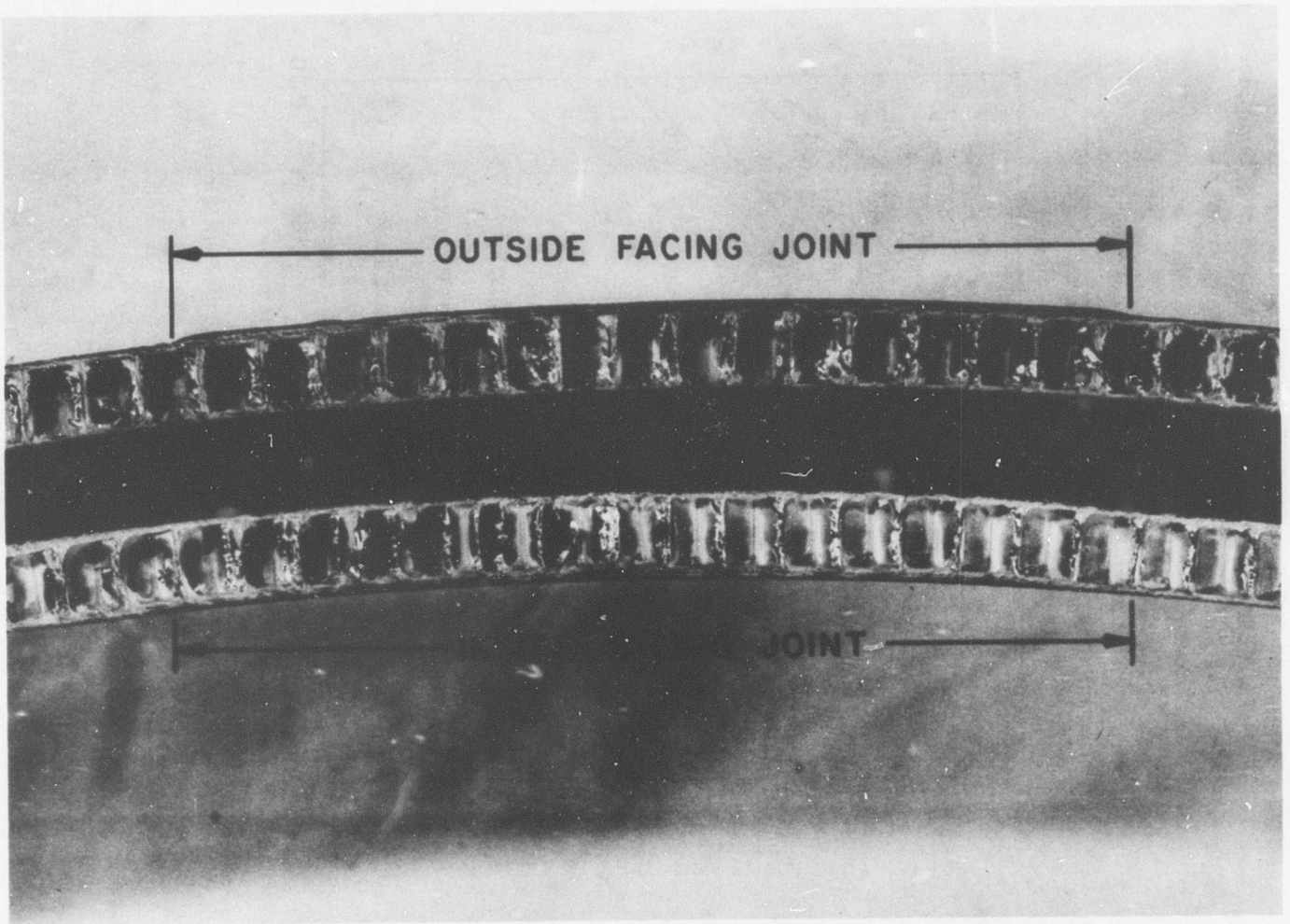

Figure 26. Cross-Sectional Pieces of Cylindrical Sandwich Showing Laminated Facing Joints.

of this type of data. This particular record represents a mid-program sampling where proficiency had been achieved. A minimum of eight men were required for each of the layup and core-rolling operations.

TABLE IV
CYLINDER FABRICATION, MAN-HOURS

Fabrication Step	Man-Hours	Total Man-Hours
A. Facing Fabrication		75
1. Prepreg Production	13	
2. Tool Preparation		
(a) Outside Facing	30	
(b) Inside Facing	10	
3. Layup (Wrapping Prepreg on Tool)		
(a) Outside Facing	10	
(b) Inside Facing	8	
4. Facing Cure (2 x 2 hrs.)	4	
B. Sandwich Shell Assembly		49
1. Rolling of Core	8	
2. Preparation of Facings	12	
3. Shell Assembly	25	
4. Shell Bonding	4	
Grand Total		124

d. Specimen Preparation and Test Procedure

(1) Curved Panels

The curved-panel test specimens were cut from the tool-length panels (80 inches long) using the table saw and roller cradle described in Section 2.b.(1). Then the compressive specimens were reinforced on the loaded ends with an epoxy-ceramic potting compound and, in some cases, with doublers or thin, narrow strips of laminate bonded to the facings. Each panel was positioned in a hydraulic testing machine so that the centroid of the cross-sectional arc was on the loading axis. The final smoothing of the specimen ends for this alignment was done by hand with a metal-cutting file.

The sides of the panels were simply supported by specially de-

signed grips consisting of steel edges bolted to aluminum angles (Page 27, Reference 26), or by grooved wooden blocks in the case of the smaller specimens. Side deflection measurements were made for each specimen tested to confirm that buckling was actually occurring (Figure 27).

The shear panels were bonded into a special gripping device to simulate the type of loading expected in an aircraft panel bordered by spars or stringers. The device is analogous to the picture-frame grip-and-linkage often used to apply shear loading to flat panels. Figure 28 shows the construction of the system and how it was attached to the torsion-bending testing machine. Torque was applied to the loading plate, and thus to the grip-and-linkage, by the moment arm and hydraulic jack shown in the figure.

(2) Complete Shells

The cylinder and cone specimens were mounted in the torsion-bending testing machine via 4-inch deep concentric steel rings similar to the method used for the curved panels (Figures 12 and 28). The specimens were fitted to the rings, aligned in the testing machine, and then tack bonded. The mounting rings were subsequently connected by steel columns to maintain the alignment while the assembly was removed for final bonding. After the back sides of the rings were sealed with tape, the specimens were cast in place using 828 epoxy and V140 polyamide curing agent mixed with a ceramic thickener (Cab-O-Lite P-1).

After curing for 48 hours at room temperature, the flanges of the rings were sanded clean of excess resin before the final mounting of the specimens. Three-element-rosette strain gages (AR-1 wire gages) were bonded to the conical specimens in order to monitor maximum facing strain. An air-operated hydraulic pump was used to increase the jack pressures in 50-psi increments, and strain readings were taken after each increase until failure.

5. Experimental Results and Evaluation

a. Curved Panels

The initial study of the structural behavior of FRP-facing sandwich panels was accomplished with small flat panels sized to buckle in a single half wave. Figure 29 shows the results of a series of tests (Reference 26) on flat panels. These were approximately 1/3 the size of the present curved panels and were constructed of similar constituents (0.2-inch-thick cores with 3/16- and 3/8-inch cells and facings of two-, three-, and four-ply thicknesses). For these panels, the analysis of Reference 32 was conservative in most cases.

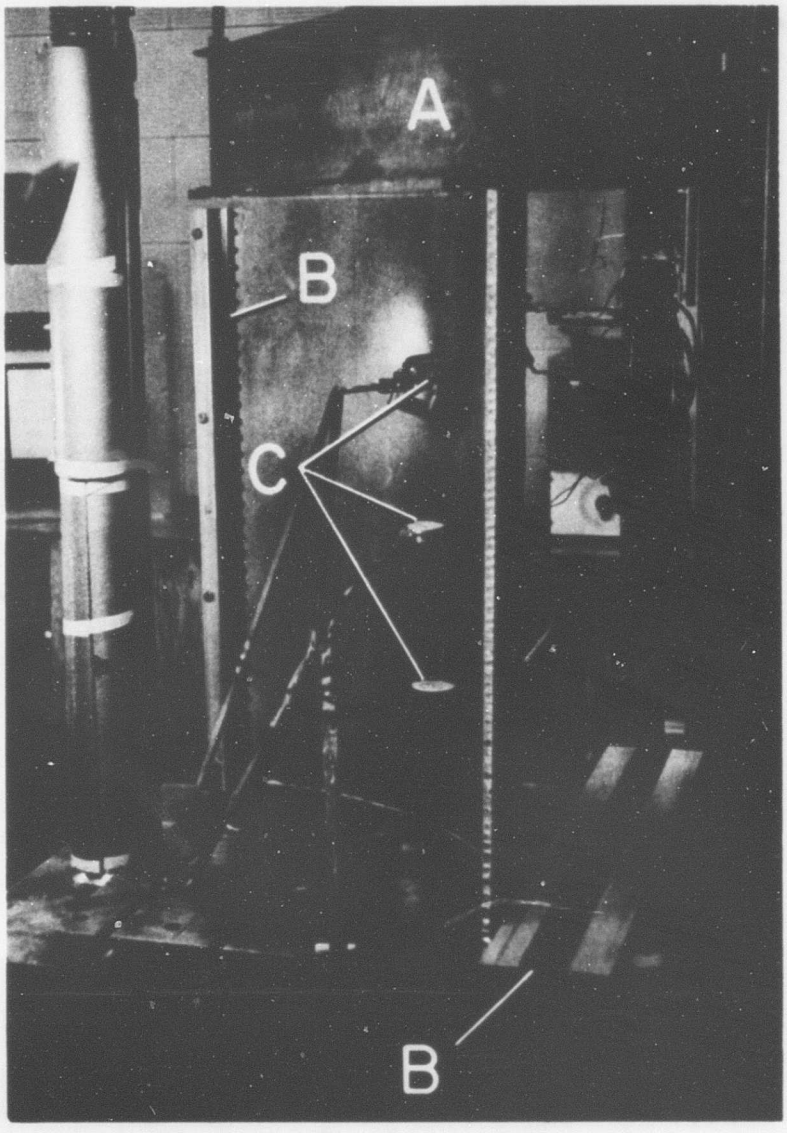

Figure 27. Test Setup for Compressive Loading of Large Curved Sandwich Panels: A, Rigid Loading Plate; B, Side Grips Providing Simply Supported Edges (One Removed to Show Knife Edges); C, Dial Gages for Monitoring Side Deflection.

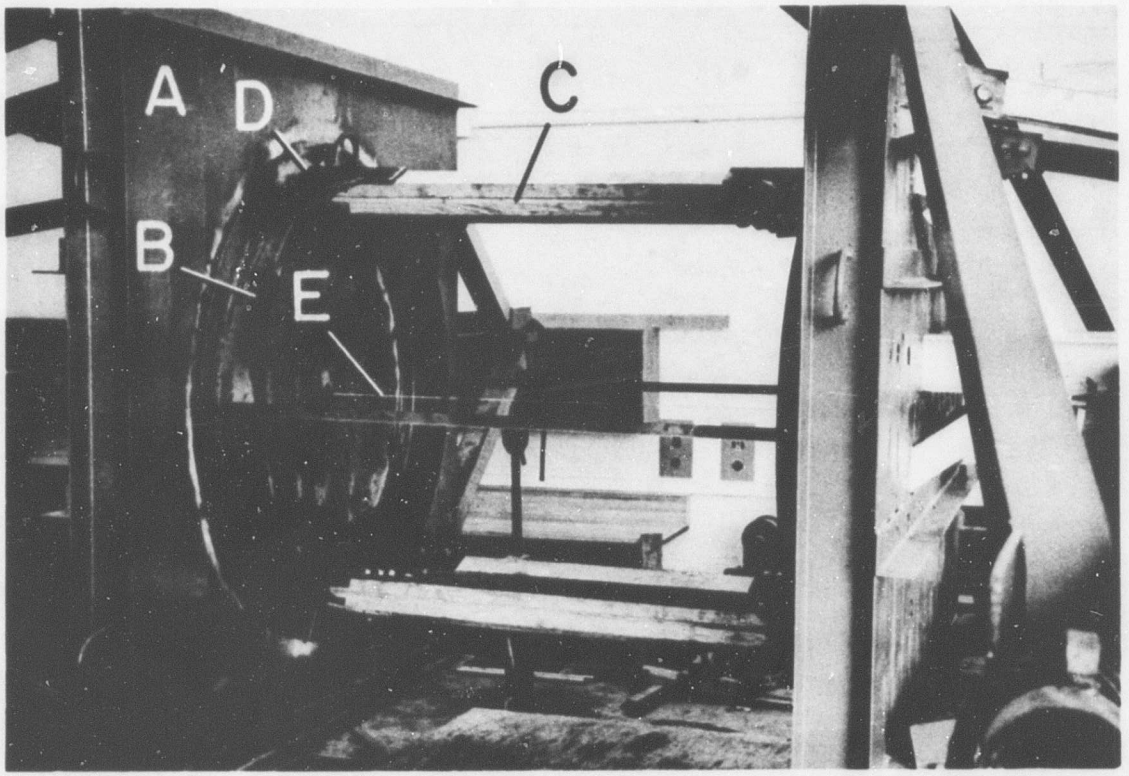

Figure 28. Gripping Device for Simultaneous Application of Shear Loads to All Edges of Curved Panels (Two Panels May Be Tested Together): A, Loading Plate for Torque Application; B, Concentric Rings for Gripping Ends of Specimens Via Resin Bond; C, Grooved Members for Gripping Edges of Specimen; D, Connecting Pin With Freedom to Rotate Parallel to Loading Plates; E, String Through System Used to Align Loading Plates.

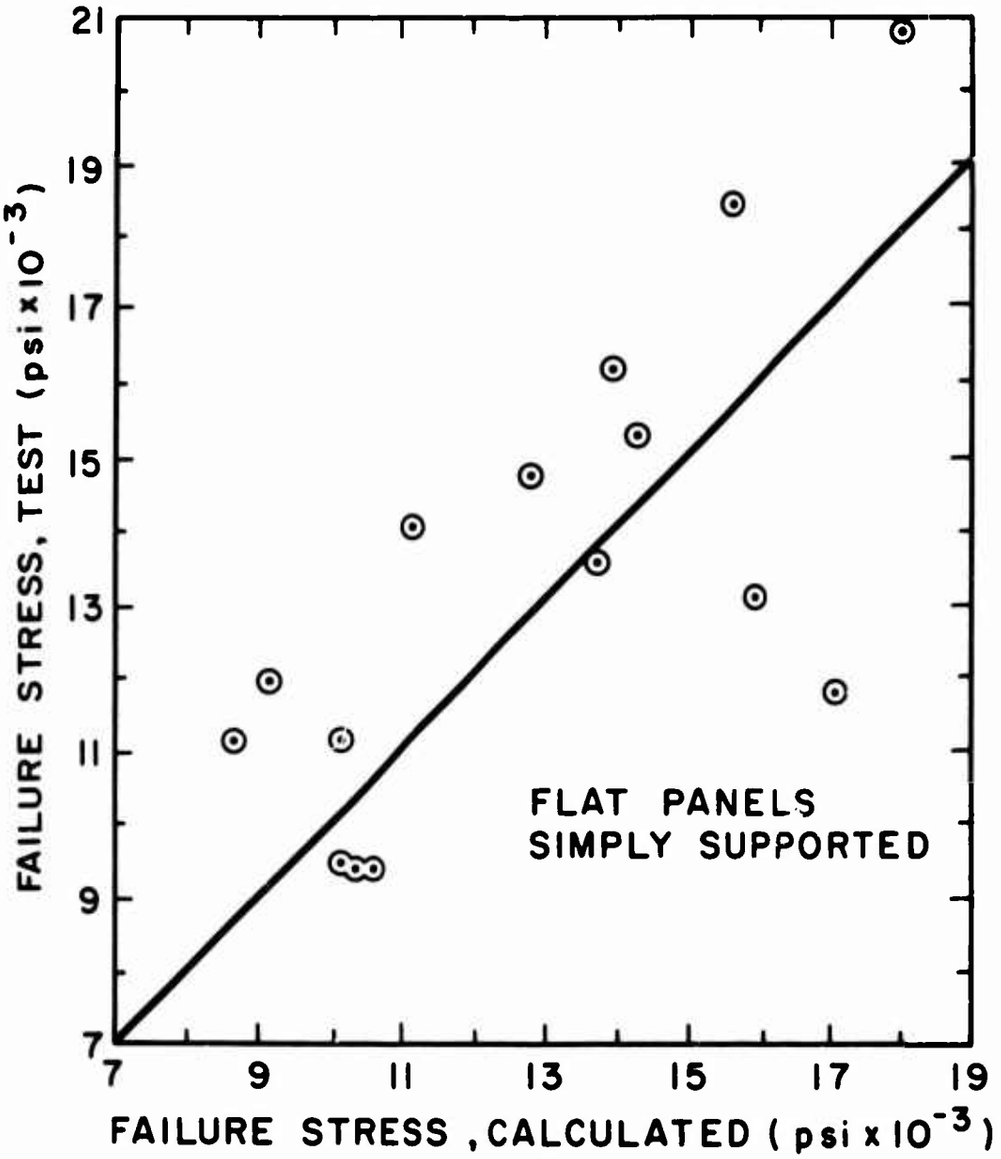

Figure 29. General Buckling of Flat Sandwich Panels With Simply Supported Edges.

The comparison of theory with test is not as clear for the series of tests on curved panels. None of the theoretical developments available to the authors for analysis of compressive buckling of curved sandwich panels take into consideration the orthotropic nature of the FRP facings used. Therefore, it is necessary to improvise either by using semiempirical analyses or by combining several rigorous analyses.

The approach recommended by the Forest Products Laboratory (Reference 18) is to use the complete-cylinder postbuckling analysis of March and Kuenzi (Reference 22), and then to add empirically the stress carried by the panel considered as a flat plate (Reference 32) when the curved panel is smaller than the ideal buckle size of the cylinder. The ratios of the experimental results to those predicted by this method are shown in the fifth column in Table V. This approach has been questioned recently, because it does not seem reasonable to use a large-deflection theory when it is observed that sandwich cylinders in the practical range of values of $R/h < 100$, where R is the nominal cylindrical radius and h is the distance between the center lines of the facings, do not undergo large deflections prior to failure. This is especially true in the case of the tests reported here, because the FRP material fractures instead of undergoing large deflections.

Another approach which appears to be more logical is to adapt the small-deflection, isotropic, sandwich-panel buckling analysis of Stein and Mayers (Reference 40) to the case of orthotropic cores and orthotropic facings (see Appendix III). This adaptation is carried out utilizing some of the results of the recent analysis by Dow and Rosen (Reference 11), which was an extension of the Reference 40 complete-cylinder analysis to the case of orthotropic facings, but with core transverse-shear deformation effects neglected completely. The following values of effective isotropic moduli were substituted for the corresponding isotropic values:

For the core: $$G_c = (G_{xz}G_{yz})^{1/2} \tag{12}$$

For the facings: $$E_f = (E_x E_y)^{1/2} \tag{13}$$

where G_{xz} and G_{yz} are the actual core transverse shear moduli in the axial and hoop (circumferential) directions, and E_x and E_y are the facing Young's moduli for the axial and hoop directions. The preceding substitutions were suggested directly by the nature of the presence of E_x and E_y in Reference 11. The effect of the facing shear modulus μ_{xy} is more subtle. It primarily affects a factor ϕ which is given by Equation (26) in Reference 11, except that if the calculated value exceeds unity, a value of unity is used for ϕ. This effect is used to obtain a correction or knockdown factor to apply to the Reference 40 isotropic analysis. If the facings were isotropic, the following familiar relation of isotropic

TABLE V
RESULTS OF CYLINDRICAL-PANEL AND COMPARISON WITH CALCULATIONS

Compression Loading

Panel No.	Facing & Core[a]	Sq. Panel Size (In.)	Experimental Buckling Stress (psi)	Ratio of Exp. to Calc. Buckling Stress	
				Large-Defl. Anal.[c]	Small-Defl. Anal.[d]
1	A,D	36	26,600	1.03	0.90
1A[b]	A,D	34	20,000	0.76	0.66
2	A,D	36	23,700	0.92	0.80
3	B,C	36	11,600	0.60	0.34
5A[b]	B,C	34	17,800	0.91	0.62

Shear Loading

Panel No.	Facing & Core[a]	Sq. Panel Size (in.)	Experimental Buckling Stress (psi) and Angle (°)		Calculated Buckling Stress (psi) and Angle, γ(°)[c]	
4	B,C	49	5,400	49	16,300	27
5[b]	B,C	49	2,600	-	16,300	27

a See Table III. Average central radii of panels are 21.99 and 21.94 for Types A-D and B-C, respectively.

b These panels loaded previously as numbers indicate. Panels 4 and 5 loaded simultaneously on first test.

c Sum of values from complete-cylinder analysis programmed for computer from equations of Reference 22 and flat-plate analysis of Reference 32. References 19 and 23 used for shear loading case.

d Analysis of Reference 40, corrected for facing orthotropy as described in text (see Appendix III).

elasticity theory would be valid:

$$\mu_i = E/[2(1 + \nu)] \tag{14}$$

where ν is the Poisson's ratio of the facing material. In Reference 11, the factor ϕ would be the same for the isotropic material as for the orthotropic one, except that it would be proportional to the square root of the appropriate shear modulus. Thus, provided that $\phi \leq 1$, the knockdown factor C_o is given by

$$C_o = (\mu_{xy}/\mu_i)^{1/2} \tag{15}$$

Although the 181-style fiber glass cloth used in laminating the facings is nearly isotropic in regard to its normal-stress stiffness (elastic moduli), it has a low in-plane shear stiffness (shear moduli) in comparison to an isotropic material. In fact, the ratio μ_{xy}/μ_i did not exceed unity; and thus, the use of Equation (15) is valid. The ratio of the experimental buckling stresses to those calculated by this second approach is presented in the sixth column of Table V. The details of all calculations are given in Appendix III, including the use of μ_{xy} obtained from shell-test strain gages, instead of coupon-test data for E_{45} from which μ_{xy} is calculated (see also Section 4.b., page 30).

In comparing columns 5 and 6 in the upper part of Table V, it is seen that the ratios for the small-deflection analysis are lower than the ratios for the large-deflection analysis; this is reasonable conceptually. However, the ratios for the large-deflection analysis in every case but one are smaller than unity, even before the inclusion of the flat-plate stress in the former values; this seems unusual. The ratios for the small-deflection analysis are all less than unity; this is reasonable. The one exceptionally low value is discussed below.

The considerations mentioned in the preceding paragraph suggest that the small-deflection analysis is an upper bound, since the calculated values in all cases were higher than the experimental ones. Even though some of the facings contained small fabricational imperfections, no failures occurred near them. Nevertheless, in only one case was the experimental value higher than the prediction of the large-deflection analysis value, which is supposedly a lower bound.

In the one case in which the experimental value was exceptionally low, failure occurred at a localized dimple which formed just before failure (Figure 30). This suggests that failure may have been due to face wrinkling. However, the semiempirical analysis of Reference 15*

* A more accurate analysis for the isotropic case is given in Reference 3.

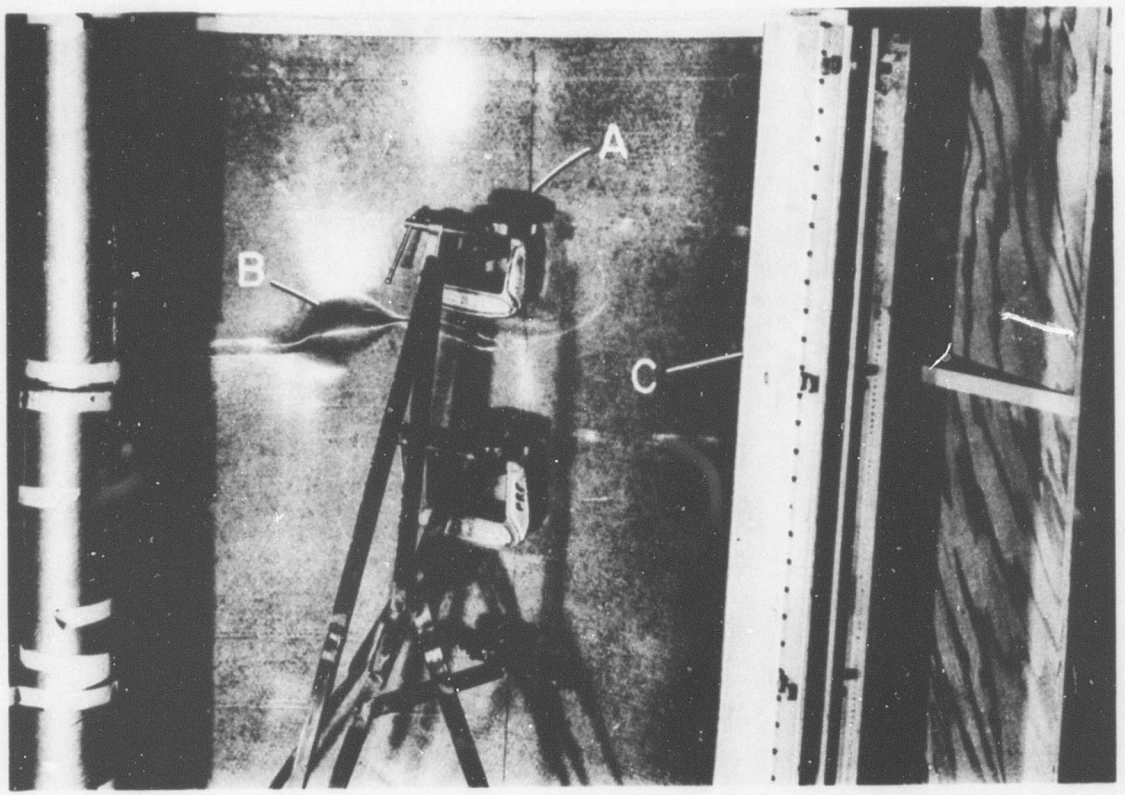

Figure 30. Typical Compressive Buckling Failure of Thin Curved Panels: A, Dial Gage for Side Deflection Measurement; B, Buckle After Panel Collapse (Panel Number 3); C, Knife-Edge Side Grip.

gave the high stress of 27,700 psi, which is in fair agreement with a value of approximately 35,000 psi measured on small sandwich compression coupons, 4 inches square, cut from the panels. Thus, it appears that the general buckle was developing (a rapid increase in side deflection at failure bears this out), and failure occurred at a local discontinuity, resulting in the large dimple which connected with the boundary as a wrinkle at panel collapse.

Load versus side deflection plots were made for all curved panels tested in compression. For each panel, data from at least one of the three dial gages showed a rapid increase in side deflection which indicated that buckling had occurred. When the program was planned, it was hoped that the Southwell method (Reference 10) could be used to predict the buckling load by using data obtained from moderate loads or prebuckling loads. However, the δ/P versus δ plots were not consistent and were not linear, so that no reliable prediction of buckling load could be obtained from the slope of these curves.

The torsional shear panels were analyzed by the semiempirical method suggested by Kuenzi (Reference 19), whereby the buckling stress for a complete cylinder (Reference 23) is added to that for the same size flat panel (Reference 20). An original estimate of 8,700 psi (buckle angle γ = 30 degrees) was obtained using secondary properties of the facings, those (E_{45} being especially significant) at a stress level above 11,000 psi, and this value compared reasonably with the first test value. However, a second calculation using initial tangent moduli (moduli at failure strain) gave a much higher value (column 6, Table V).

This large difference between theory and test suggests the possibility of a shortcoming in the analysis or the existence of secondary loading at the longitudinal boundary in the test. Figure 31 shows the buckle that occurred on the first shear panel (Number 4). Buckle formation started on the second panel but did not completely develop before the panel failed by tearing at a loading ring.

b. Cylinders

As mentioned in Section 4.b., page 30, strain-gage measurement of E_{45}, accomplished on the cone torsion test, yielded higher values than the coupon tests. This was most noticeable at the higher strain levels. Utilization of these E_{45} values resulted in much higher and more reasonable buckling stresses. The calculations are given in Appendix III.

(1) Pure Bending

The calculation of buckling due to pure bending moment in sand-

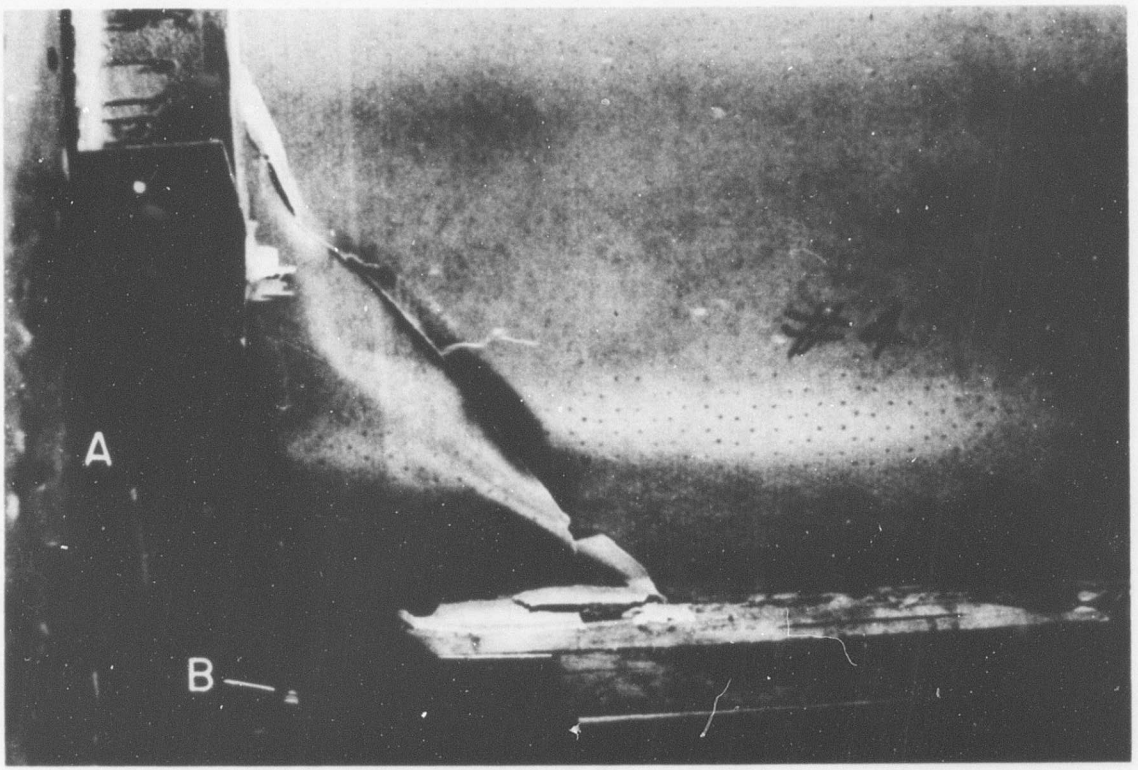

Figure 31. Curved-Panel Shear Failure: A, Torque Plate and Ring End-Grip; B, Tilting Pin.

wich cylindrical shells with orthotropic facings and orthotropic core is severely limited because such an analysis does not exist on a rigorous basis. In fact, there are very few analyses for this loading even in the isotropic case. Due to the paucity of appropriate analyses which are directly applicable, it is the usual practice to relate the maximum fiber stress at which buckling occurs in a cylinder subject to pure bending $(\sigma_{cr})_b$ to that of an identical cylinder subject to axial compression $(\sigma_{cr})_a$. This raises the controversial question as to what is the correct relationship of the buckling stresses for the two kinds of loading.

Early tests by Donnell and others (see Reference 41 for discussion) indicated that for homogeneous, isotropic cylinders $(\sigma_{cr})_b \simeq 1.4\ (\sigma_{cr})_a$. According to small-deflection theory of homogeneous, isotropic cylinders (References 1, 6, and 38), $(\sigma_{cr})_b \simeq (\sigma_{cr})_a$; thus, the factor 1.4 has been attributed to the nonuniformity in circumferential distribution of axial stress and to large deflections and imperfections. In fact, Yao's analysis (Reference 45) indicates that the ratio $(\sigma_{cr})_b/(\sigma_{cr})_a$ increases from a value of unity at radius/thickness (R/h) ratio of 45 to a value of 1.3 at R/h of approximately 200. However, more recently a very careful statistical analysis of tests on more than 300 cylinders (Reference 17) indicates that this ratio is essentially equal to unity.

Turning now to sandwich-type cylinders, small deflection analyses (References 12 and 43) indicate that just as in the homogeneous, isotropic case, $(\sigma_{cr})_b/(\sigma_{cr})_a \simeq 1$. The experimental results seem to be inconclusive: Gerard (Reference 13) found a ratio of approximately 1.32, North (Reference 33) obtained 1.99, and Peterson and Anderson (Reference 35) achieved 1.00. In view of these results, it appears that more tests are necessary to definitely resolve this question in the case of sandwich cylinders.

The situation regarding calculation of the buckling stress for complete sandwich cylinders subject to axial compression is similar to that discussed in the previous section for the curved panels, except that here there are even more theories available.

Use of the large-deflection theory of March and Kuenzi (Reference 22) gives a value of 18,300 psi for $(\sigma_{cr})_a$. However, as previously discussed, this theory does not appear to be valid here because large deflections do not take place physically, and the assumed form of the buckle wave-form shape will not permit the equations to reduce to the correct form for small deflections.

All of the small-deflection analyses available at present are for the case of isotropic facings. The infinite-length analysis

of Zahn and Kuenzi (Reference 47), the analysis of Almroth (Reference 2), and that of Peterson and Anderson (Reference 35) all give a buckling stress of 45,300 psi. The finite-length analysis of Stein and Mayers (Reference 40) yields a value of 40,100 psi.

In order to incorporate orthotropic facings, in particular the effect of the low in-plane shear stiffness, the knockdown factor of 0.545, derived in Appendix III on the basis of Reference 11 can be applied to the values listed in the preceding paragraph with the following results: 24,700 psi for the infinite length and 21,900 psi for the finite length. Thus, it is seen that the small-deflection analyses do in fact stand as the upper bound as expected. The test value of 14,100 psi is lower than the value from the large-deflection analysis (18,300 psi) which was not expected; but this was probably due to imperfections in the test specimen, as it was the first shell fabricated in the program. It should be mentioned that the particular mode of buckling could not be identified in the present test, as the failure was explosive in nature.

A new unified sandwich instability theory (Reference 3) considers face wrinkling as well as general instability and thus may give more accurate predictions, if it were modified to consider orthotropic facings.

(2) Pure Torsion

The small-deflection theory of Reference 23 was used for the analysis of the sandwich cylinder loaded in torsion. As explained in Section 5.a. for the curved-panel shear case, a conservative initial estimate of the buckling stress was made using the secondary values of the facing elastic moduli. This calculated facing stress was 5,390 psi. The test result was 8,560 psi which confirmed that failure did occur in the higher strain region as anticipated; however, in an effort to obtain a more accurate calculation, the E_{45} value obtained from shell strain-gage data (see Appendix III) was used in a second calculation rather than the values obtained from the coupon tests. This calculation gave a buckling stress of 10,700 psi.

Observations indicated that failure may have started near a poorly bonded spot on the outside facing; this fact suggests that the test value may be slightly low. Should this be the case, the gap between theory and test would be less than indicated above, which would lend support to the idea that a linear theory gives an accurate prediction of the buckling stress, provided the material properties at the failure stress are used (in particular, the E_{45} value). Of course, an iteration procedure would have to be used to apply this to design.

Figure 32 is an action shot of the failure showing the huge

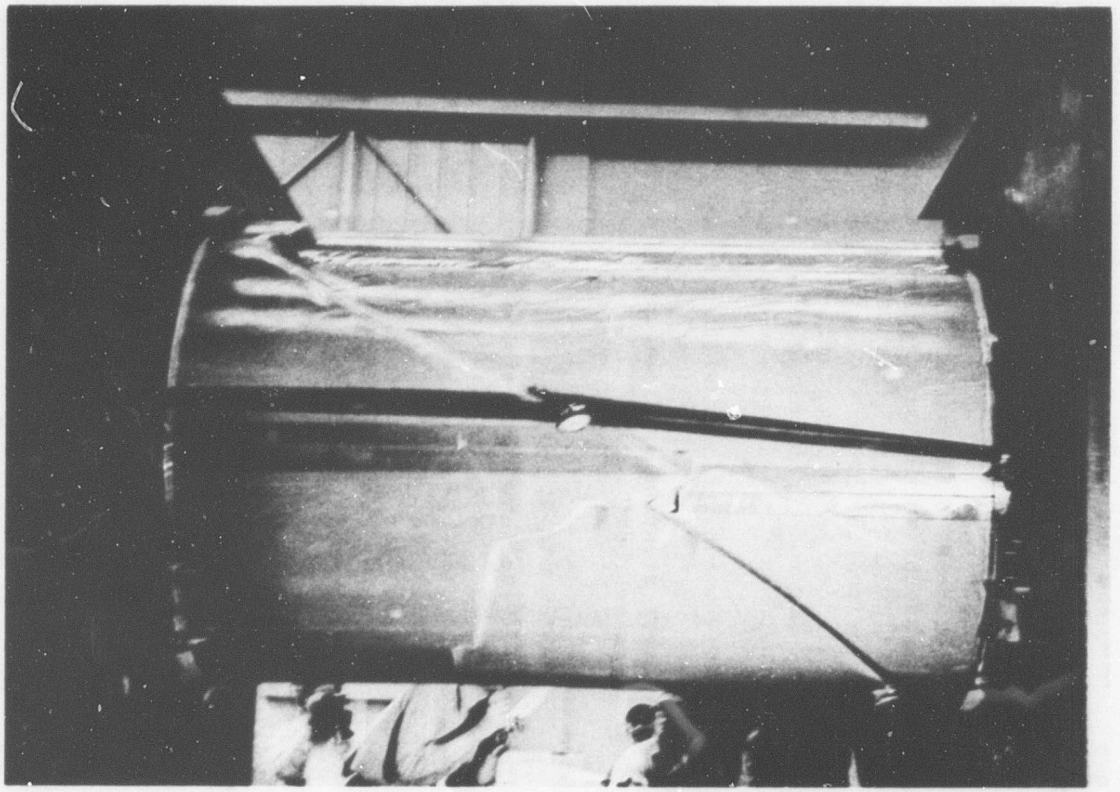

Figure 32. Torsional Buckling of Sandwich Cylinder in Progress.

buckle that developed across the cylinder. The buckle angle was 29 degrees measured from the cylinder axis. The calculated values of this angle corresponding to stress levels of 5,390 psi and 10,700 psi were 30 degrees and 23 degrees, respectively.

(3) Combined Torsion and Bending

The third specimen in the cylinder program was loaded with approximately equal torque and bending moments which gave a bending-to-torsion stress ratio of two. The three data points from the program are plotted in Figure 33 and compared with the interaction equation of Wang, Vaccaro, and DeSanto (Equation (6) of Section 3.d), where the calculated values of References 22, 23, and 40 (modified) were used as anchor points.

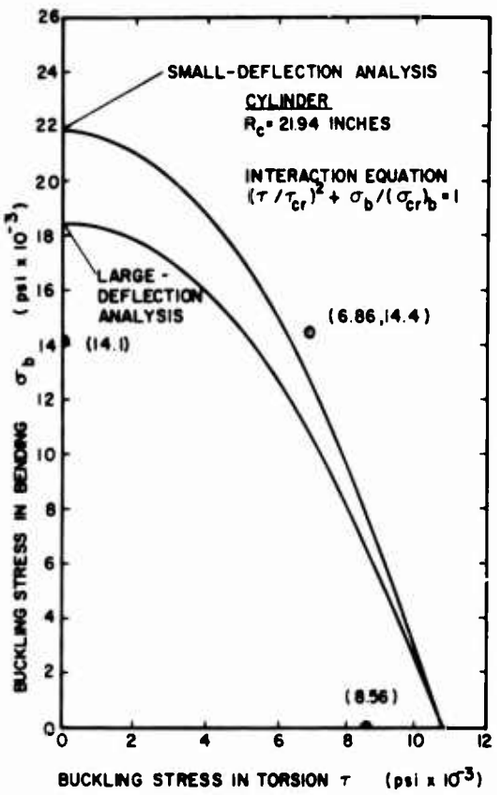

Figure 33. Interaction Curve for Buckling of Sandwich Cylinders.

These limited data appear to fit Equation (6) reasonably well, especially when it is realized that the low values at the end points may be due to shell imperfections. (These were the first complete-shell specimens fabricated and tested.) However, another interaction equation suggested by Bruhn (Reference 7) as being used by several aerospace companies (not specifically referenced) contains the ratio σ_b/σ_{bcr} to the 1.5 power rather than 1.0. This would result in a curve somewhat fuller than the Reference 44 curve shown in Figure 33. Thus, to identify the precise interaction curve more clearly, at least three specimens should be tested at each location. Furthermore, at least one more location should be provided, possibly at a bending-to-torsion stress ratio of 1/2. This additional research would be extremely valuable to the body of knowledge needed to bring full acceptance of reinforced plastics as

primary load-bearing structures for aircraft, in that available information of this type is very limited.

As for the separately loaded cases, the failure here was also sudden, producing a very loud report. The failed condition of the specimen was particularly interesting in that the characterestics of both torsion and bending were present. The photo of Figure 34 captures the important features. As can be seen, compressive collapse occurred in the region farthest from the neutral axis and changed into a pure torsional buckle at the neutral axis. On the tension side, the torsional buckle progressively disappears with distance from the neutral axis.

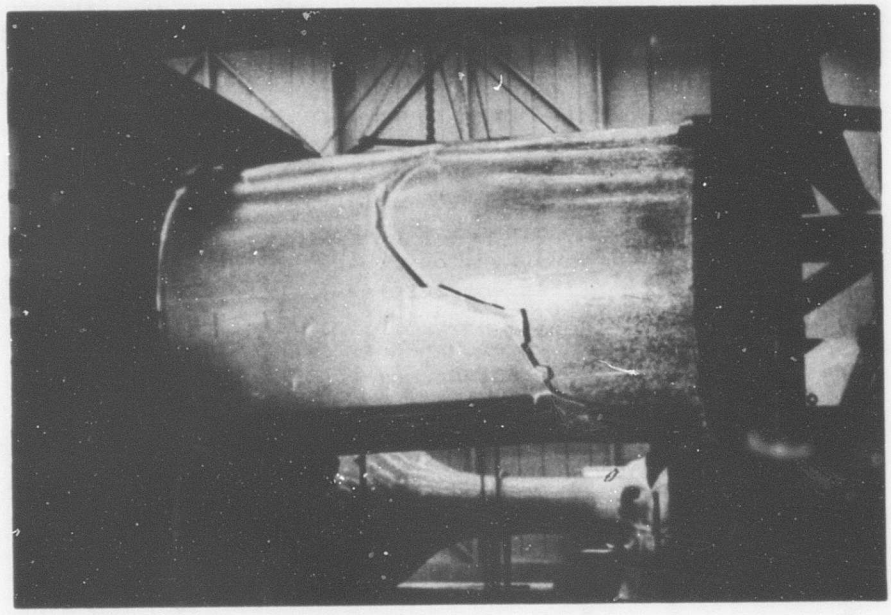

Figure 34. Torsion-Bending Failure of Sandwich Cylinder.

c. Cones

(1) Pure Bending

To the authors' knowledge, there is no theoretical analysis available for the bending of sandwich cones. The method proposed by Seide (Equation (10) of Section 3.e.) was used as a first approximation in the present program. This is tantamount to saying that the buckling stress of the cone is the same as a cylinder of radius equal to that at the small end of the cone, since the cosine squared factor also appears in the denominator of the stress σ_b.

Unexpectedly, the experimental value of 26,000 psi from the first cone-bending test was much higher than the predicted

value of 17,600 psi, where the cylinder buckling stress was taken as that in axial compression using Reference 22. As in all the buckling calculations, the E_{45} value obtained from shell strain-gage data (1.4×10^6 psi) was used in favor of that from the coupon tests (again see Appendix III and Section 4.b., page 30). Possible sources of error include the approximate buckling analysis and the unknown relation between the axial compression and the bending phenomena (see Section 5.b. (1)). In the latter case, the uncertainty is much worse than for cylinders, as test data are even more sparse (Reference 39).

It was believed initially that the test value could be improved by accounting for the possible shift in neutral axis due to the different tension and compression stress-strain curves found in FRP and by increasing the area moment of inertia (used to calculate stress) to account for the presence of the facing joints; however, limited rosette strain-gage data obtained from the second test more closely agreed with the original MR/I calculation of 26,000 psi, based on the experimental value of M.

Failure occurred prematurely in the second bending test because of a local bond crack on the tension side of the boundary at the small end of the shell. This resulted in a tearing of the shell in the vicinity of the neutral axis. The bending stress had reached 17,400 psi when the shear failure was discovered.

Pullout occurred on the small-end tension side of the boundary during the first test; however, because of the high stress level achieved, it appears that compressive failure did play a role in this collapse. The appearance of the compressive failure was similar to that of the cylinder.

(2) Pure Torsion

There is also a lack of theoretical buckling analyses for sandwich cones in torsion. Again the Seide equations (in particular, Equations (7), (8), and (9), Section 3.e.) were used to estimate sandwich buckling. This was done by using Equation (7) to obtain the ratio of τ_{cone} to $\tau_{cylinder}$ and by multiplying this ratio by the torsional buckling stress of the cylinder (8,300 psi using Reference 23). The result was 9,600 psi, which compares favorably with the test value of 11,500 psi.

Figure 35 shows that the same type of buckle occurred as did in the cylinder test. The buckle angle was measured at 34 degrees from the shell axis as compared to the calculated value of 24 degrees (Reference 23). Proof that the shell underwent pure torsion was provided by strain-gage readings. The 45-degree arm of the rosette strain gage indicated a total of 9,850 micro-inches of strain, whereas the changes in the

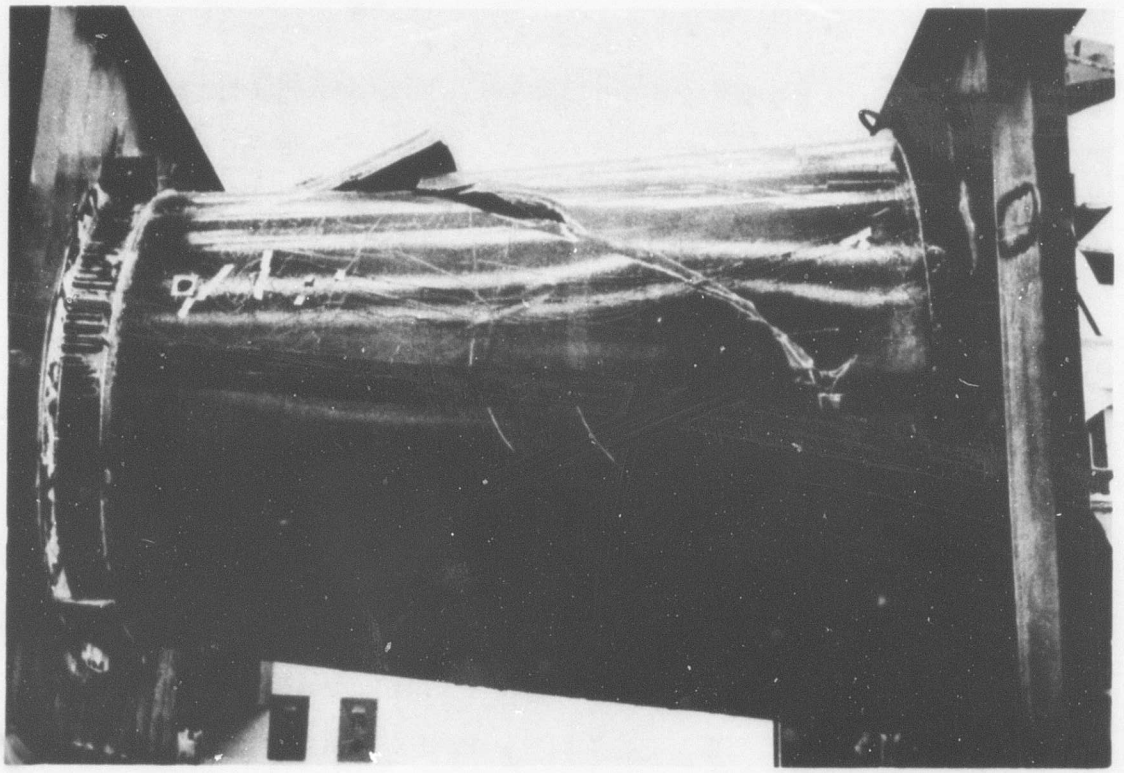

Figure 35. Torsional Buckle of Sandwich Cone.

longitudinal and hoop readings were nil. (See Appendix IV for discussion.)

(3) Combined Torsion and Bending

The fourth sandwich cone was loaded with approximately equal torque and bending moments which gave a bending-to-torsion stress ratio of two, as in the case of the cylinders. The three test points obtained in the cone program are plotted in Figure 36 and compared with the same interaction equation used for the cylinders (Equation (6) of Section 3.d.), since in Reference 21, the same equation was found to be valid for monolithic cones.

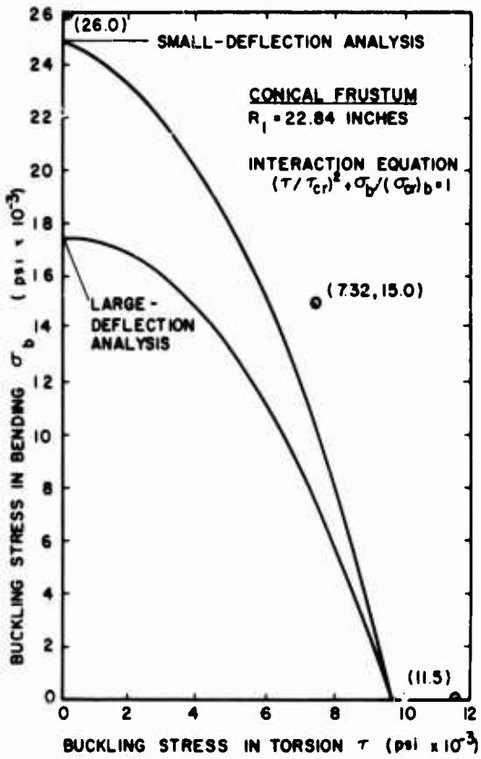

Figure 36. Interaction Curve for Buckling of Sandwich Cones.

About the same agreement as obtained for the cylinders is present here for the pure torsion and combined loading cases; however, there is very poor agreement in the pure bending case. Until a theoretical analysis is provided for the bending of sandwich cones (see Section 5.c.(1) discussion), little more

can be said of the interaction equation. Also, before any proposed interaction relation can be confirmed, more test specimens are needed. At least three specimens are needed at each of the present loadings, and furthermore, another load combination should be provided. Needless to say, these data would be invaluable to the designer of FRP structures.

The cone failure under combined loading was abrupt, and the buckles were similar in appearance to those of the cylinder (see Section 5.b.(3) for discussion). Figure 37 is a photo showing the torsion and compression buckles.

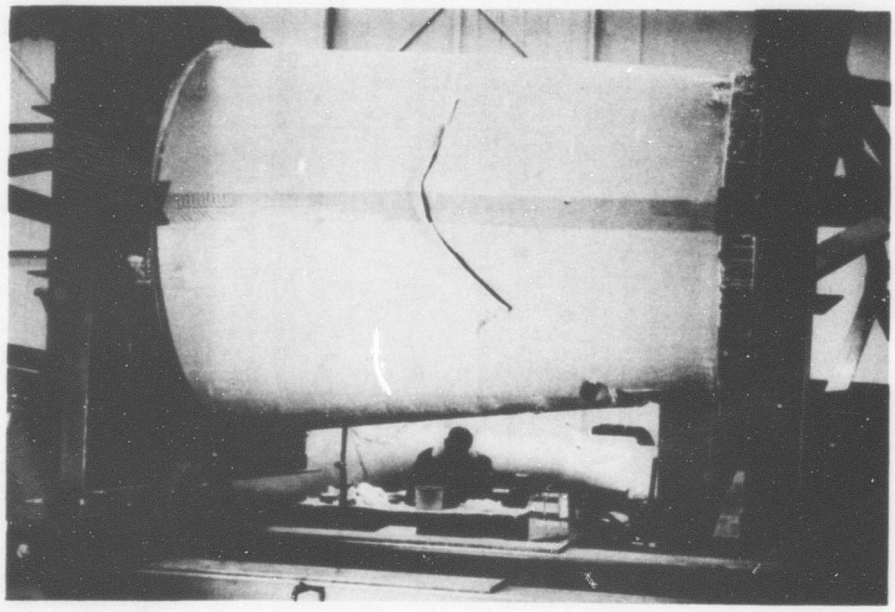

Figure 37. Torsion-Bending Failure of Sandwich Cone.

6. Conclusions and Recommendations

a. Fabrication

(1) Uniform multilayer impregnations of fiber glass fabric and 828-Z epoxy resin can be produced in lengths greater than 700 inches using the resin-coating machine developed at the University of Oklahoma.

(2) The fabrication procedures and techniques revealed by the present large structures research using well-known materials are believed to be basic in nature and should apply to the newer reinforcing materials such as S-glass, carbon, boron, etc., with only minor modifications.

(3) To permit optimal structural design, it is recommended that research be conducted to obtain basic joint information, with consideration being given to such factors as specific strength, joint fabrication, type of adhesive, and aerodynamic smoothness.

(4) Research should be continued on facing laminate materials, especially in regard to complex loadings such as biaxial tension, in regard to optimum reinforcement and load orientation, and in regard to the effect of cutouts.

(5) The use of thin, stretchable prepregs in the layup of very large components often poses problems in regard to fiber misalignment and localized wrinkles. Extra care must be exercised in the handling of these materials in order to obtain smooth, uniform thickness laminates. It is possible that a program to fabricate specimens with a compound curvature may suggest handling and wrapping techniques which would minimize these deviations in smoothness.

(6) Probably the most prevalent difficulty in the autoclave cure of reinforced plastics is the pressure blanket leak. When possible, the use of dissimilar materials at connections should be avoided, and blankets of durable materials should be used in conjunction with self-tightening edge seals.

(7) In the assembly of very large sandwich structures for final bonding, the positioning on the core of the second of the prelaminated facings must be accurate or such as to permit limited sliding into the final location as the bonding pressure and temperature are applied. If the proper positioning of constituents is not achieved, the excess facing will often bulge into a wrinkle and result in a poorly bonded area.

(8) It is especially recommended that advantage be taken of the present research as soon as possible by way of the fabrication and structural evaluation of a complex aircraft component, possibly an aerodynamic structure such as a wing section.

b. Structural Evaluation

(1) The results of the present research indicate that sandwich shells are not as sensitive to small imperfections as monolithic shells.

(2) To obtain more conclusive information on the phenomenon of curved-panel shear, it is recommended that tests be conducted using Forest Products Laboratory (FPL) type picture-frame loading apparatus (Reference 19).

(3) The torsion-bending testing machine developed in the present program was very successful in applying pure torsion, pure bending, and any desired combination of the two. There were

no problems associated with its use. The basic design concepts of the testing machine could be applied to design of machines to test any large aircraft-type structure.

(4) The testing of one specimen each in torsion, in bending, and in combined torsion and bending has established preliminary interaction relationships for buckling of sandwich cylinders and cones, but does not conclusively indicate the validity of these interaction equations for design use. Thus, it is recommended that a follow-on program of research be conducted to test at least three specimens at each load condition and that one more point on the interaction curve be established in a similar manner.

(5) Rigorous theoretical buckling analyses for several sandwich structures of simple, basic geometry possessing orthotropic facings and cores do not exist; yet these are vitally needed for the design of composite structures for Army aircraft. Such structures include (a) curved panels subjected to both shear and axial compression loadings, (b) cylinders subjected to pure bending, and (c) cones subjected to both pure bending and pure torsion. It is recommended that research be initiated in these areas as soon as possible.

(6) Comparisons of experimental results with available theoretical buckling analyses for the cases in which they are available indicated that a small-deflection-analysis prediction represents an upper bound which is not exceeded in experiments. It is assumed that the analysis is made using material properties associated with the stress level at which failure occured in the experiments.

(7) The small-deflection shell buckling predictions are fairly sensitive to changes in facing shear modulus μ_{xy} and care must be used in experimentally determining this value. It has been found that μ_{xy} values obtained by calculation from uniaxial-coupon-test data are too low. Thus, this method is not recommended.

REFERENCES

1. Abir, D., and S. V. Nardo, "Thermal Buckling of Circular Cylindrical Shells Under Circumferential Temperature Gradients", Journal of Aerospace Sciences, Volume 26, 1959, pp. 803-808.

2. Almroth, B. O., Buckling of Axially Compressed Sandwich Cylinders, Technical Report Number 6-62-64-9, Lockheed Missiles and Space Company, Sunnyvale, California, July 1964.

3. Bartelds, G., and J. Mayers, Unified Theory for the Bending and Buckling of Sandwich Shells - Application to Axially Compressed Cylindrical Shells, SUDAER Report Number 287, Stanford University Department of Aeronautics and Astronautics, November 1966; also American Institute of Aeronautics and Astronautics/American Society of Mechanical Engineers Eighth Structures, Structural Dynamics and Materials Conference, Palm Springs, California, March 1967, pp. 619-637.

4. Bert, C. W., W. C. Crisman, and G. M. Nordby, "Fabrication and Full-Scale Structural Evaluation of Glass-Fabric Reinforced Plastic Shells", American Institute of Aeronautics and Astronautics/American Society of Mechanical Engineers Eighth Structures, Structural Dynamics and Materials Conference, Palm Springs, California, March 1967, pp. 352-362.

5. Bert, C. W., D. J. Wilkins, and W. C. Crisman, "Damping in Sandwich Beams With Shear-Flexible Cores", Paper Number 67-Vibr-11, American Society of Mechanical Engineers Vibration Conference, Boston, Massachusetts, March 1967.

6. Bijlaard, P. P., and R. H. Gallagher, "Elastic Instability of a Cylindrical Shell Under Arbitrary Circumferential Variation of Axial Stress", Journal of Aerospace Sciences, Volume 27, 1960, pp. 854-859.

7. Bruhn, E. F., Analysis and Design of Flight Vehicle Structures, Tri-State Offset Company, Cincinnati, Ohio, 1965, pp. c8.17, c8.20.

8. California Institute of Technology, Some Investigations of the General Instability of Stiffened Metal Cylinders II - Preliminary Tests of Wire-Braced Specimens and Theoretical Studies, July 1943, also Technical Note 906, National Advisory Committee for Aeronautics, July 1943.

9. Crisman, W. C., G. M. Nordby, and C. W. Bert, "Automated Multilayer Prepreg Production", Modern Plastics, Volume 42, Number 12, August 1965, pp. 118, 121.

10. Donnell, L. H., "On the Application of Southwell's Method for the Analysis of Buckling Data", Stephen Timoshenko 60th Anniversary Volume, The Macmillan Company, New York, 1938, pp. 27-38.

11. Dow, N. F., and B. W. Rosen, "Structural Efficiency of Orthotropic Cylin-

drical Shells Subjected to Axial Compression", American Institute of Aeronautics and Astronautics Journal, Volume 4, 1966, pp. 481-485.

12. Gellatly, R. A., and R. H. Gallagher, "Sandwich Cylinder Instability Under Nonuniform Axial Stress", American Institute of Aeronautics and Astronautics Journal, Volume 2, 1964, pp. 398-400.

13. Gerard, G., "Bending Tests of Thin-Walled Sandwich Cylinders", Journal of Aeronautical Sciences, Volume 20, 1953, pp. 639-641.

14. Greszczuk, L. B., Elastic Constants and Analysis Methods for Filament Wound Shell Structures, Douglas Aircraft Company, Inc., Missile & Space Systems Division, Santa Monica, California, Report Number SM-45849, January 1964.

15. Harris, B. J., and W. C. Crisman, "Face-Wrinkling Mode of Buckling of Sandwich Panels", Journal of the Engineering Mechanics Division, Proceedings of the American Society of Civil Engineers, Volume 91, Number EM3, June 1965, pp. 93-111.

16. Hoff, N. J., "Thin Shells in Aerospace Structures" (4th von Karman Lecture), Astronautics and Aeronautics, Volume 5, Number 2, February 1967, pp. 26-45.

17. Horton, W. H., and J.W. Cox, The Stability of Thin-Walled Unstiffened Circular Shells Under Nonuniformly Distributed Axial Load, SUDAER Report Number 220, Stanford University Department of Aeronautics and Astronautics, February 1965.

18. Kuenzi, E. E., Design Criteria For Long Curved Panels of Sandwich Construction in Axial Compression, Report Number 1558, Forest Products Laboratory, Madison, Wisconsin, December 1946.

19. Kuenzi, E. W., Stability of a Few Curved Panels Subjected to Shear, Report Number 1571, Forest Products Laboratory, Madison, Wisconsin, May 1947.

20. Kuenzi, E. W., W. S. Erickson, and John J. Zahn, Shear Stability of Flat Panels of Sandwich Construction, Report Number 1560, Forest Products Laboratory, Madison, Wisconsin, May 1947, revised May 1962.

21. MacCalden, P. B., and R. B. Matthiesen, "Combination Torsion and Axial Compression Tests of Conical Shells", American Institute of Aeronautics and Astronautics Journal, Volume 5, Number 2, February 1967, pp. 305-309.

22. March, H. W., and E. W. Kuenzi, Buckling of Cylinders of Sandwich Construction in Axial Compression, Report Number 1830, Forest Products Laboratory, Madison, Wisconsin, June 1952, revised December 1957.

23. March, H. W., and E. W., Kuenzi, Buckling of Sandwich Cylinders in Torsion, Report Number 1840, Forest Products Laboratory, Madison, Wisconsin, June 1953, revised January 1958.

24. Nordby, G. M., C. W. Bert, and W. C. Crisman, "Buckling of Large Fiberglass-Honeycomb Core Sandwich Structures in Torsion and Bending", presented at the American Society of Civil Engineers Conference, Session on Materials for Structures in the Atomic Space Age, Seattle, Washington, May 1967.

25. Nordby, G. M., and W. C. Crisman, Research In the Field of Fiberglass-Reinforced Sandwich Structure for Airframe Use, TRECOM Technical Report 64-37, U. S. Army Transportation Research Command, Fort Eustis, Virginia, July 1964.

26. Nordby, G. M. and W. C. Crisman, Strength Properties and Relationships Associated with Various Types of Fiberglass-Reinforced Facing Sandwich Structure, Technical Report 65-15, U. S. Army Aviation Materiel Laboratories, Fort Eustis, Virginia, August 1965.

27. Nordby, G. M., and W. C. Crisman, "Fabricating Laminates for Specific Properties", Modern Plastics, Volume 44, Number 2, October 1966, pp. 135, 136.

28. Nordby, G. M., and W. C. Crisman, "Fatigue Characteristics of An RP Sandwich Structure", Modern Plastics, Volume 43, Number 10, June 1966, pp. 120 ff.

29. Nordby, G. M., and W. C. Crisman, "Anatomy of an Autoclave", to be published.

30. Nordby, G. M., W. C. Crisman, and C. W. Bert, Dynamic Elastic Damping, and Fatigue Characteristics of Fiberglass-Reinforced Sandwich Structure, Technical Report 65-60, U. S. Army Aviation Materiel Laboratories, Fort Eustis, Virginia, October 1965.

31. Nordby, G. M. , W. C. Crisman, and C. W. Bert, The Effect of Resin Content and Voids on The Strength of Fiberglass-Reinforced Plastics for Airframe Use, Technical Report 65-66, U. S. Army Aviation Materiel Laboratories, Fort Eustis, Virginia, November 1965.

32. Norris, C. B., Compressive Buckling Curves For Simply Supported Sandwich Panels With Glass-Fabric-Laminate Facings and Honeycomb Cores, Report Number 1867, Forest Products Laboratory, Madison, Wisconsin, December 1958.

33, North, L. O., Design Data on High Temperature Resistant Reinforced Plastics and the Design, Fabrication, and Evaluation of a Reinforced-Plastic Missile Component, Technical Report 56-355, Part I, Wright Air Development Center, Wright-Patterson Air Force Base, Ohio, November 1956.

34. Owens-Corning Fiberglas Corporation, Office of Aerospace and Defense, Mechanical Properties of Aerospace Fiberglass Fabric Laminates, March 17, 1965.

35. Peterson, J. P. and Anderson, J. K., Structural Behavior and Buckling Strength of Honeycomb Sandwich Cylinders Subjected to Bending, Technical Note D-2926, National Aeronautucs and Space Administration, Langley Research Center, Virginia, August 1965.

36. Plantema, F. J., Sandwich Construction, John Wiley and Sons, Inc., New York, New York, 1966.

37. Seide, P., "On the Buckling of Truncated Conical Shells in Torsion", Journal of Applied Mechanics, Volume 29, 1962, Transactions of the American Society of Mechanical Engineers, Volume 84E, 1962, pp. 321-328.

38. Seide, P., and V. I. Weingarten, "On the Buckling of Circular Cylindrical Shells Under Pure Bending", Journal of Applied Mechanics, Volume 28, 1961, Transactions of the American Society of Mechanical Engineers, Volume 83E, 1961, pp. 112-116.

39. Seide, P., V. I. Weingarten, and E. J. Morgan, The Development of Design Criteria for Elastic Stability of Thin Shell Structures, Final Report Number STL/TR-60-0000-19425 (EM10-26), Space Technology Laboratories, Los Angeles, California, December 1960.

40. Stein, M., and J. Mayers, Compressive Buckling of Simply Supported Curved Plates and Cylinders of Sandwich Construction, Technical Note 2601, National Advisory Committee for Aeronautics, Langley Aeronautical Laboratory, Hampton, Virginia, January 1952.

41. Timoshenko, S. P., and J. M. Gere, Theory of Elastic Stability, Second Edition, McGraw-Hill Book Company, Inc., New York, 1961, pp. 484-485.

42. Tsai, S. W., Strength Characteristics of Composite Materials, Report Number CR-224, National Aeronautics and Space Administration, Washington, D.C., April 1965.

43. Vogt, C. W., E. S. Haniuk, and J. M. Trice, Jr., "Evaluation of Testing Techniques for Filament Wound Composites", Testing Techniques for Filament Reinforced Plastics, Technical Report AFML-TR-66-274, Air Force Materials Laboratory, Wright-Patterson Air Force Base, Ohio, September 1966.

44. Wang, C. T., and D. P. Sullivan, "Buckling of Sandwich Cylinders Under Bending and Combined Bending and Axial Compression", Journal of Aeronautical Sciences, Volume 19, 1952, pp. 468-470.

45. Wang, C. T., J. R. Vaccaro, and D. E. DeSanto, "Buckling of Sandwich Cylinders Under Combined Compression, Torsion, and Bending Loads", Journal of Applied Mechanics, Volume 22, 1955, Transactions of the American Society of Mechanical Engineers, Volume 77, 1955, pp. 324-328.

46. Yao, J. C., "Large-Deflection Analysis of Buckling of a Cylinder Under Bending", Journal of Applied Mechanics, Volume 29, 1962, Transactions of the American Society of Mechanical Engineers, Volume 84E, 1962, pp. 708-714.

47. Zahn, J. J., and E. W. Kuenzi, Classical Buckling of Cylinders of Sandwhich Construction in Axial Compression -- Orthotropic Cores, Report Number FPL-018, Forest Products Laboratory, Madison, Wisconsin, November 1963.

APPENDIX I

BUCKLING OF FRP SANDWICH CYLINDERS IN TORSION

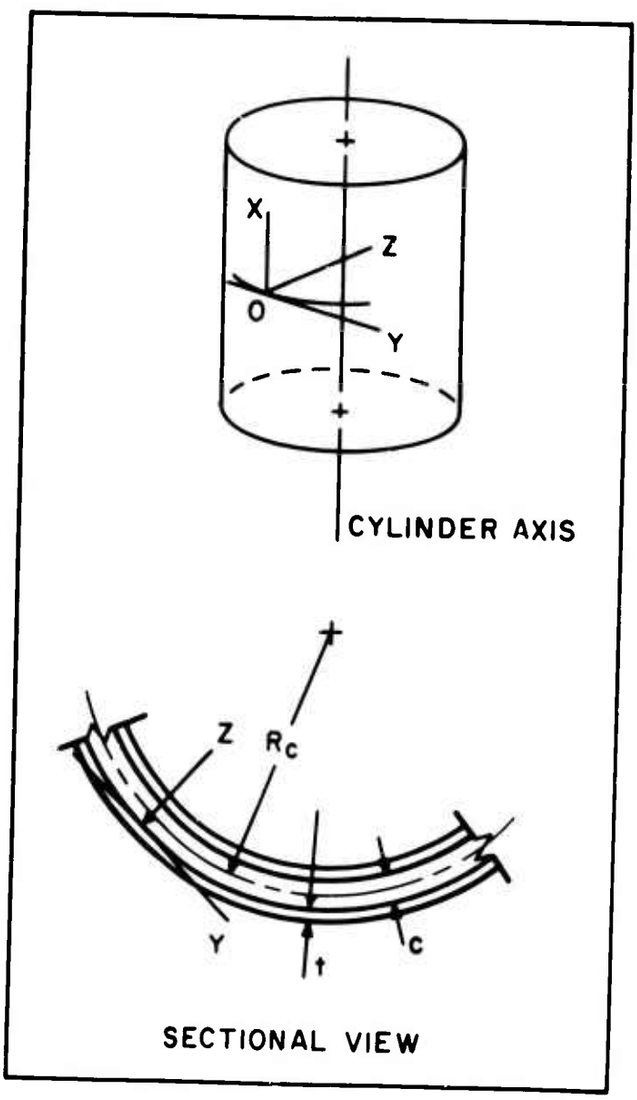

Figure 38. Coordinate System Used in the Cylinder Analyses.

The torsional analysis developed by March and Kuenzi of FPL in Reference 23 was used in the present study of FRP sandwich cylinders and curved panels. The formulas which account for orthotropic facings and cores were obtained using a small-deflection theory and the energy method of analysis.

Assuming a form of the buckled surface based on experiments with plywood shells, expressions were written for the various sandwich strains from which the energy of deformation was obtained. Facing membrane and flexural strains and the core transverse shear strains were considered. From the energy balance with the applied loads, an expression for the shear stress τ was obtained and the minimum was then located by minimizing τ with respect to (1) the inclination of the buckles from the cylinder axis γ (in radians), and (2) the parameter ρ containing the number of circumferential buckles n. The procedure is briefly discussed in the next few paragraphs in order to present the computer program developed for the calculations.

In programming the equation for minimum τ, an error was discovered in FPL equations number 48 (Reference 23). These are too large by a factor of 2, which was carried over into several of the remaining transformations of the original equation for minimum τ. However, a comparison of the results from the equations as printed and the graphs included in that report indicates that this was simply a typing error. The corrected equations employing a more convenient notation are as follows:

$$\tau_{cr} = K_f E_x \frac{H}{R_c} \tag{16}$$

where

$$K_f = \psi_1 + \psi_2 \tag{17}$$

$$\psi_1 = \frac{J\rho^2}{\pi^2 \gamma} \left[\frac{T_1^4}{\frac{E_x}{E_y} T_1^4 + \left[\frac{E_x}{\mu_{xy}} - 2\nu_{xy} \right] T_1^2 + 1} + \frac{T_2^4}{\frac{E_x}{E_y} T_2^4 + \left[\frac{E_x}{\mu_{xy}} - 2\nu_{xy} \right] T_2^2 + 1} \right] \tag{18}$$

$$T_1 = \gamma + \rho \tag{19}$$

$$T_2 = \gamma - \rho \tag{20}$$

$$\psi_2 = \frac{\pi^2}{\left(1 - \frac{c}{H}\right) 4J\rho^2 \gamma} \left[\frac{\frac{I}{H^3} \left[B_1 + B_2 \frac{\pi^2 \lambda}{2J\rho^2} \left(\frac{S_x}{A_4} + S_y \right) \right]}{1 + \frac{\pi^2 \lambda}{2J\rho^2} \left(S_x \frac{A_1}{A_4} + S_y A_3 \right) + \frac{\pi^4 \lambda^2}{4J^2 \rho^4} S_x \frac{B_2}{A_4} S_y + \frac{I_f}{H^3} B_1} \right] \tag{21}$$

$$I = \frac{t}{8} (H + c)^2 \tag{22}$$

$$B_1 = A_1 + 2A_2 + A_3 \tag{23}$$

$$B_2 = A_1A_3 - A_2^2 \tag{24}$$

$$A_1 = \frac{2}{\lambda}(\gamma^4 + 6\gamma^2\rho^2 + \rho^4) + \frac{2\mu_{xy}}{E_y}(\gamma^2 + \rho^2) \tag{25}$$

$$\mu_{xy}^{-1} = \frac{4}{E_{45}} - \frac{1 - \nu_{xy}}{E_x} - \frac{1 - \nu_{yx}}{E_y} \tag{26}$$

$$A_2 = 2\left[\frac{\nu_{yx}}{\lambda} + \frac{\mu_{xy}}{E_x}\right](\gamma^2 + \rho^2) \tag{27}$$

$$A_3 = 2\frac{E_y}{E_x\lambda} + 2\frac{\mu_{xy}}{E_x}(\gamma^2 + \rho^2) \tag{28}$$

$$A_4 = \gamma^2 + \rho^2 \tag{29}$$

$$S_x = \frac{E_x ct}{2\lambda G_{zx} R_c H} \tag{30}$$

$$S_y = \frac{E_x ct}{2\lambda G_{yz} R_c H} \tag{31}$$

$$I_f = t^3/6 \tag{32}$$

The minimum τ was calculated from the equations by an iterative procedure because of the complexity of the equations. Several values of ρ were estimated, and then for each ρ, the minimum buckling coefficient K_f with respect to γ was found with the aid of a digital computer. These values of K_f were then accurately plotted versus ρ to locate the relative minimum of K_f. Figure 39 shows the flow chart for the computer program, and Figure 40 illustrates the procedure used to locate the final minimum. The value of γ at minimum K_f can then be obtained from a cross plot of γ and K_f, as shown in the figure.

The initial calculations made in the research program were for the design of the specimens (see Section 3). To be specific, the first set of calculations was exploratory in nature to determine the approximate material sizes such as facing and core thickness and core cell size. Table VI and Figure 41 display the results of this effort. The second set of calculations was for the probable material sizes and was later compared with similar calculations for the axial compression case in order to finalize the material sizes and shell geometry. Table VII and Figure 42 exhibit these data. The detail calculations for comparison with tests are contained in the result sections.

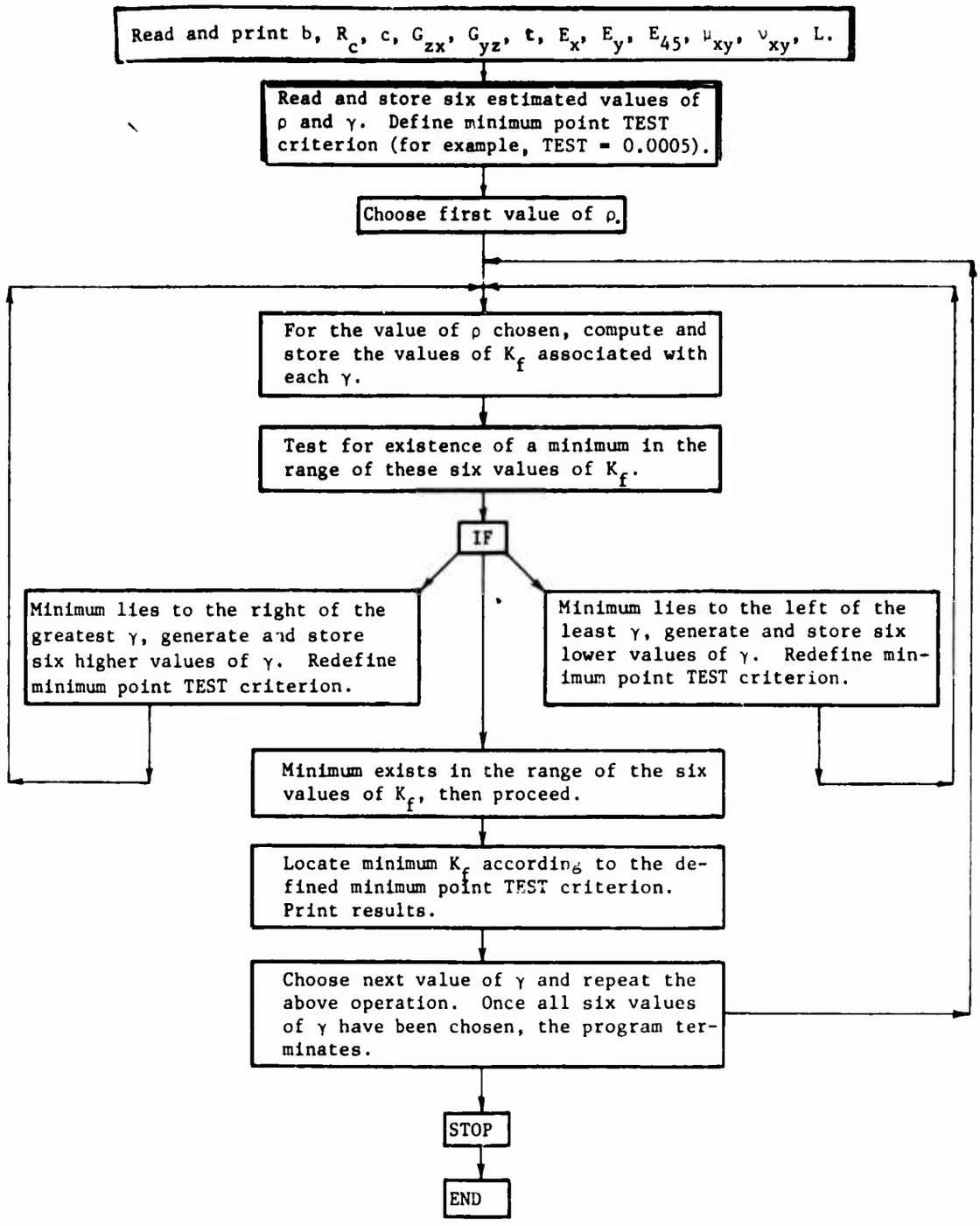

Figure 39. Flow Chart for Computer Program Used To Locate Minimum Values of Torsional-Buckling Coefficient K_f With Respect to γ.

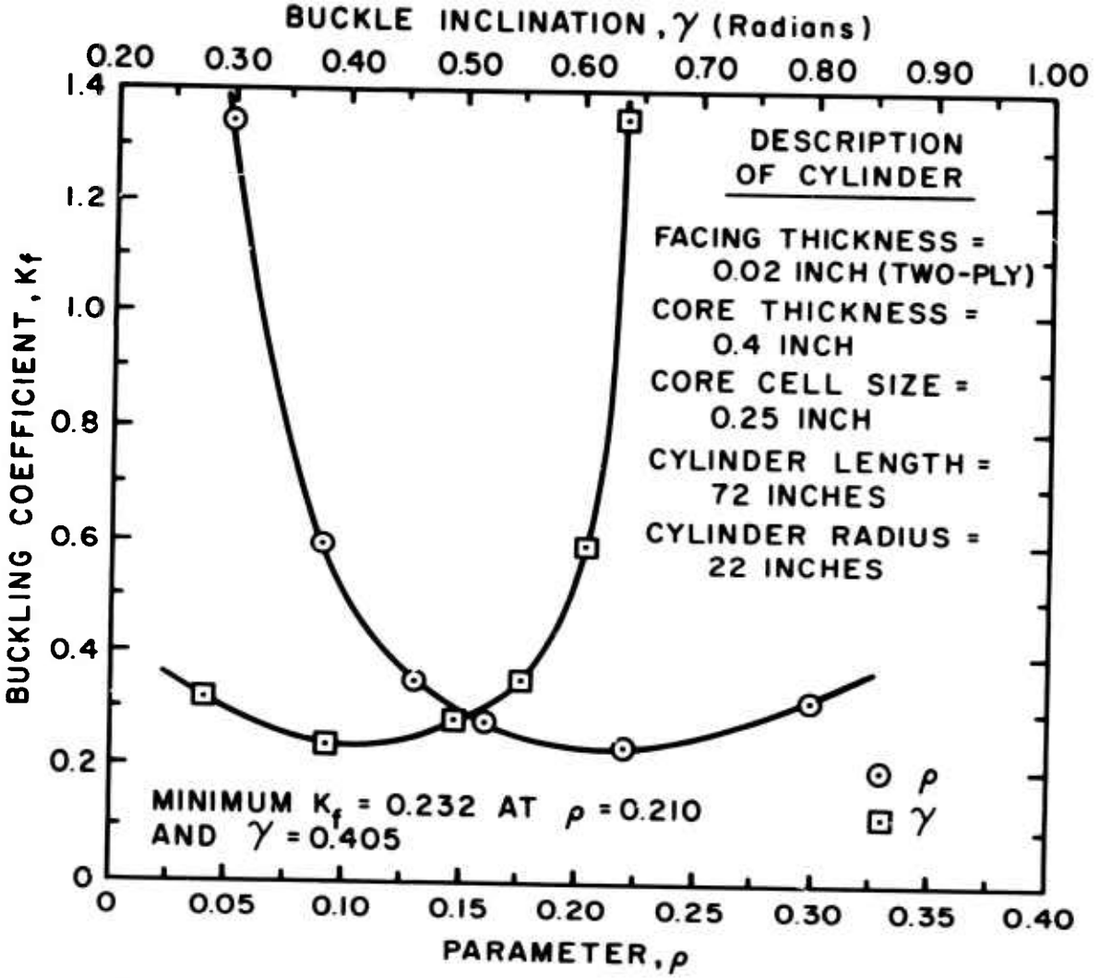

Figure 40. Typical Plot Used To Locate the Minimum Values of Buckling Coefficient K_f and the Inclination of the Buckles γ. The data were obtained from the computer analysis.

TABLE VI
PRELIMINARY CALCULATED VALUES I,
TORSIONAL-BUCKLING STRESS OF CYLINDERS

Cell Size (in.)	Core Thick. (in.)	G_{xz} * (psi)	G_{yz} * (psi)	Number Facing Plies	Facing Thickness,* t (in.)	E_x * (10^{-6} psi)	E_y ** (10^{-6} psi)	Radius, R_c (in.)	Buckling Coef., K_f ***	Critical Stress,*** τ (psi)
3/8	0.75	17,700	6,850	2	0.020	3.07	2.91	14	0.235	40,710
								18	0.249	33,550
								22	0.270	29,760
	0.40	22,000	8,700	2	0.020	3.07	2.91	14	0.209	20,170
								18	0.220	16,510
								22	0.230	14,120
	0.20	21,600	11,100	2	0.020	3.07	2.91	14	0.179	9,420
								18	0.178	7,290
								22	0.195	6,540
	0.75	17,700	6,850	3	0.025	4.06	3.85	14	0.198	45,940
								18	0.210	37,890
								22	0.220	32,480
	0.40	22,000	8,700	3	0.025	4.06	3.85	14	0.178	23,230
								18	0.192	19,490
								22	0.199	16,530
	0.20	21,600	11,100	3	0.025	4.06	3.85	14	-	-
								18	0.162	9,140
								22	0.172	7,940
3/16	0.75	34,800	19,900	2	0.020	3.07	2.91	14	0.242	41,920
								18	0.258	34,760
								22	0.270	29,750
	0.40	40,500	20,300	2	0.020	3.07	2.91	14	0.213	20,550
								18	0.222	16,660
								22	0.235	14,430
	0.20	47,400	27,000	2	0.020	3.07	2.91	14	0.180	9,470
								18	0.189	7,760
								22	0.198	6,630

* Average values taken from USAAVLABS TR 65-15 (Poisson's ratios ν_{xy}, ν_{yx} assumed equal to 0.13 for simplicity).
** E_y obtained as described on page 68, USAAVLABS TR 65-15. E_{45} also taken from page 68 of this report.
*** All values for cylinders 72 inches long.

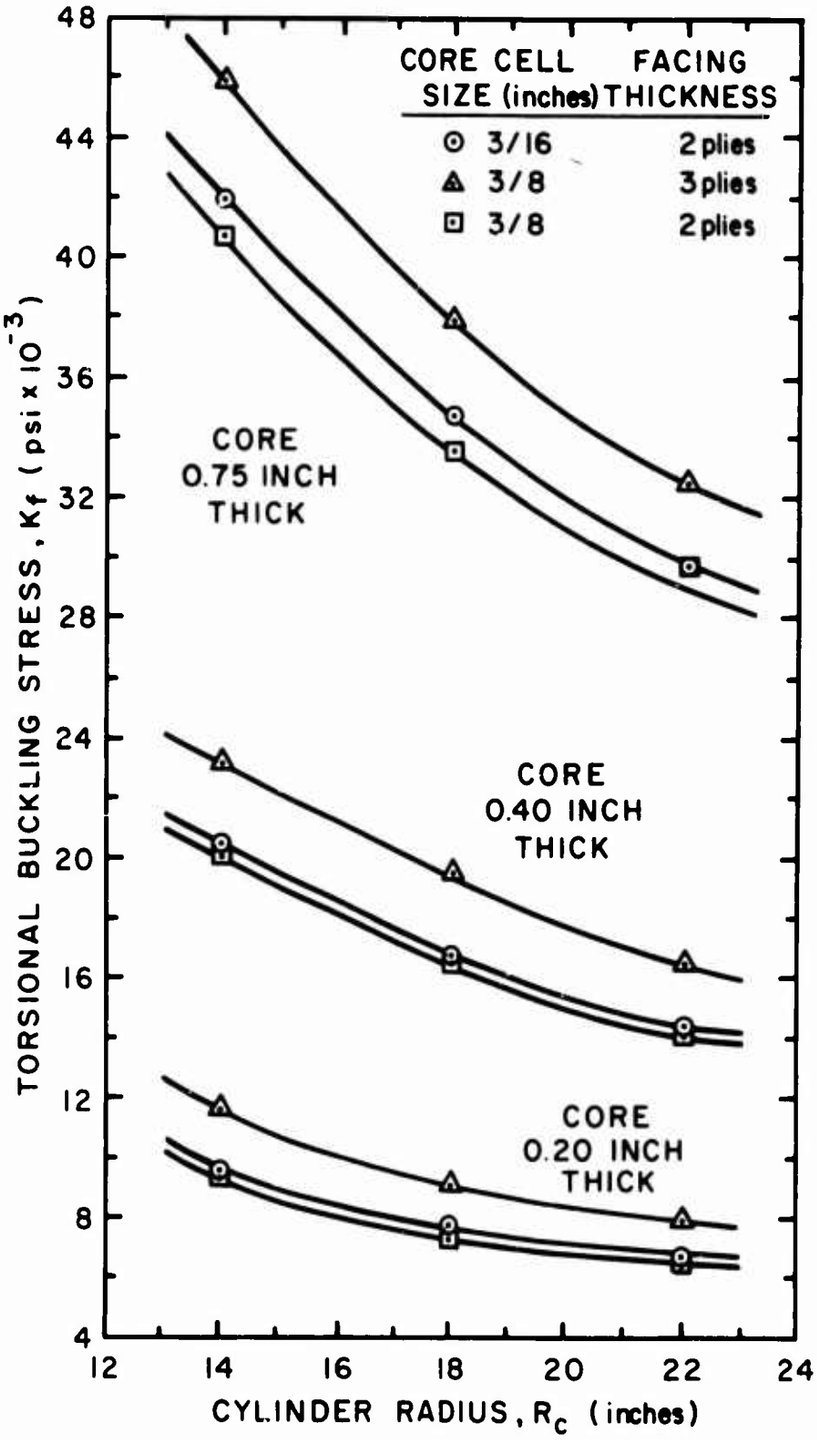

Figure 41. Effect of Constituent Materials and Geometry on Torsional-Buckling Stress of Sandwich Cylinders.

TABLE VII
PRELIMINARY CALCULATED VALUES II,
TORSIONAL-BUCKLING STRESS OF CYLINDERS

Constituent Properties					Buckling Data					
Thickness Core, Facing (in.)	Core Moduli (psi) G_{xz}*	G_{yz}*	Facing Moduli (10^{-6} psi) E_x*	E_y**	Radius, R_c (in.)	Buckling Coef., K_f	Critical Stress, τ (psi)	Calc. n	Number Buckles Possible	Inclination Buckles, γ (radians)
0.4, 0.02 (2-ply)	30,200	14,600	3.07	2.91	14	0.205	19,800	3.49	3 or 4	0.365
					18	0.222	16,700	4.03	4 or 5	0.382
					22	0.232	14,200	4.53	4 or 5	0.405
0.3, 0.02 (2-ply)	30,200	14,600	3.07	2.91	14	0.196	14,600	3.87	3 or 4	0.308
					18	0.204	11,800	4.29	4 or 5	0.345
					22	0.218	10,300	4.80	4 or 5	0.360
					24	0.225	9,800	5.11	5 or 6	0.372
					26	0.229	9,200	5.28	5 or 6	0.370

* Average values taken from pages 63 and 66 of USAAVLABS TR 65-15 (core cells = 1/4-inch width, 1-mil-thick 5052 aluminum foil; facing $E_{45} = 2.20 \times 10^6$).

** E_y obtained as described on page 68 of USAAVLABS TR 65-15, see E_F (=W).

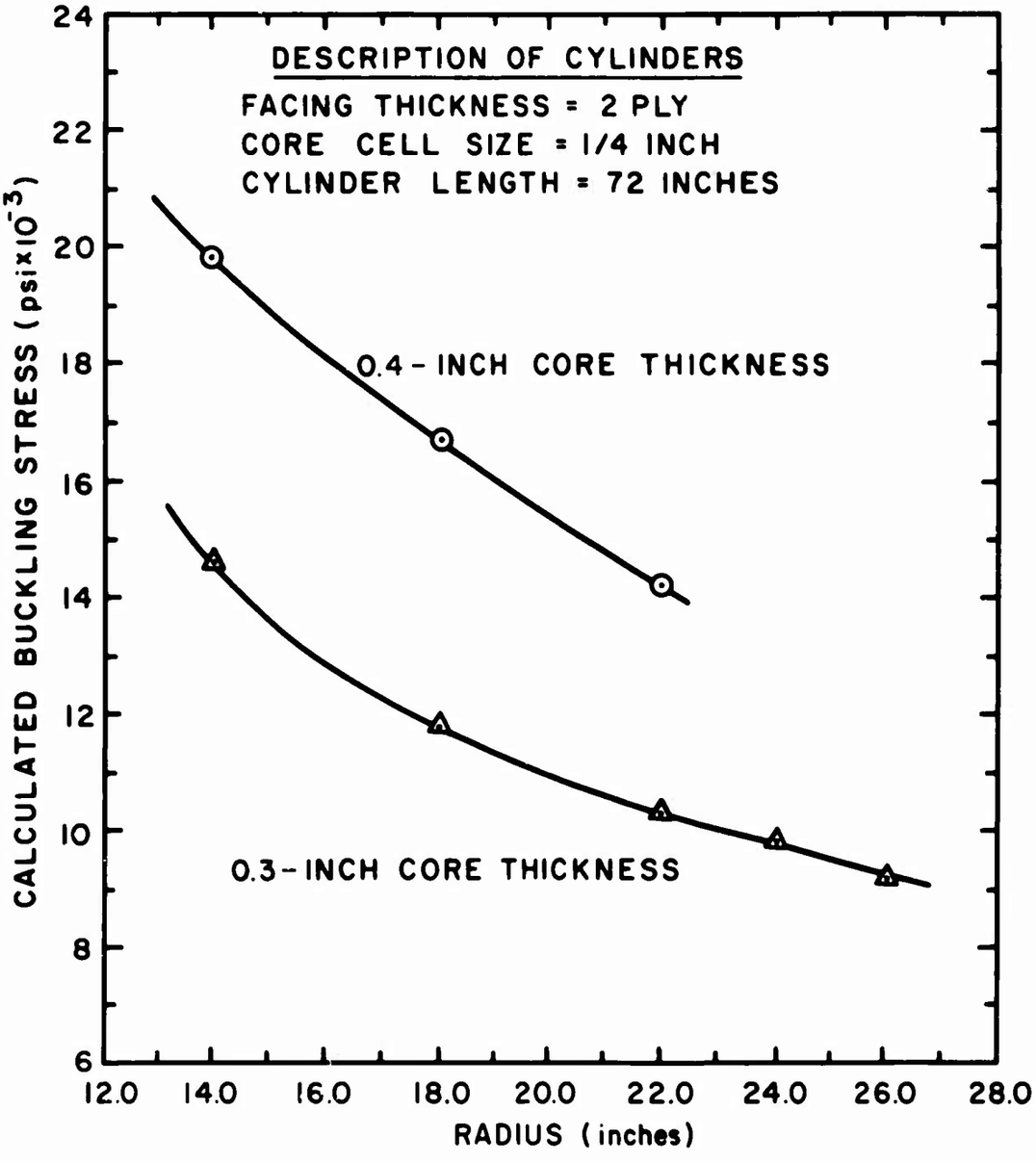

Figure 42. Approximate Relations Between Calculated Torsional-Buckling Stress and Cylinder Radius in the Vicinity of the Design Point. Consult the result sections for precise values.

APPENDIX II

BUCKLING OF FRP SANDWICH CYLINDERS IN AXIAL COMPRESSION (LARGE-DEFLECTION THEORY)

A mathematical analysis developed by March and Kuenzi for compressive buckling (Reference 22) was also used in the present study of sandwich cylinders and curved panels, especially in the shell design phase. In the FPL formulation of the problem, the energy method was used in conjunction with a large-deflection theory, and the core and facings are taken to be orthotropic.

Assuming a diamond form of the buckled surface of the shell (Figure 43), based on extensive experiments with plywood shells (Reference 22), expressions were written for the various sandwich strains from which the energy of deformation of the buckled shell was obtained. Again the facing membrane and flexural strains and the core transverse shear strains were considered in the development. The vanishing of the derivatives of the total energy expression, which included the energy of the compressive load, with respect to the various unknown parameters then led to an equation for the critical buckling stress σ_{cr} as follows:*

$$\sigma_{cr} = KE_x \frac{H}{R_c} \tag{33}$$

where μ_{xy} is given by Equation (26), and

$$K = \frac{64}{3\zeta^2}\left[\frac{\beta_3}{\eta} - \frac{9\beta_2^2}{32\beta_1\eta} + \beta_4\eta\right] \tag{34}$$

$$\beta_1 = C_1 + C_2 + C_3 + C_4 + C_5 \tag{35}$$

$$\beta_2 = C_6 + C_7 \tag{36}$$

$$\beta_3 = C_8 + C_7 \tag{37}$$

$$C_1 = \frac{\zeta^4}{4096} \tag{38}$$

$$C_2 = \frac{E_y}{4096\ E_x} \tag{39}$$

*See Figure 39 of Appendix I for coordinate definitions.

$$C_3 = \frac{\zeta^4}{512\left[\zeta^4 \frac{E_x}{E_y} + 81 + \frac{9\zeta^2 E_x}{\mu_{xy}} - 18\nu_{xy}\zeta^2\right]} \tag{40}$$

$$C_4 = \frac{\zeta^4}{512\left[81\zeta^4 \frac{E_x}{E_y} + 1 + 9\zeta^2 \frac{E_x}{E_y} - 18\nu_{xy}\zeta^2\right]} \tag{41}$$

$$C_5 = \frac{17\zeta^4}{2048\left[\zeta^4 \frac{E_x}{E_y} + 1 + \frac{\zeta^2 E_x}{\mu_{xy}} - 2\nu_{xy}\zeta^2\right]} \tag{42}$$

$$C_6 = \frac{E_y}{512\ E_x} \tag{43}$$

$$C_7 = \frac{\zeta^4}{32\left[\zeta^4 \frac{E_x}{E_y} + 1 + \frac{\zeta^2 E_x}{\mu_{xy}} - 2\nu_{xy}\zeta^2\right]} \tag{44}$$

$$C_8 = \frac{E_y}{256\ E_x} \tag{45}$$

$$\beta_4 = \frac{N}{32\lambda H^2 t}\left[\frac{I + \frac{I}{Q}\ B\ \frac{\eta}{E_x}\left(\frac{W_x}{\zeta^2} + W_y\right)}{1 + \frac{\eta d_1 W_x}{E_x\zeta^2} + \frac{\eta d_3 W_y}{E_x} + \frac{\eta^2 B W_x W_y}{E_x^2\zeta^2}} + I_f\right] \tag{46}$$

$$Q = 3E_x\zeta^4 + 3\ E_y + 2\ (E_x\nu_{yx} + 2\lambda\mu_{xy})\zeta^2 \tag{47}$$

$$B = d_1 d_3 - d_2^2 \tag{48}$$

$$d_1 = 3E_x\zeta^4 + \lambda\mu_{xy}\zeta^2 \tag{49}$$

$$d_2 = (E_x\nu_{yx} + \lambda\mu_{xy})\zeta^2 \tag{50}$$

$$d_3 = 3E_y + \lambda\mu_{xy}\ \zeta^2 \tag{51}$$

$$I = t/2\, h^2 \tag{52}$$

$$I_f = t^3/6 \tag{53}$$

$$W_x = \frac{E_x ct}{3\lambda G_{zx} R_c H} \tag{54}$$

$$W_y = W_x \frac{G_{zx}}{G_{yz}} \tag{55}$$

It was then finally necessary to minimize Equation (34) with respect to (1) the parameter η proportional to the number of circumferential buckles n, and (2) the parameter ζ which is the aspect ratio of the buckles b/a. This minimizing process was accomplished with the aid of a digital computer using a trial and error procedure similar to that used for the torsional analysis presented in Appendix I. In particular, several values of ζ were estimated, and a minimum buckling coefficient with respect to η was located by the computer for each of these ζ. These values of K were then plotted against the chosen values of ζ to obtain the desired relative minimum of K. Figure 44 shows the flow chart for the computer program, and Figure 45 illustrates the plotting procedure used to locate the final minimum. The value of η at the minimum K was then obtained from a plot of K versus η, as shown in the figure.

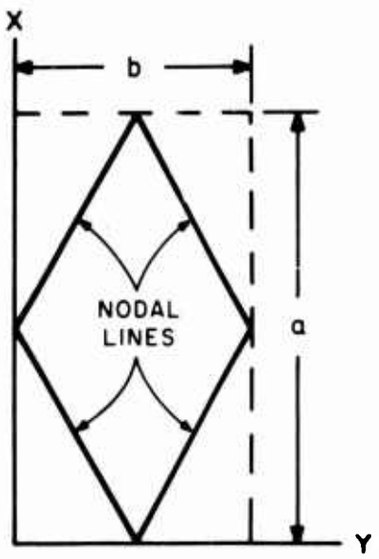

Figure 43. Assumed Diamond-Shaped Buckle.

Table VIII contains the preliminary values of compressive buckling stresses and the corresponding buckle sizes which were calculated using the first estimates of material properties after probable material sizes had been established by the torsion analysis (Appendix I). Figure 46 summarizes these values that served to confirm the cylinder design. The final calculations with more precise material properties can be found in the result sections.

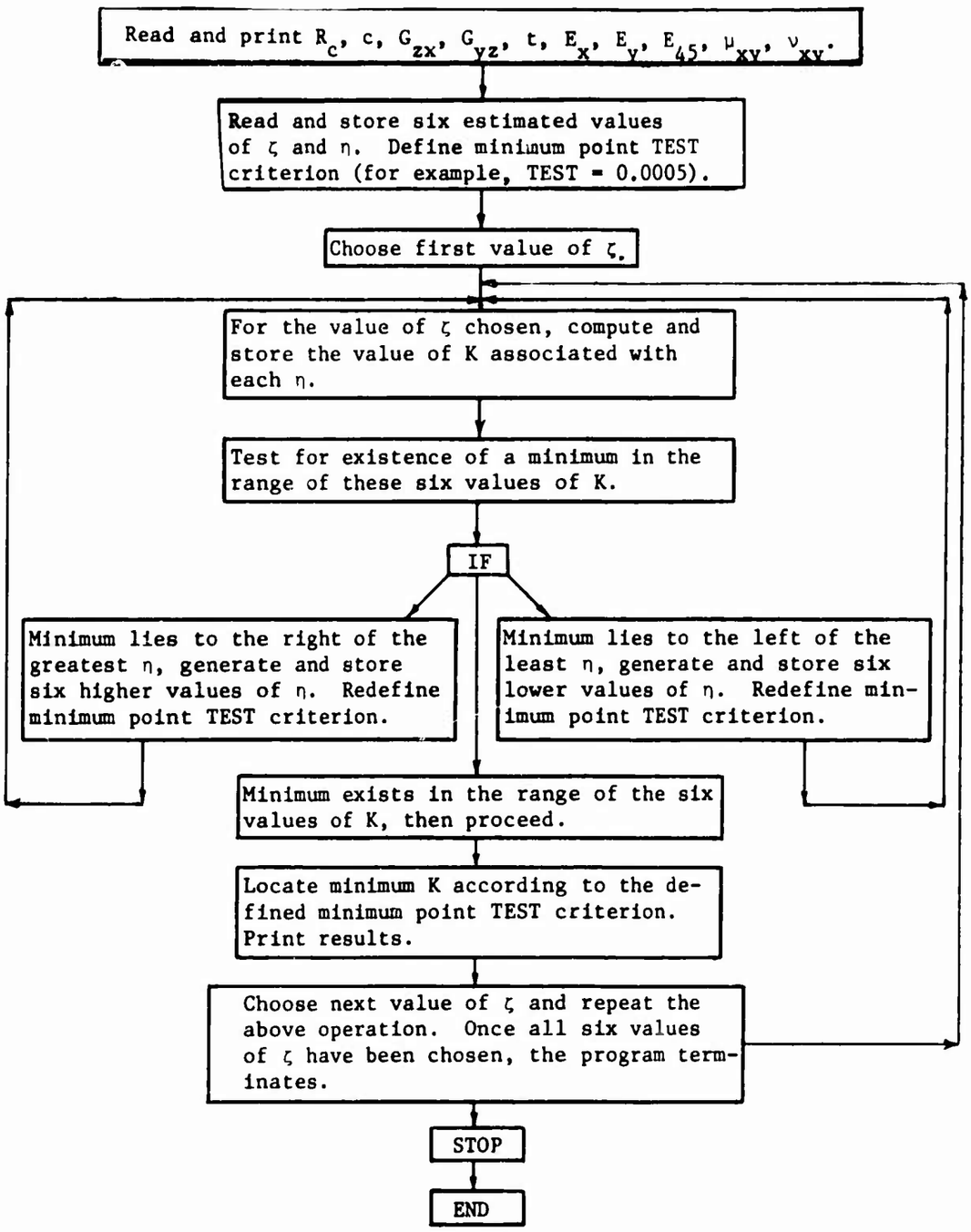

Figure 44. Flow Chart for Computer Program Used To Locate Minimum Values of Compressive Buckling Coefficient K With Respect to η.

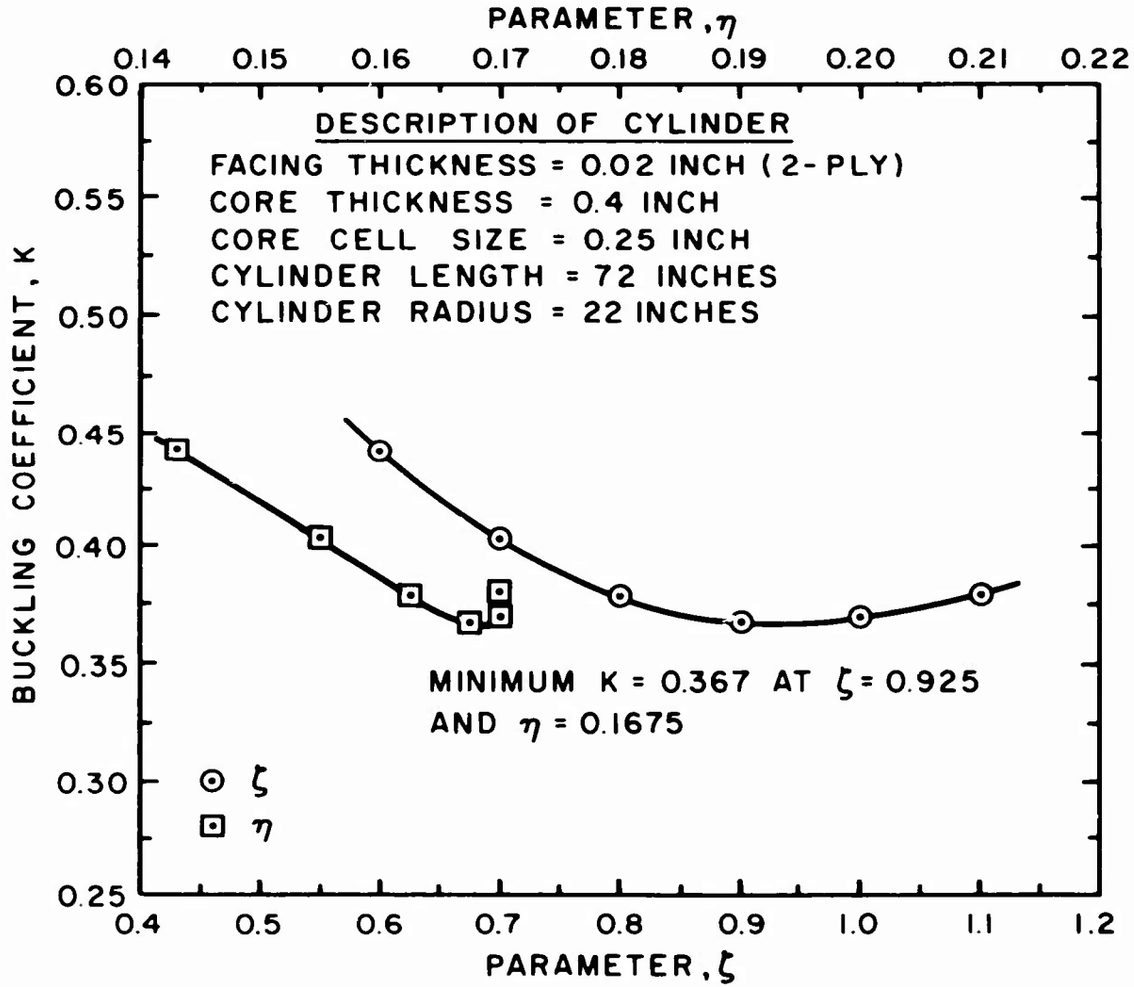

Figure 45. Typical Plots Used To Locate the Relative Minimum of Buckling Coefficient K and Parameter η. The data were obtained from the computer analysis.

TABLE VIII
PRELIMINARY CALCULATED VALUES,
AXIAL COMPRESSIVE-BUCKLING STRESS OF CYLINDERS

Constituent Properties					Buckling Data					
Thickness Core, Facing (in.)	Core Moduli (psi) G_{zx}*	G_{yz}*	Facing Moduli (10^{-6} psi) E_x*	E_y**	Radius, R_c (in.)	Critical Stress, σ (psi)	Calc. n	Number Buckles Possible	Buckle Size (in.) b	a
0.4, 0.02 (Two-ply)	30,200	14,600	3.07	2.91	14	34,500	2.32	2	44.0	47.6
								3	29.3	31.7
					18	27,500	2.64	2	56.6	61.1
								3	37.7	40.3
					22	22,500	2.89	2	69.1	74.7
								3	46.1	49.8
					24	20,700	3.02	3	50.3	54.4
								4	35.2	38.0
					26	19,100	3.14	3	54.5	58.9
								4	40.8	44.2
0.3, 0.02 (Two-ply)	30,200	14,600	3.07	2.91	14	26,800	2.65	2	44.0	46.8
								3	29.3	31.2
					18	20,900	3.00	3	37.7	40.1
					22	17,200	3.31	3	46.1	49.0
								4	34.6	36.8
					24	15,700	3.46	3	50.3	52.9
								4	37.7	39.7
					26	14,600	3.61	3	54.5	58.5
								4	40.8	43.9

* Average values taken from USAAVLABS TR 65-15. Core cell = 1/4-inch, 1-mil-thick 5052 aluminum foil, facing $E_{45} = 2.20 \times 10^{-6}$.
** E_y obtained as described on page 68, USAAVLABS TR 65-15, see E_f (-W).

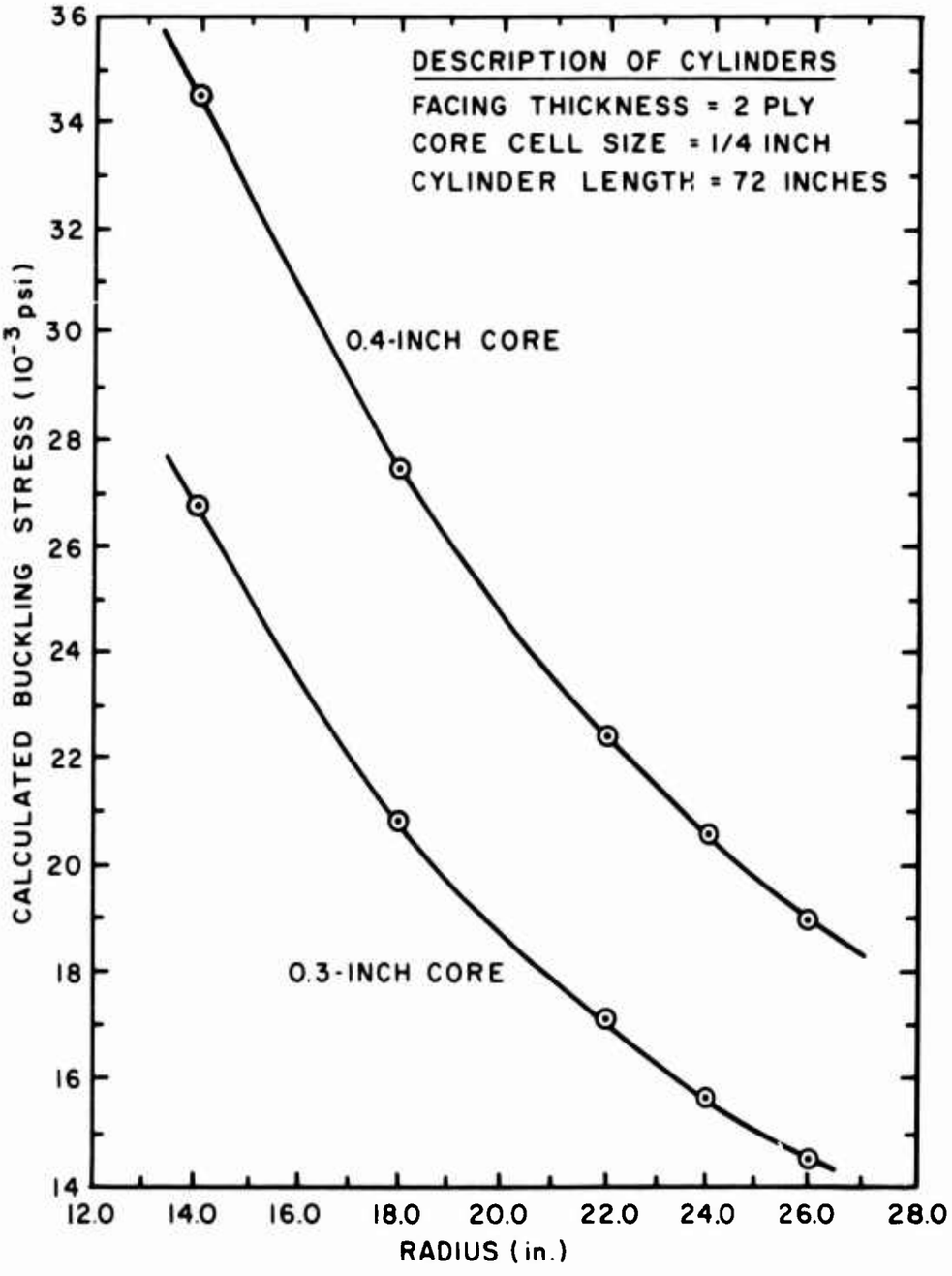

Figure 46. Approximate Relations Between Calculated Compressive-Buckling Stress and Cylinder Radius in the Vicinity of the Design Point. Consult the result sections for precise values.

APPENDIX III

MODIFIED SMALL-DEFLECTION BUCKLING CALCULATIONS

As pointed out in the body of the report, apparently at present there is no small-deflection axial-compression buckling analysis of cylindrically curved panels and of complete cylinders for sandwich construction with orthotropic facings (such as FRP laminates). Therefore, the approach used here is to use the various analyses for sandwich construction with isotropic facings, and then to apply an approximate correction or knockdown factor to account for facing orthotropy.

1. Derivation of Correction Factor to Account for Orthotropic Facings

For the case of infinitely long cylinders (or cylindrical panels) with perfect cores (i.e., infinite core shear rigidity), Dow and Rosen (Reference 11) extended the isotropic-facing analysis of Stein and Mayers (Reference 40) to orthotropic facings with the material-symmetry axes lined up in the axial and hoop directions. The result of their analysis can be expressed as follows:

$$\sigma_{cr} = (2t/R)\{[1 + (c/2t)]^3 - [c/2t]^3\}^{1/2}[E_x E_y/3(1 - \nu_{xy}\nu_{yx})]^{1/2}\phi \qquad (56)$$

where σ_{cr} = critical axial buckling load per unit facing cross-sectional area; t = facing thickness; R = mean radius of cylinder; c = core depth; E_x, E_y = facing elastic moduli in the axial and hoop directions; ν_{xy}, ν_{yx} = facing Poisson's ratios; and ϕ = a shear-stiffness factor given by the following expressions:

$$\phi = \begin{cases} \phi_1 = \{2\mu_{xy}[1 + (\nu_{xy}\nu_{yx})^{1/2}]/(E_x E_y)^{1/2}\}^{1/2} \text{ if } \phi_1 < 1 \\ \phi_2 = 1, \text{ if } \phi_1 \geq 1 \end{cases} \qquad (57)$$

where μ_{xy} = facing shear modulus. It is noted that the way in which the elastic moduli and Poisson's ratios enter into Equation (57) is always as a square root of the product. Thus, the effective isotropic modulus and Poisson's ratio would be

$$E_f = (E_x E_y)^{1/2} \; ; \; \nu_f = (\nu_{xy}\nu_{yx})^{1/2} \qquad (58)$$

Now if the facings were isotropic, the following familiar relationship of isotropic elasticity theory would be valid:

$$\mu_1 = E_f/[2(1 + \nu_f)] \qquad (59)$$

In inserting Equations (58) and (59) in Equation (57) for the parameters involved in the cylindrical panels and cylinders used here, the isotropic factor $\phi_i \simeq 1$. However, when the actual (orthotropic) value of μ_{xy}, which is approximately 30 percent of μ_i, is used, the orthotropic $\phi_o < \phi_i$; specifically

$$\phi_o/\phi_i = (\mu_{xy}/\mu_i)^{1/2} \tag{60}$$

Thus, the correction factor which is applied to the results of an isotropic buckling analysis to account for orthotropic facings is

$$C_o = \phi_o/\phi_i = (\mu_{xy}/\mu_i)^{1/2} \tag{61}$$

2. Stein-Mayers Curved-Panel Compression Buckling Analysis

To utilize the curves presented by Stein and Mayers (Reference 40), it is necessary to assume the core to be isotropic. Here this is accomplished by using the following relation

$$G_c = (G_{xz}G_{yz})^{1/2} \tag{62}$$

A sample calculation is carried out for Panel No. 1 as follows:

$$G_c = (0.0306 \times 0.0179)^{1/2} \times 10^6 = 0.0234 \times 10^6 \text{ psi}$$

$$E_f = (E_x E_y)^{1/2} = (3.23 \times 3.09)^{1/2} \times 10^6 = 3.16 \times 10^6 \text{ psi}$$

$$\nu_f^* = (\nu_{xy}\nu_{yx})^{1/2} \simeq 0.13 \quad \text{(dimensionless)}$$

$$h = c + t = 0.40 + 0.02 = 0.42 \text{ in.}$$

$$z_a = (2a^2/hR)(1 - \nu_f^2)^{1/2} = 278 \quad \text{(dimensionless)} \tag{63}$$

where a = panel length (36 in.)

$$r_a = (\pi/a)^2(E_f tc/2G_c)(1 - \nu_f^2)^{-1} = 0.00418 \quad \text{(dimensionless)} \tag{64}$$

$$a/b = 36/36 = 1 \quad \text{(dimensionless)}$$

where b = panel circumferential width

From Figure 6 in the report by Stein and Mayers, for the above values

*ν_{xy} and ν_{yx} assumed equal for simplicity.

of z_a, r_a, and a/b, one obtains $K_{xa} = 50$. Now K_{xa} is defined as

$$K_{xa} = (a/\pi)^2 N_{cr}/D_f \tag{65}$$

where N_{cr} = critical axial buckling load and D_f = flexural rigidity of facings about the composite neutral axis, $E_f th^2/[2(1 - \nu_f^2)]$.

Thus, the critical buckling load per unit facing area is

$$N_{cr}/2t = (\pi h/2a)^2 K_{xa} E_f/(1 - \nu_f^2) = 54{,}000 \text{ psi}$$

The above value obtained by isotropic analysis is multiplied by the factor C_o to account for orthotropic facings. To obtain C_o one needs μ_i and μ_{xy}.

$$\mu_i = E_f/[2(1 + \nu_f)] = 1.40 \times 10^6 \text{ psi}$$

The actual orthotropic μ (denoted by μ_{xy}) is best calculated from the experimental strain measurements taken in a shell torsion test as follows:

$$\mu_{xy} = \Delta\tau/\Delta\gamma = (R/J)(\Delta T/2\Delta\epsilon_{45}) \tag{66}$$

where $\Delta\tau$ = torsional shear-stress increment, $\Delta\gamma$ = shear strain increment, T = applied torque increment, ϵ_{45} = measured normal-strain increment at an angle of 45 degrees to the major material-symmetry axis (shell axis). It is noted that the expression (R/J) T is valid for a thin shell in torsion even though the stress-strain curve is not linear, because the effective radius of the material remains the same regardless of the nonlinearity of the material. The factor of two in Equation (66) is due to the nature of the Mohr strain circle for pure shear which gives $\Delta\gamma/2$ = radius of circle = $\Delta\epsilon_{45}$. A plot of torsional shear stress versus shear strain is given in Figure 47 for the conical shell.

For a normal-stress level σ_{cr} of 26,600 psi (reached in the experiment), the equivalent shear stress using the von Mises criterion is $0.577\ \sigma_{cr}$ = 15,400 psi. This is in the tertiary region of Figure 47, which has a shear modulus

$$\mu_{xy} = 0.416 \times 10^6 \text{ psi}$$

Then

$$C_o = [0.416 \times 10^6)/(1.40 \times 10^6)]^{1/2} = 0.545$$

Thus, the final buckling load per unit facing area is

$$\sigma_{cr} = 0.545 \times 54{,}000 = \underline{29{,}400 \text{ psi}}$$

Since the experimental value was 26,600 psi, the ratio of the experimental value to the small-deflection analysis value is 0.90 (see column 6, Table V).

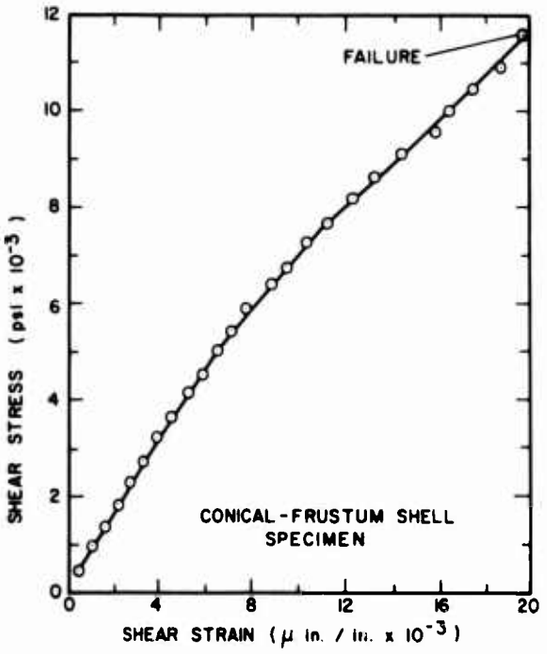

Figure 47. Typical Shear Stress-Strain Curve Obtained During Torsion Test of Conical Shell.

3. Stein-Mayers Complete-Cylinder Compression Buckling Analysis

This analysis (Reference 40) is very similar to the one just described above. A sample calculation follows:

$$G_c = (0.032 \times 0.0183)^{1/2} \times 10^6 = 0.0242 \times 10^6 \text{ psi}$$

$$E_f = (3.28 \times 3.14)^{1/2} \times 10^6 = 3.21 \times 10^6 \text{ psi}$$

$$\nu_f = 0.13 \quad \text{(dimensionless)}$$

$$h = c + t = 0.30 + 0.02 = 0.32 \text{ in.}$$

$$z_a = (2L^2/hR)(1 - \nu_f^2)^{1/2} = 1464 \text{ (dimensionless)} \qquad (67)$$

where L = active length of cylinder (72 in.)

$$r_a = (\pi/L)^2 (E_f tc/2G_c) (1 - \nu_f^2)^{-1} = 0.0006 \text{ (dimensionless)} \quad (68)$$

From Figure 5 in the report by Stein and Mayers, for the above values of z_a and r_a, one obtains $K_{xa} \simeq 250$.

Thus

$$N_{cr}/2t = 40{,}100 \text{ psi}$$

Here the correction factor for facing orthotropic behavior is 0.545, and thus

$$\sigma_{cr} = 0.545 \times 40{,}100 = \underline{21{,}900 \text{ psi}}$$

4. Zahn-Kuenzi Complete-Cylinder Compression Buckling Analysis

The factors needed to use the curves presented by Zahn and Kuenzi (Reference 47), which account for orthotropic core but not orthotropic facings, are:

$$G_{xz}/G_{yz} = 0.0320 \times 10^6/0.0183 \times 10^6 = 1.749$$

$$V = (E_f ct/2hRG_{xz})(1 - \nu_f^2)^{-1/2} = 0.0425 \quad (69)$$

From Zahn and Kuenzi's Figure 3, $K' \simeq 0.96$.

Then

$$N_{cr}/2t = (K'E_f h/R)(1 - \nu_f^2)^{-1/2} = 45{,}300 \text{ psi}$$

Applying the correction factor to account for orthotropic facings gives

$$\sigma_{cr} = 0.545 \times 45{,}300 = \underline{24{,}700 \text{ psi}}$$

5. Almroth Complete-Cylinder Compression Buckling Analysis

In the analysis by Almroth (Reference 2), which also is for an infinitely long cylinder with isotropic facings and orthotropic core, the following factors are used:

$$G_{xz}/G_{yz} = 1.749; \; V = 0.0425$$

$$F = (1/3)(t/h)^2 = 0.00130$$

From the curve given by Almroth, $K' \simeq 0.96$.

Then

$$N_{cr}/2t = (E_f hK'/R)(1 - \nu_f^2)^{-1/2} = 45,300 \text{ psi}$$

Applying the orthotropic-facing correction

$$\sigma_{cr} = 0.545 \times 45,300 = \underline{24,700 \text{ psi}}$$

6. Peterson-Anderson Complete-Cylinder Compression Buckling Analysis

Peterson and Anderson (Reference 35) presented an analysis which considers the effects of decreased core shear stiffness due to incipient buckling and isotropic facings with a nonlinear stress-strain curve. By neglecting these two effects, their equations reduce to the following expression:

$$N_{cr}/2t = (E_f h/R)(1 - \nu_f^2)^{-1/2}[1 - (E_f ct/2RhG_{xz})(1 - \nu_f^2)^{-1/2}] = 45,300 \text{ psi}$$

Applying the orthotropic-facing correction:

$$\sigma_{cr} = 0.545 \times 45,300 = \underline{24,700 \text{ psi}}$$

APPENDIX IV

INTERPRETATION OF STRAIN-ROSETTE DATA FOR ORTHOTROPIC MATERIAL

In isotropic materials, those having material properties which are independent of directional orientation, the principal-strain directions coincide with the principal-stress directions. However, in general, for anisotropic materials, which have material properties which depend upon the directional orientation, the principal-strain directions do not coincide with the principal-stress directions.

In the conical-shell torsion test, the 45-degree arm of the strain rosette indicated a total strain of 9,850 microinches per inch, while the meridional and circumferential readings were nil. These results are interpreted in terms of principal stresses in the following paragraphs.

In view of the reported strain readings, the principal-strain direction θ_ε is obviously 45 degrees. What remains to be determined is the principal-stress direction θ_σ.

Greszczuk (Reference 14) has derived the following equation expressing the relationship between the principal-stress direction θ_σ and the principal-strain direction θ_ε for the case of a thin layer of orthotropic material (such as the FRP facings used on the shells covered in this report):

$$\tan \theta_\sigma / \tan 2\theta_\varepsilon = \mu_{xy} \{[(1 + \nu_{xy})/E_x] - [(1 + \nu_{yx})/E_y] \tan^2 \theta_\sigma\} \quad (64)$$

From the preceding equation and the trigonometrical double-angle relation [$\tan 2\theta_\varepsilon = 2 \tan \theta_\varepsilon / (1 - \tan^2 \theta_\varepsilon)$], it can be shown that in order for θ_ε and θ_σ to coincide, the following condition must be met:

$$\tan^2 \theta_\sigma = [1 - 2(1 + \nu_{xy})(\mu_{xy}/E_x)] / [1 - 2(1 + \nu_{yx})(\mu_{xy}/E_y)] \quad (65)$$

For the present facings, $E_y \approx E_x$. Then, diagonal symmetry of the general anisotropic stress-strain relations requires that $\nu_{yx} \approx \nu_{xy}$.

Thus, the right-hand side of the preceding equation is unity. Finally, since $\tan \theta_\sigma = 1$, $\theta_\sigma = 45$ degrees. A stress field characterized by $\theta_\sigma = 45$ degrees is a pure-shear stress state, which means that the testing machine was applying this type of loading. (Parenthetically, even though the material is orthotropic, for this special case when $E_x \approx E_y$ and $\theta_\sigma = 45$ degrees, the principal-strain direction does coincide with the principal-stress direction.)

Unclassified
Security Classification

DOCUMENT CONTROL DATA - R & D

(Security classification of title, body of abstract and indexing annotation must be entered when the overall report is classified)

1. ORIGINATING ACTIVITY (Corporate author) University of Oklahoma Research Institute Norman, Oklahoma	2a. REPORT SECURITY CLASSIFICATION Unclassified 2b. GROUP

3. REPORT TITLE

FABRICATION AND FULL-SCALE STRUCTURAL EVALUATION OF SANDWICH SHELLS OF REVOLUTION COMPOSED OF FIBER GLASS REINFORCED PLASTIC FACINGS AND HONEYCOMB CORES

4. DESCRIPTIVE NOTES (Type of report and inclusive dates)

Final Report 1 April 1965 - 31 March 1967

5. AUTHOR(S) (First name, middle initial, last name)

Nordby, Gene M.
Crisman, W. C.
Bert, Charles W.

6. REPORT DATE	7a. TOTAL NO. OF PAGES	7b. NO. OF REFS
November 1967	110	47

8a. CONTRACT OR GRANT NO.	9a. ORIGINATOR'S REPORT NUMBER(S)
DA 44-177-AMC-164 (T) b. PROJECT NO. c. 1P121401A14176 d.	USAAVLABS Technical Report 67-65 9b. OTHER REPORT NO(S) (Any other numbers that may be assigned this report)

10. DISTRIBUTION STATEMENT

This document has been approved for public release and sale; its distribution is unlimited.

11. SUPPLEMENTARY NOTES	12. SPONSORING MILITARY ACTIVITY
	U.S. Army Aviation Materiel Laboratories Fort Eustis, Virginia

13. ABSTRACT

Large sandwich cylinders, truncated cones, and curved panels composed of fiber glass-epoxy facings and honeycomb cores were fabricated and tested as a part of a larger research program designed to bring acceptability of reinforced plastics for primary load-bearing members of Army aircraft structures. The many aspects of tooling for and fabrication of these large shells (up to 58-inch diameter and 72 inches long) by autoclave cure were examined in detail. To generate preliminary data on this mode of shell failure, the shells were designed to fail in buckling. The tests were carried out on a testing machine capable of applying 3,000,000 inch-pounds of bending moment, of torque, or of each in combination. Curved-panel compressive test values agreed reasonably well with the approximate theoretical analyses available, but agreement of test and analysis was not good for the shear loading. Preliminary interaction relations were confirmed tentatively for the combined torsion and bending of the cylinders and truncated cones.

DD FORM 1 NOV 1473 REPLACES DD FORM 1473, 1 JAN 64, WHICH IS OBSOLETE FOR ARMY USE.

Unclassified
Security Classification

14. KEY WORDS	LINK A		LINK B		LINK C	
	ROLE	WT	ROLE	WT	ROLE	WT
Aircraft Structures						
Buckling						
Composite Materials						
Design Criteria						
Fabrication						
Sandwich Construction						
Shell Structures						
Structural Analysis						